

This work is protected by copyright and other intellectual property rights and duplication or sale of all or part is not permitted, except that material may be duplicated by you for research, private study, criticism/review or educational purposes. Electronic or print copies are for your own personal, non-commercial use and shall not be passed to any other individual. No quotation may be published without proper acknowledgement. For any other use, or to quote extensively from the work, permission must be obtained from the copyright holder/s.

**Neural immune cell responses to clinically relevant ligands of the  
niacin receptor (Gpr109a): niacin and monomethyl fumarate**

**Amy Louise Brown-Lyons**

**A thesis submitted for the degree of Master of Philosophy  
(Neuroscience)**

June 2023

Keele University





# Abstract:

**Background:** Inflammation is a major driver, and perhaps cause, of neurodegeneration, suggesting neuroimmunomodulation as a therapeutic strategy. Microglia, the primary mediators of neuroinflammation, switch between three activation states [surveillant/unactivated (M0), proinflammatory (M1), anti-inflammatory/pro-repair (M2)], with M1 being associated with worsening pathology, while M2 is associated with reduced severity. Microglia reportedly express Gpr109a, a receptor predicted, but not demonstrated, to reduce M1 and induce M2 phenotype switching. If Gpr109a ligands do reduce M1 and promote M2 microglial activation, this may be therapeutically beneficial. Astrocytes are secondary immunocompetent glial cells, which can express Gpr109a, although most astrocytes are reportedly Gpr109a<sup>-</sup>. It remains unclear whether Gpr109a ligands induce responses in Gpr109a<sup>+</sup> astrocytes.

**Methods:** Primary rat cortical microglia and astrocyte cultures were assessed for Gpr109a expression, and treated with Gpr109a ligands (niacin, monomethyl fumarate). Controls included nicotinamide (similar metabolic effects to niacin, but without Gpr109a activation) and lipopolysaccharide (LPS, positive inflammatory control). Microglial and astrocyte responses were assessed by marker expression (immunostaining: Arg1, Gpr109a, Iba1, Nox2) and morphometric analyses.

**Results:** Expression of Gpr109a was demonstrated for rat microglia and astrocytes, with the majority of cells being Gpr109a<sup>+</sup>. Clear glial responses to Gpr109a ligands were not reproducibly demonstrated for either microglia or astrocytes. For Gpr109a ligands and for LPS, no consistent dose-response effects were seen in expression of Gpr109a, Nox2, Iba1

or Arg1. Morphological measurements showed no consistent responses to Gpr109a ligands or LPS treatment (Cell area, perimeter, Feret's max/min diameter, aspect ratio, circularity index).

**Conclusion:** Gpr109a represents a promising target for neuroimmunomodulatory therapies, as clinically approved ligands have good safety profiles, and neural immune cells express Gpr109a. Future studies should employ more sophisticated CNS models, including injury/disease to determine whether Gpr109a ligands may generate beneficial responses in neuroimmune cells already undergoing inflammatory/pathological activation.

# Acknowledgements

I would like to thank Dr Stuart Iain Jenkins for accepting me as an MPhil student. It takes so much time and effort to train us and that has not gone unnoticed. Thank you for your support, guidance, and patience throughout this experience. You have been such a supportive supervisor going above and beyond for not just me but all your students. Thank you for sharing your time and providing a wonderful environment for me to develop the knowledge and skills I shall hopefully take with me in my continuing career. You've allowed me to enjoy my time here and completing the MPhil possible!

I would like to extend my gratitude to other members of the Harvey laboratory, especially Dr Sama al Shaheeb and Dr Emma Green. I would like to thank them for their guidance and help within the laboratory. I hope you all the best in your future career paths!

Some of the raw microglia data (cell counts, morphological measurements) were generated by undergraduate students, and my thanks are extended to: Luke Marney, Isabella Hibell, Binh Dang and Aiden O'Grady.

I would like to thank my Mum for her emotional support. You are a strong independent woman and without you this wouldn't be possible. You saw potential in me that I couldn't see. You've encouraged me from primary school to university to pursue my dreams.

I would like to thank my Grandad Trevor throughout my educational career I never thought I would be here where I am today. By sharing your experience at school through to your own time at university you have helped me to push through my self-doubt and overcome difficulties. Thank you and to my Nanny Pat and uncle Paul for always being there. Coming

to visit after long days at uni to say hello would always brighten the day. Those cups of tea and treats didn't go unappreciated.

I would like to say thank you to Matt who has supported me emotionally throughout both my undergraduate and postgraduate degree. Providing hot chocolate, treats, and company during the tough study sessions. The little comic strips you drew of us kept me smiling. It didn't go unnoticed.

Dad, stepmum Gemma, little brother Olly, and Nana Linda. Thank you for asking how life and university is going over Sunday lunches. Encouraging me to take time out and focus on life outside of education, learning skills like learning to drive, at last!

Last but by most certainly not least Grandad David. It's been over a year since you passed. You came to my undergraduate graduation and you were so proud. You pointed out the sacrifices I had made to pursue a career in medicine and research even when they were not obvious to myself. You might not be there in body at my next graduation but certainly in memory.

# Contents

Abstract: .....	i
Acknowledgements .....	iii
Contents .....	v
List of tables and figures .....	ix
Abbreviations .....	xii
Chapter 1: General introduction .....	1
1.1. Neurodegenerative diseases lack effective therapies.....	1
1.2. Neuroinflammation is common to many neurological disorders .....	1
1.3. Microglia are major regulators of neuroinflammation: Physiological roles .....	4
1.4. Microglial activation involves switching between phenotypes .....	7
1.4.1. M0: Surveillance microglial phenotype .....	9
1.4.2. M1: Pro-inflammatory microglial phenotype.....	10
1.4.3. M2: Anti-inflammatory / pro-repair microglial phenotype .....	11
1.4.3.1 M2a .....	11
1.4.3.2 M2b .....	14
1.4.3.3 M2c .....	14
1.5. Microglial morphology is suggested to be related to activation status.....	16
1.6. Microglial activation and its role in neurodegenerative disease.....	31
1.7. Microglial activation in models of neurodegenerative disease.....	34
1.8. Immunomodulatory targets for therapy .....	36
1.9. Evidence for microglial expression of GPR109a.....	37
1.10. How do microglia respond to GPR109a ligands? .....	40
1.10.1. Microglial response to BHBA .....	40



1.10.2.	Microglial response to Niacin .....	43
1.10.3.	Dimethyl fumarate (DMF) and its metabolites: Dimethyl Fumarate-glutathione conjugate (DMF-GSH) and Monomethyl fumarate (MMF).....	44
1.10.4.	How do DMF and MMF affect gene expression and inflammatory response in primary microglia? .	47
1.10.5.	Evidence for astrocyte expression of GPR109a .....	48
1.11.	Neuroimmunomodulatory agents in clinical trials .....	53
1.12.	Ligands of the Gpr109a receptor may have therapeutic potential.....	56
1.13.	Aims and Objectives .....	63
Chapter 2:	Materials and Methods.....	64
2.1.	Rationale for experimental design .....	64
2.2.	Antibodies, equipment, and reagents used .....	68
2.3.	Preparation of cell adhesion surfaces.....	69
2.4.	Dissection, establishing, and maintenance of primary mixed glial, microglial, and astrocyte cultures .....	69
2.4.1.	Dissection .....	69
2.4.2.	Establishing mixed glial culture protocol .....	70
2.4.3.	Enriched microglia culture protocol .....	70
2.4.4.	Enriched astrocyte culture protocol.....	71
2.4.5.	Cell counting .....	71
2.5.	Experimental procedures .....	72
2.6.	Fixation and Immunocytochemistry .....	72
2.6.1.	Fixation .....	72
2.6.2.	Staining .....	72
2.7.	Image acquisition for cellular analysis .....	73
2.7.1.	Fluorescence microscopy .....	73
2.7.2.	Justification of markers .....	73

2.8.	Analyses .....	76
2.8.1.	Cell counts .....	76
2.8.2.	Morphometric analysis and antibody analysis .....	76
2.8.3.	Statistical analyses and data presentation .....	78
Chapter 3:	Do neural immune cells express Gpr109a, and respond to Gpr109a ligands? ....	80
3.1.	Introduction .....	80
3.2.	Objectives .....	81
3.3.	Results .....	82
3.3.1.	Primary rat microglia and astrocyte cultures successfully established .....	82
3.3.2.	Primary rat microglia expressed Gpr109a .....	82
3.3.3.	Impact of LPS, NA, Nm, and MMF treatment on microglial cell count .....	84
3.3.4.	Microglial response to LPS: Iba1 and Nox2 fluorescence .....	86
3.3.5.	Microglial response to LPS: Arg1 and Gpr109a fluorescence .....	89
3.3.6.	Microglia responses to niacin (NA): Iba1 and Nox2 expression .....	92
3.3.7.	Primary rat microglia responses to niacin (NA): Arg1 and Gpr109a .....	93
3.3.8.	Microglia responses to nicotinamide (Nm): Iba1 and Nox2 .....	94
3.3.9.	Microglia responses to nicotinamide (Nm): Arg1 and Gpr109a .....	95
3.3.10.	Microglia responses to monomethyl fumarate (MMF): Iba1 and Nox-2 .....	96
3.3.11.	Microglia responses to monomethyl fumarate (MMF): Arg1 and Gpr109a .....	97
3.3.12.	Microglial morphological responses to LPS, Nm and Gpr109a ligands .....	98
3.3.13.	Primary rat astrocytes expressed Gpr109a .....	104
3.4.	Discussion .....	105
3.4.1.	Efficacy of the anti-GPR109a antibody was confirmed .....	105
3.4.2.	Microglia express Gpr109a .....	105
3.4.3.	Astrocytes express Gpr109a .....	106

3.4.4.	Gpr109a expression was nuclear localised in both microglia and astrocytes .....	108
3.4.5.	Primary rat microglia response to LPS, nicotinamide, and Gpr109a ligands .....	109
3.4.6.	Morphometry .....	113
3.5.	Summary / conclusions .....	120
Chapter 4:	General Discussion and Conclusions .....	122
4.1.	Neural immune cells express Gpr109a, but did not show detectable responses to Gpr109a ligands .....	122
4.2.	Limitations of experimental design used here and ideas for future experimental work	123
4.2.1.	Microglial responses to Gpr109a ligands were only assessed in the absence of pro-inflammatory stimuli	123
4.2.2.	3D cultures may better replicate <i>in vivo</i> cellular functions .....	124
4.2.3.	The process of establishing cultures may alter inflammatory profiles, at least initially .....	125
4.2.4.	Do other cell types need to be included during testing? .....	125
4.2.5.	More complex models: 3D co-cultures, organotypic slice cultures, <i>in vivo</i> .....	127
4.2.6.	Disease modelling .....	131
4.2.7.	Assays and analyses .....	132
4.3.	Phenotypic markers and terminology .....	134
4.4.	Prophylaxis as a clinical consideration .....	136
4.5.	Conclusion .....	137
Appendix	.....	138
References	.....	150

# List of tables and figures

Figure 1.1: The four phases of neuroinflammation along with key events.....	3
Figure 1.2: Microglial activation statuses cover a range of behaviours. ....	8
Table 1.1: Descriptors of microglial morphologies and/or functions, as reported in the literature .....	17
Table 1.3: Definitions for morphological descriptors and how they pertain to cell shape .....	22
Table 1.4: Summary of length and perimeter morphometrics applied to microglia.....	23
Table 1.5: Summary of area and volume morphometrics applied to microglia.....	25
Table 1.6: Summary of cell circularity measurements applied to microglia .....	26
Table 1.7: Summary of cell process complexity measurements applied to microglia .....	29
Table 1.10: Evidence for microglial expression of Gpr109a .....	38
Table 1.11: Effects of Gpr109a ligands on primary microglia.....	46
Table 1.12. Microglial gene expression is substantially altered by the fumarate drugs, DMF and MMF.....	47
Table 1.13: Evidence for astrocyte expression of Gpr109a .....	49
Table 1.14: Summary of experimental data for potential therapeutic targets NF- $\kappa$ B, Nrf2, and the JAK-STAT3 pathway .....	50
Table 1.15: Potentially neurotherapeutic agents in clinical trials, with suspected neuroimmunomodulatory action .....	55
Table 1.16: Clinical use of Gpr109a ligands .....	58
Table 1.17 Experimental evidence for Gpr109a ligands directly affecting microglia.....	59
Figure 1.3: Schematic showing Gpr109a and Nrf2 mediated effects. ....	61
Table 2.1: Gpr09a ligand options, with expectation of Gpr109a and Nrf2 activation .....	65
Table 2.2: Primary antibodies and dilutions .....	68

Table 2.3: Secondary antibodies and dilutions .....	68
Table 2.4: Primary and secondary antibody pairings .....	68
Table 2.5: Reagents .....	69
Figure 2.1: Examples of cell morphometrics using fluorescence micrographs. ....	77
Table 2.6: Morphological measurements used in this study. ....	78
Figure 3.1. Gpr109a immunostaining of primary microglia was dose-dependent. ....	82
Figure 3.2. Intensity of Gpr109a immunostaining in primary microglial cultures was antibody-dose-dependent. ....	83
Figure 3.3. Microglial cell counts were reduced at high LPS concentration, but unaltered by Gpr109a ligands.....	85
Figure 3.4. LPS increased microglial staining intensity for Iba1 and Nox2, except at the greatest concentration, which reduced both. ....	87
Figure 3.5. Microglia were Iba1 <sup>+</sup> and Nox2 <sup>+</sup> , with and without LPS treatment. ....	88
Figure 3.6. LPS decreased microglial staining intensity for Gpr109a and Arg1.....	90
Figure 3.7 LPS treatment of microglial cultures diminished Gpr109a and Arg1 expression.....	91
Figure 3.8 Niacin-treated microglial cultures, staining intensity for Iba1 and Nox2.....	92
Figure 3.9. Niacin-treated microglial cultures, microglial staining intensity for Arg1 and Gpr109a, in niacin-treated cultures. ....	93
Figure 3.10. Nicotinamide-treated microglial cultures, microglial staining intensity for Iba1 and Nox2.....	94
Figure 3.11. Nicotinamide treated microglial cultures, microglial staining intensity for Arg1 and Grp109a individual cells.....	95
Figure 3.12 MMF-treated microglial cultures, microglial staining intensity for Iba1 and Nox2 expression.....	96
Figure 3.13 MMF-treated microglial cultures, staining intensity for Arg1 and Gpr109a.....	97
Figure 3.14. Microglial cell area was unaffected by LPS, Nm or Gpr109a ligands. ....	98

Figure 3.15. Microglial cell perimeter was unaffected by LPS, Nm or Gpr109a ligands.....	99
Figure 3.16. Microglial cell Feret’s maximum diameter was unaffected by LPS, Nm or Gpr109a ligands.....	100
Figure 3.17. Microglial cell Feret’s minimum diameter was unaffected by LPS, Nm or Gpr109a ligands.....	101
Figure 3.18. Microglial cell aspect ratio was unaffected by LPS, Nm or Gpr109a ligands.....	102
Figure 3.19. Microglial cell circularity index was unaffected by Gpr109a ligands, or Nm, but increased at high LPS concentration.....	103
Figure 3.20. Primary rat astrocytes expressed Gpr109a with nuclear localisation. ....	104
Table 3.1 comparing thesis data vs literature for inflammatory stimuli impact on area and volume morphometric for microglia.....	115
Table 3.2 comparing thesis data vs literature for inflammatory stimuli impact on Feret’s Max and Circularity.....	117
Figure 4.1: Experimental conditions typically involve a trade-off, with increasing complexity being associated with a loss of experimental control .....	129
Table 1.2: Studies reporting objective morphometric values for microglia .....	139
Table 1.8: Evidence for microglial involvement in neurological conditions, from human patients .....	145
Table 1.9: Microglial involvement in neuroinflammation in animal models.....	148

# Abbreviations

A $\beta$	Amyloid Beta
ACC	Anterior cingulate cortex
AD	Alzheimer's Disease
AIDS	Acquired immune deficiency syndrome
ALGERNON2	Altered generation of neurons 2
ALS	Amyotrophic Lateral Sclerosis
Arg1	Arginase-1
BA	Basilar artery
BBB	Blood Brain Barrier
BHBA	Beta Hydroxybutyric acid
CHA	Convex Hull Analysis
CHC	Convex Hull Circularity
CHSR	Convex Hull Span Ratio
CIE	Chronic intermittent ethanol
C1q	Complement component 1q
CNS	Central nervous system
CSF	Cerebral spinal fluid
CTCF	Corrected total cell fluorescence
CytoTOF	Cytometry time-of-flight
C3	Complement protein 3
DA	Dopamine
DAPI	4',6-diamidino-2-phenylindole
DAM	Disease Associated Microglial
DAMP	Damage Associated Molecular Pattern
ddH <sub>2</sub> O	Double distilled water
DIO	Diet-induced obesity
DIV	Days <i>in vitro</i>
DLPFC	Dorsolateral prefrontal cortex
DMEM	Dulbecco's modified Eagle's medium
DMF	Dimethyl Fumarate
DMF-GSH	Dimethyl Fumarate–glutathione conjugate
D10	Supplemented Dulbecco's modified Eagle's medium
EC <sub>50</sub>	Half maximal effective concentration
ECM	Extracellular Matrix
ELISA	Enzyme-linked immunosorbent assay
ERG	Electroretinography
FACS	Fluorescence-Activated Cell Sorting
FBS	Fetal Bovine Serum
FDA	Food and Drug Administration
FJB	Fluoro-Jase B
FIZZ1	Found in Inflammatory Zone 1
GFAP	Glial fibrillary acidic protein
Gpr109a	G-protein coupled receptor 109a
HCA2	Hydroxycarboxylic acid receptor 2
HIV	Human immunodeficiency virus

HLA-DR	Human Leukocyte Antigens
HMC3	Human Microglial Cell line 3
IC <sub>50</sub>	Half maximal inhibitory concentration
IFN $\gamma$	Interferon Gamma
IGF-1	Insulin-like growth factor 1
IL-1 $\beta$	Interleukin 1 beta
IL-3	Interleukin 3
IL-10	Interleukin 10
IgG	Immunoglobulin G
iNOS	Inducible nitric oxide synthase
JAK2-STAT3	Janus Kinase signal transducer and activator of transcription pathway
Keap1	Kelch-like ECH-associated protein 1
LIR	Light induced retinopathy
LPS	Lipopolysaccharide
M0	Surveillant / unactivated microglial phenotype (default)
M1	Pro-inflammatory microglial phenotype (classically activated)
M2	Alternatively activated microglial phenotype (anti-inflammatory)
MACO	Middle cerebral artery occlusion
MAG1	Matrix antigen 1
MCI	Mild cognitive impairment
MDMi	Monocyte-derived microglia-like cells
MHC1	Major Histocompatibility Complex 1
MHC2	Major Histocompatibility Complex 2
miR-155	MicroRNA-155
MMF	Monomethyl Fumarate
MPTP	1-methyl-4-phenyl-1,2,3,6-tetrahydropyridine
MPP <sup>+</sup>	1-methyl-4-phenylpyridinium
MS	Multiple Sclerosis
MSACH	Maximum span across the convex hull
NICE	The National Institute for Health and Care Excellence
NF- $\kappa\beta$	Nuclear Factor Kappa Beta
NLRP3	Nucleotide-binding domain and leucine-rich repeat family pyrin domain containing 3
NMDA	N-Methyl-D-aspartic acid
NO	Nitric Oxide
NPC1	Niemann-Pick disease type, C1
Nrf2	Nuclear factor erythroid-2 related factor 2
NSC	Neural Stem Cell
OGD/R	Oxygen and glucose deprivation
OPC	Oligodendrocyte precursor cells
PBS	Phosphate-buffered saline
PCR	Polymerase Chain Reaction
PET	Positron emission tomography
PD	Parkinson's Disease
PDD	Parkinson's Disease Dementia
PDL	Poly-D-lysine
PFA	Paraformaldehyde
pMCAO	Permanent medial cerebral artery occlusion
PUMA-G	a.k.a. Gpr109a
qRT-PCR	Real-Time Quantitative Reverse Transcription Polymerase Chain Reaction
RNS	Reactive Nitrogen Species



ROS	Reactive Oxygen Species
SN	Substantia nigra
SNpc	Substantia nigra pars compacta
STAT1	Signal Transducer And Activator of Transcription
Tak1	Transforming growth factor $\beta$ -activated kinase
TBI	Traumatic brain injury
TIF	Tag Image File Format
Tgf- $\beta$	Transforming Growth Factor Beta
TLR4	Toll Like Receptor 4
tMCAO	Transient middle cerebral artery occlusion
TNF $\alpha$	Tumour necrosis factor alpha
UPDRS	Unified Parkinson's Disease Rating Scale
VTA	Ventral tegmental area
WBC	White blood cells
WT	Wild type
7-OZ	5Z-7-oxozeanol

# Chapter 1: General introduction

## **1.1. Neurodegenerative diseases lack effective therapies**

Neurodegenerative disease is characterised by the progressive impairment and/or destruction of cells in the central nervous system (CNS). Neurological disease or injury can be particularly debilitating and place a lot of emotional and physical stress on the patient, family and wider carers. Prominent neurological disorders include Alzheimer's disease (AD), dementia, stroke, and Parkinson's disease (PD)<sup>1,2</sup>. Neurological disorders frequently lead to disability and premature death, and represent a major cause of disability globally, with substantial financial burden on a state's economy<sup>1</sup>.

There are very few treatments for neurological disorders which can halt or reverse tissue damage, with most therapeutics merely limiting symptoms, and being part of palliative care. There is a great need to focus on understanding the pathology of individual conditions in greater detail to develop effective therapies, and hopefully cures.

The immune system is increasingly recognised as having a role in neurodegenerative diseases, with a focus on the potential for modulation of neuroinflammatory processes to produce beneficial effects, a strategy referred to as immunomodulation.

## **1.2. Neuroinflammation is common to many neurological disorders**

Aetiologies of neurodegenerative diseases are commonly sporadic, however neuroinflammation is now considered a common denominator with chronic inflammation typically being detrimental to neurological function, and there is evidence that anti-inflammatory therapies may alleviate neurological deficits<sup>3</sup>. Whilst the causative mechanisms differ across conditions such as amyotrophic lateral sclerosis (ALS), PD, AD,

multiple sclerosis (MS), and stroke, they are all associated with chronic neuroinflammation, hence representing viable targets for developing immune-related therapies <sup>3</sup>.

Neuroinflammation can act in response to pathogens, trauma, toxic protein aggregates, toxic metabolites, apoptotic cell bodies, and dysfunctional cells. Mediators of neuroinflammation include resident glia (microglia, astrocytes) and infiltrating peripheral cells (macrophages, dendritic cells) <sup>3</sup>. Acute inflammation typically has protective properties, but chronic inflammation, often associated with AD and PD, is ultimately damaging to neuronal integrity <sup>3</sup>.

Neuroinflammation can be considered to exhibit four stages, beginning with the initiation phase, where surveillant microglia detect infection, tissue damage and/or cellular debris (**Fig 1.1**). A localised inflammatory response follows, with microgliosis and astrocytosis, along with secretion of inflammatory factors and chemoattractants. This leads to a blood-brain barrier (BBB) leakage where peripheral immune cells are recruited across the BBB. During the latest stages resolution of inflammation should occur where astrocytes and microglia secrete anti-inflammatory and neurotrophic factors to promote neurogenesis, remyelination, vascularisation, and build-up of the extracellular matrix. Microglia are thought to be the main mediators of the neuroinflammatory response acting as the macrophages of the CNS hence the main target for therapies <sup>4</sup>.

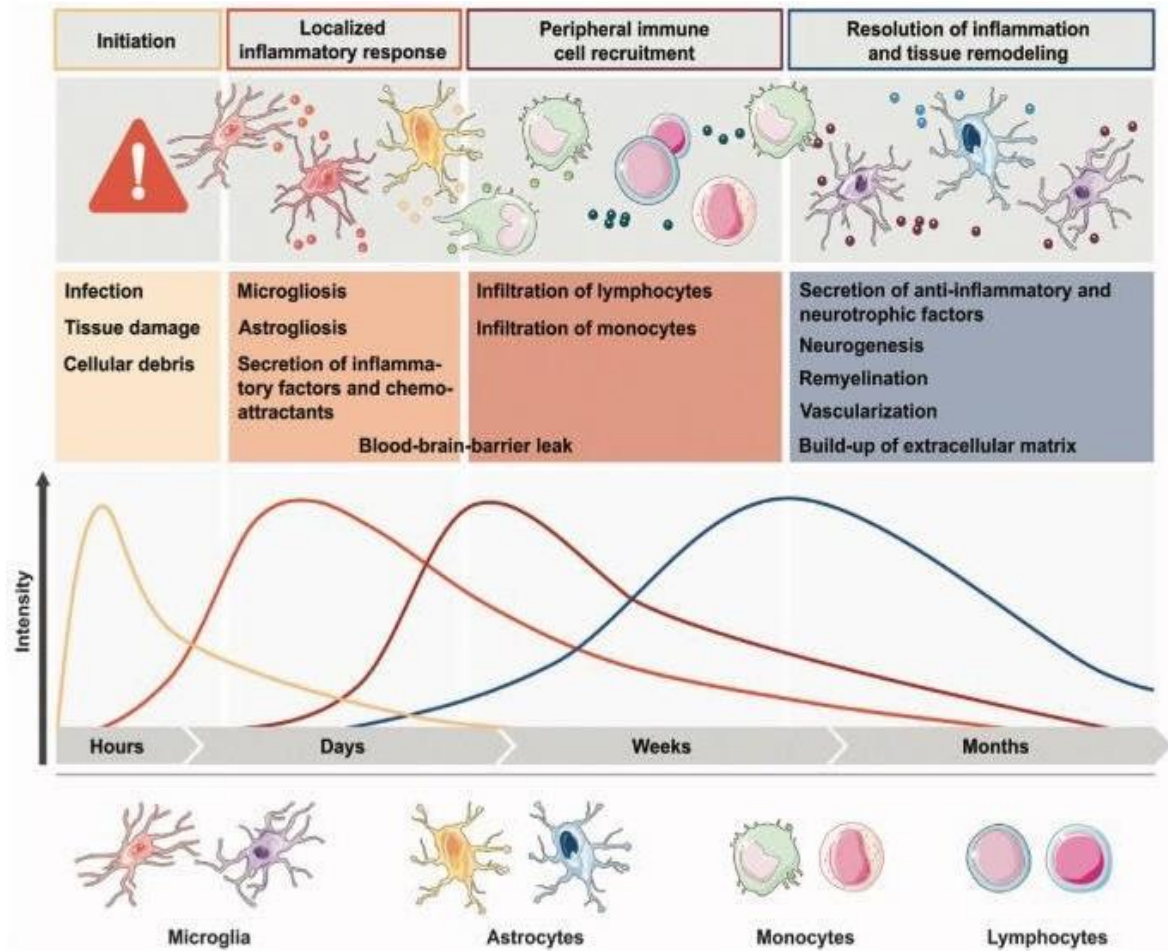


**Figure 1.1: The four phases of neuroinflammation along with key events.** The initiation phase. A localised inflammatory response phase characterised by microgliosis and astrocytosis, and secretion of other pro-inflammatory mediators. This leads to a blood-brain barrier (BBB) leakage where peripheral immune cells infiltrate. The latest stage is resolution of inflammation where astrocytes and microglia secrete anti-inflammatory and neurotrophic factors to promote growth and repair. Adapted from <sup>4</sup>.

### 1.3. Microglia are major regulators of neuroinflammation: Physiological roles

Microglia are the main mediators of neuroinflammation and are known as the macrophages of the CNS. Microglia typically react earliest to pathological stimuli, can induce microgliosis and astrogliosis, and can recruit peripheral immune cells <sup>5</sup>. Peripheral macrophage phenotypes (activation states) have been characterised as M0 (surveillant), M1 (pro-inflammatory), and M2 (anti-inflammatory, with subtypes M2a, M2b, and M2c). Due to their shared lineage and functions with macrophages, this naming convention is also frequently used with microglia <sup>6</sup>. Whether these labels accurately define different microglial phenotypes, microglial activation status has been shown to dramatically alter microglial functions.

Based on the emergence of single-cell RNA sequencing and cytometry time-of-flight (CyTOF) mass spectrometry, the M1/classical activation and M2/alternative activation phenotype classification has been called into question <sup>7</sup>. A comparison of M1 and M2 gene expression profiles (five public microarray datasets) show M1 and M2 sharing common signalling pathways, blurring the distinction between M1 and M2 <sup>8</sup>. Additionally microglia have been demonstrated, using single-cell analysis, to be capable of simultaneously expressing both M1 and M2 markers <sup>9,10</sup>.

M2 is associated with a wide variety of functions, pathways, and markers. As such, there have been attempts to define subcategories within M2 as M2a, M2b, and M2c <sup>11-13</sup>. All these subtypes are based on *in vitro* research and there is considerable controversy over whether they exist in these forms *in vivo*. There is a lack in consistency in which genes/proteins are described as being M2 markers. Individual M2 markers have been shown to lack correlation with other M2 markers. In order for any M2 marker to be

considered reliable, it will need to accurately and reliably predict the presence/absence (or expression levels) of other markers.

Current research understanding is based around categorising microglia based upon distinct phenotypes (M0, M1, and M2) which are primarily acquired in response to external cues in the microenvironment. However, microglial subtypes are reported to exist, with subtype being a separate concept from microglial reactive state (phenotype). Microglial subtypes have defining properties independent of phenotypic activation state. As the subtype-defining property could be morphological, genetic, protein expression, or behavioural, it would be of value to study all of these features <sup>14</sup>. Putative subtypes include satellite microglia, keratan sulphate proteoglycan (KSPG) microglial, and dark microglia <sup>14</sup>.

Satellite microglia interact with the “axonal initial segment” (axon hillock) of neurons within the healthy brain with a single overlapping segment. This subtype may be preferentially associated with excitatory neurons. Satellite microglia are IBA1<sup>+</sup>/CD11b<sup>+</sup>/CXCR1<sup>+</sup>, which is common for microglia, and no markers are known to be specific to satellite microglia. Therefore, they are defined as satellite microglia by the location of their physical interaction with neurons <sup>14</sup>.

KSPG microglia are defined by their expression of KSPG, which is found in the ECM and on the cell surface of KSPG microglia. KSPG microglia are thought to have a role in cellular adhesion and growth of axons. Previous studies have found them to have ramified morphologies and express IBA1, CR3, and CD11b. KSPG microglia have been found in the olfactory bulb, hippocampus, brainstem, spinal cord, retina, cerebellum and cerebral cortex <sup>14</sup>.

High spatial resolution electron microscopy allowed for the identification of dark microglia, defined by their ultrastructural “dark” appearance, distinct from typical microglia. This dark

appearance may be due to oxidative stress, which is consistent with their condensed, electron dense cytoplasm and nucleoplasm. These microglia are IBA1<sup>low</sup>, CX3CR1<sup>low</sup>, CD11b<sup>+</sup>, TREM2<sup>+</sup>, 4d4<sup>+</sup>, and are found within the cortex, hippocampus, hypothalamus, and amygdala <sup>14</sup>. Dark microglia are thought to indicate pathology as they are rarely present under healthy conditions, but abundant during chronic stress, normal aging, and AD pathology. They are highly ramified with thin processes contacting synaptic clefts, encircling axon terminals and dendritic spines. They are highly phagocytic, engulfing synaptic elements suggesting a role in pathological remodelling of neuronal circuits. Microglial subtypes are not often referred to in the literature. Given the differences between sub-types it is important to consider both the sub-type and phenotype of microglia when reporting experimental data <sup>15</sup>.

Recent advances have highlighted heterogeneity within microglial populations, with researchers suggesting any population of microglia is likely to be a heterogeneous mixture of cell profiles: the presence of one or few markers does not account for the full transcriptomic profiles within a population <sup>10</sup>. When studying the activation status of microglia it is desirable to monitor multiple markers of both 'M1' and 'M2' in combination <sup>14,15</sup>. This is in order to accurately assess expression profiles, as it cannot be reliably inferred from the presence of an 'M2 marker', that there is an absence of 'M1 markers'.

Given the complications surrounding M1/M2 nomenclature, it is likely to be replaced in the future. This is largely because describing a microglial cell/population as 'M2' does not reliably indicate the profiles of gene expression, protein expression, or cell behaviours of all cells in that population. The terms are, however, still in widespread use and no other standardised alternative exists. Therefore, M1/M2 terminology has been used here in the discussion of the literature, with specific reference to relevant stimuli/markers.

#### **1.4. Microglial activation involves switching between phenotypes**

Much of the literature refers to three broad states of microglial activation which will be discussed in this section. These activation states are M0, surveillance microglia, M1, classically activated inflammatory microglia, and M2, alternatively activated microglia. M2 microglia have been proposed to exist as at least three subtypes: M2a, M2b, and M2c (**Fig 1.2**). There has even been discussion of the potential for M3 and Disease Associated Microglial (DAM) phenotypes. Microglial activation has frequently been described as existing on a spectrum of activation, from M1 through M0 to M2. However, some evidence suggest that no individual microglial cell belongs exclusively to M1 or M2 as a discrete activation state, and the spectrum description is falling out of favour with some researchers<sup>14,15</sup>. Describing the states of microglial activation, much like macrophage activation, is still an area of contention.



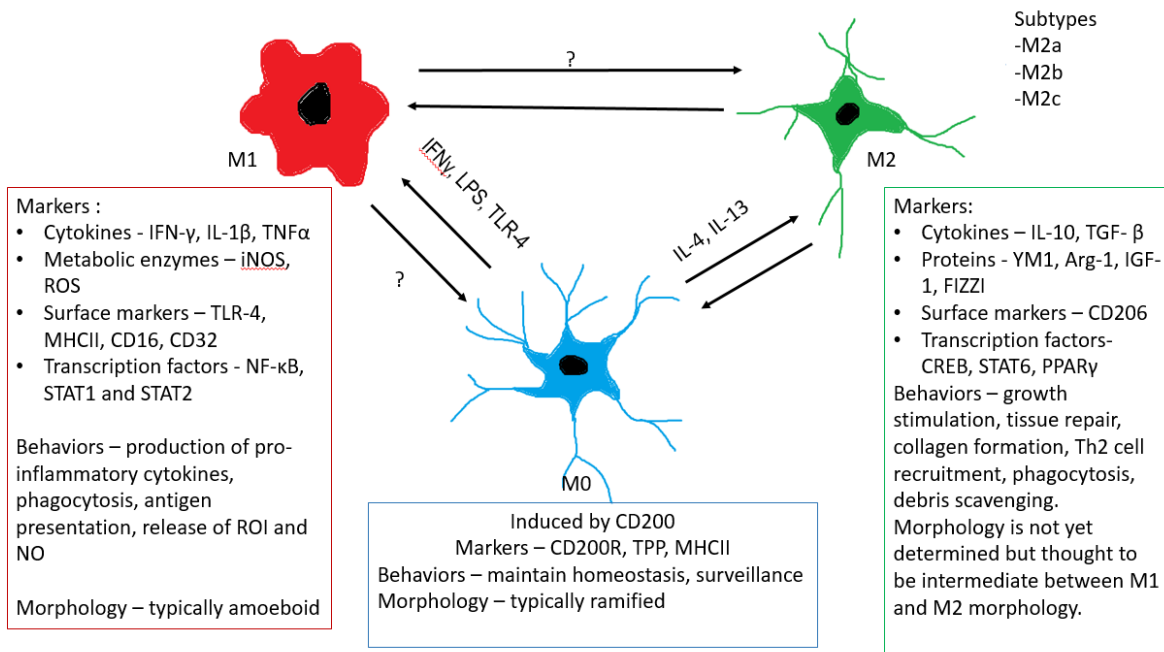


**Figure 1.2: Microglial activation statuses cover a range of behaviours.** M0 microglia predominate in healthy tissue, and are surveillant, maintaining homeostasis. Pro-inflammatory M1 microglia release reactive oxygen species (ROS) and reactive nitrogen species (NOS), actively phagocytose, and can present antigen. M2 microglia promote neuroprotection and tissue repair. Typically, these phenotypes are identified by behaviour, morphology, protein/transcriptomic profiles, and behaviours<sup>16–18</sup>. M1 microglia can be induced from M0 by exposure to IFN $\gamma$ , LPS, TLR4 or from M2 microglia exposed to chronic inflammatory conditions. Increased numbers of M2 microglia could be a result of M1 resolution to the M2 phenotype, or M1 apoptosis followed by new M2 cells generated from the M0 pool; a consensus has not yet been met, indicated by “?”. The ability of M2 microglia to change back to ramified forms has been demonstrated but the mechanism is not yet known<sup>19</sup>. Adapted from<sup>20</sup>.

#### 1.4.1. M0: Surveillance microglial phenotype

Under physiological conditions microglia exist in a surveillant form, exhibiting a ramified morphology with a small soma and tendril-like processes that constantly probe the microenvironment for stimuli. Hence M0 microglia can be thought of as a 'surveillance' phenotype. Original thought was that M0 microglia's main purpose was to survey the brain parenchyma for infection/trauma and mediate an appropriate response<sup>21-22</sup>.

Recent studies show that M0 microglia may have functions including roles in tissue development, homeostasis, and brain remodelling. They support neurogenesis by forming, and maintaining survival of, neural circuits by inducing programmed cell death of immature or defective neurons and phagocytosing the remaining debris. They continue to play significant roles in neuronal development and maintaining neuronal function into adulthood. This is achieved via the release of trophic factors examples include IGF-1, nerve growth factor, and BDNF<sup>23</sup>.

Microglia have roles in synaptic plasticity, by pruning redundant and excessive synaptic connections in order to promote mature and effective neuronal circuits, one of the mechanisms underpinning learning<sup>24</sup>.

It is difficult to identify the M0 phenotype of microglia, as their morphology tends to be fluid and plastic. Typically M0 tend to display a ramified morphology whereby the cell shows a small soma (cell body) with many fine cellular processes<sup>25-30</sup>. There are no well-validated markers available to identify M0 microglia. M0-inducing factors include CD200, which is expressed by all CNS neurons and acts on the microglial CD200 receptor (CD200R). CD200R is generally expressed to a lesser extent than its ligand and in the CNS is mainly expressed by microglia. Neurons are thought to express CD200 as a self-protective mechanism as it binds to CD200R on the surface of microglia preventing secondary

neuronal injury caused by microglia. This may play a key role in keeping the microglia in the resting state. Neuronal loss leads to reduction in CD200-CD200R signalling and potentially may lead to M1 microglial activation <sup>31-33</sup>

#### **1.4.2. M1: Pro-inflammatory microglial phenotype**

If the local microenvironment is disturbed by either exogenous factors, such as bacteria or viruses, or endogenous factors, such as dead, degenerating, or apoptotic cells, microglia become activated by detection of pathogen associated molecular patterns (PAMPs) and/or damage-associated molecular patterns (DAMPs). M1 (“classically activated”) microglia typically retract their processes, enlarge their soma and undergo proliferation at the site of injury or infection, these processes together being called microgliosis. Although these behaviours are usually beneficial and protective, M1 microglia have been implicated in exacerbating neurodegenerative diseases such as PD and AD where they are thought to damage and even kill otherwise viable glia and neurons <sup>34</sup>.

The M1 phenotype can be characterised by marker expression (e.g. upregulated TLR4, MHCII), secretion of pro-inflammatory cytokines (e.g. TNF- $\alpha$ , IL-1 $\beta$ , IL-6), morphological changes (e.g. becoming more amoeboid), and release of reactive oxygen species (ROS) and reactive nitrogen species (RNS; Figure 1.2). TLR4 recognises both damage-associated molecular patterns (DAMPs) and pathogen associated molecular patterns (PAMPs) modulating neuroinflammatory signalling via activation of the NF- $\kappa$ B signaling pathway. Upregulation of the NF- $\kappa$ B signaling pathway results in microglial secretion of pro-inflammatory cytokines including TNF- $\alpha$ , IL-1 $\beta$ , IL-6<sup>35</sup>.

Major histocompatibility complex II (MHCII) is a transmembrane receptor expressed on the surface of the M1 phenotype. MHCII is responsible for antigen recognition and activation

of the peripheral immune system by activating T-cells of the peripheral immune system recruiting them for defence against pathogenic insult <sup>36</sup>.

Identifying microglial activation states via morphological analysis can be a difficult task. Phagocytic behaviours are often associated with amoeboid morphology, but ramified microglia have also been shown to be phagocytic, including phagocytosis of amyloid beta plaques <sup>37</sup>. Microglia have highly active membranes and cytoskeletons and, under time-lapse (dynamic/video) microscopy, show constant remodelling with rapid changes between amoeboid and ramified forms, with such changes being observed in micrograph frames less than a minute apart <sup>38</sup>. Therefore, microglial morphology at any specific moment in time may not be reliably indicative of activation status. There are several commonly used phenotypic markers for M1 microglia (Figure 1.2), although as they are not exclusively expressed by the M1 phenotype, therefore they may be unreliable markers.

#### **1.4.3. M2: Anti-inflammatory / pro-repair microglial phenotype**

Referred to as 'alternative' activation, and having multiple anti-inflammatory behaviours, the M2 phenotype is potentially neuroprotective and neurorestorative. The M2 phenotype has been proposed to include a subset of activation states: M2a, 2b, and 2c. The subsets are considered to be separate however there is considerable overlap in their activities and protein expression profiles. This overlap leads to the idea that the M2 phenotype may be more of a collection of activities rather than discrete subtypes.

##### **1.4.3.1 M2a**

M2a microglia carry out anti-inflammatory functions. The M2a phenotype is characterised by upregulation of tissue repair and remodelling, upregulation of scavenger receptors for phagocytosis of debris, and suppression of inflammation. Upregulation of tissue repair and remodelling had been induced *in vitro* by both microglia and macrophages via the

activation of IL-4R $\alpha$  with interleukins IL-4 and IL-13. M2a tissue repair has been associated with rescue of damaged and apoptotic neurons, and recruitment of stem/precursor cells. Molecules associated with, and therefore used as markers for, tissue repair and remodelling are Arg1, YM1, FIZZ1, and IGF-1<sup>39,40,41,42</sup>. Arg1 is an enzyme that catalyses the conversion of L-arginine to ornithine, which ultimately promotes cell proliferation, wound healing, ion channel function, and neuroprotection. Arg1 competes with inducible nitric oxide synthase (iNOS) for L-arginine, inhibiting the production of NO<sup>-</sup>, a molecule known to damage healthy tissue<sup>43</sup>.

YM1 chitinase-like protein-3 is a chitin-degrading enzyme protecting against chitin containing pathogens. Ym1 is secreted by M2 macrophages, neutrophils, and microglia. In the CNS its expression is upregulated in neurotrauma and neurodegeneration. Proposed functions are to facilitate ECM remodelling, and in demyelination events it may bind to epidermal growth factor receptor of neural stem cells and promote oligodendrogenesis.

Given the lack of consensus for M2 marker expression, there are suggestions that (putative) phenotypes may be best indicated by stating the stimulus used for induction. E.g. 'Il-4-induced activation of microglia', rather than 'M2a'. This may then be more clearly associated with events downstream of Il-4R activation, for example<sup>44,45</sup>. *In vitro* treatment of the BV2 microglial cell line with Il-4 reduced the expression of inflammatory markers (CD16/32) and cytokines; whilst increasing the expression of CD206 (a proposed 'M2' marker) and anti-inflammatory cytokines<sup>45</sup>. Additionally, Il-4 administration *in vivo* (mouse model of intracerebral haemorrhage) lowered levels of pro-inflammatory cytokines (Il-6, TNF- $\alpha$ ), and increased levels of anti-inflammatory cytokines (Il-10, Tgf- $\beta$ ), with this being associated with decreased neurological deficits, brain oedema, and infarct lesion.

Tingting Yu (2019) <sup>46</sup> showed that M2a microglia have a neuroprotective role in kainic acid induced neurotoxicity. In an *in vitro* model, neurons were cultured with kainic acid, an analogue of glutamate. Glutamate is an excitotoxic neurotransmitter involved in the pathogenesis of numerous neurodegenerative conditions and is proven to cause pathological changes in rodent brains. M2a microglia were characterised by stimulation with Il-4, Il-10, and Tgf- $\beta$ , and by expression of Arg1 and CD206. M2a microglia promoted neuronal survival, decreased production of pro-inflammatory cytokines (TNF- $\alpha$ , IFN- $\gamma$ , and IL-6), NO, NF- $\kappa\beta$  and caspase 3 signalling pathways whilst promoting neuronal survival and release of anti-inflammatory cytokines (Il-4 and Il-10).

M2a microglia function may be impaired with age and this could be a causative factor in neurodegenerative disease. After disease/injury is resolved it has been postulated that the M2 phenotype returns to the ramified M0, of which the mechanisms of action are not yet known. **Fig 1.2** shows markers commonly used for identifying M2a microglia. Arg1 has the most evidence to support its claim for identifying M2a <sup>41</sup>.

#### 1.4.3.2 M2b

M2b is proposed to mediate cell maturation, tissue stabilisation, angiogenesis, extracellular matrix (ECM) synthesis and immunoregulation, all of which could be beneficial therapeutically<sup>47</sup>. Stimuli such as IgG, TLR agonists, IL-1R, and immunoglobulin Fc gamma receptor ligands are reported to generate the M2b microglial response<sup>20</sup>. This results in a decrease in IL-12 alongside increases in IL-10 and HLA-DR expression, which may be the most reliable marker profile of M2b<sup>40</sup>.

They can produce high levels of both anti-inflammatory cytokines (e.g. IL-10, although this is also M2c-associated) and pro-inflammatory cytokines (which are M1-associated). This suggests both pro-inflammatory and anti-inflammatory behaviours, and complicates phenotype identification. In addition, gene expression studies show that some of the same genes expressed by M1 and M2c may be seen in M2b, showing the difficulties in reliably distinguishing between microglial phenotypes<sup>48</sup>.

Glioma-conditioned media and LPS-IFN $\gamma$  conditioned media induced the M2b activation phenotype. M2b microglia upregulate the gene expression of IL-10 and Tgf- $\beta$ <sup>40</sup>. Acting as a negative feedback loop, M2b secretion of IL-10 can cause an increase in the levels of microglial- and astrocyte-produced Tgf- $\beta$ <sup>49</sup>. Tgf- $\beta$  reportedly induces the macrophage M2c phenotype and due to their shared lineage with microglia this is thought to also occur in microglia<sup>50</sup>. In the BV2 mouse microglial cell line, IL-10 induces M2c activation<sup>51</sup>. It could be postulated that the M2b phenotypic production of IL-10 and TGF- $\beta$  facilitates the phenotypic conversion from M2b to M2c.

#### 1.4.3.3 M2c

M2c microglia reportedly exhibit rounded morphologies with multiple processes, difficult to distinguish from M0. M2c has been associated with tissue remodelling and matrix deposition in response to inflammation<sup>41</sup>, anti-inflammatory effects on the innate immune system<sup>52</sup>, scavenging of debris<sup>20,41,50</sup>, and increasing NSC proliferation<sup>53</sup>. In an *in vivo* rat spinal cord compression injury model, a positive correlation was found between the increased expression of Tgf- $\beta$ , SOCS3, and ILR4 $\alpha$  (M2c markers) and CD206 (M2a) with improved functional recovery (walking test)<sup>54</sup>.

There are several proposed M2c markers (**Fig 1.2**), but the most reliable seems to be Tgf- $\beta$ . The BV2 microglial cell line, treated with 10 ng/mL of IL-10, showed increased M2c activation<sup>51</sup>. The mechanisms of this process in microglia are unknown but its anti-inflammatory action is thought to centre around the down-regulation of SLP-76 an actin-rich phagosome. An *in vitro* macrophage model, treated with IL-10, Tgf- $\beta$  or glucocorticoids, reportedly switched to an M2c phenotype, and this is thought to be mediated by downregulating STAT1 and NF- $\kappa\beta$ <sup>20,50,55</sup>.

These M0, M1 and M2 activation states all have roles in normal tissue homeostasis, and in resolution of damage/infection. However, evidence suggests that microglia can become inappropriately activated under some circumstances, adopting ineffective, or even harmful, phenotypes. For example, failure to resolve M1 activation, leading to increased oxidative stress and damage to otherwise healthy neural tissue. Understanding how to identify different activation states, and what stimuli cause transition between them, will be of great advantage in understanding and treating neurological disorders. Identifying changes in marker expression is the routine technique applied, but there is emerging considerable evidence to suggest morphological features may be characteristic of activation status.



### 1.5. Microglial morphology is suggested to be related to activation status

Microglia are highly plastic cells, with a wide range of morphologies. Different morphologies have been described as indicating activation status, especially the transition between M0 (ramified) and M1 (amoeboid). **Table 1.1** summarises morphological descriptors used for microglia, and illustrates that the high degree of variability in microglial morphology is attracting research attention. Some of these terms are widely used and understood, while others exist in only a single published article. Further, these descriptive terms are highly subjective, and not yet clearly associated with function/behaviour. It is difficult to reconcile across studies, and be confident that the same microglial phenotype/morphology is being discussed in different reports.

Table 1.1: Descriptors of microglial morphologies and/or functions, as reported in the literature					
Descriptor: morphology	Functional description	Source of microglia	Culture details (ref)	Treatment	Morphological/functional response to treatment
<b>Amoeboid:</b> Enlarged cell body with few (thick) primary processes (lacking secondary branches), or no identifiable processes at all	M1 inflammatory	Primary human resected tissue (intractable epilepsy)	<i>In vitro</i> cell culture (>90% microglia) <sup>56</sup>	E.coli bio-particle exposure (1 h; no controls)	<ul style="list-style-type: none"> <li>• 16.9% amoeboid</li> <li>• Increase in phagocytic activity, similar to pseudopodic</li> </ul>
		Mouse	Coronal sections <sup>57</sup>	TBI, tMCAO, and pMCAO	
		Male rat	Coronal sections of the hippocampus <sup>58</sup>	Pilocarpine-induced SE	<ul style="list-style-type: none"> <li>• Control: 0-64% amoeboid</li> <li>• SE: 38-64% amoeboid</li> <li>• Increase in amoeboid at 3 and 14 d post-SE</li> </ul>
<b>Bushy</b>		Male rat	Coronal sections of the hippocampus <sup>58</sup>	Pilocarpine-induced SE	<ul style="list-style-type: none"> <li>• Control: 0-19%</li> <li>• SE: 19-64%</li> </ul>
<b>Dark</b>	Phagocytic and oxidative	APP-PS1 mice 6-, 14-, and 21-months old; wild type littermates	<i>In vivo</i> rat microglia. Transverse sections of CA1, prefrontal cortex, amygdala, or hypothalamus <sup>59</sup>	Chronic unpredictable stress experiments	<ul style="list-style-type: none"> <li>• Microglia near A<math>\beta</math> plaques show signs of oxidative stress; condensation, darkening of cytoplasm/nucleoplasm, autophagic vacuoles.</li> <li>• In CA1 of stressed CX3CR1 knockout mice, microglia were 'highly ramified with thin processes'.</li> <li>• Microglia form 'acute angles' interacting with neuropil</li> </ul>
	Active -"Engulfing"	NPC1 mouse model. Age related illness.	<i>In vivo</i> . Sagittal cerebellar slice of mouse brain <sup>60</sup>	Age related illness.	<ul style="list-style-type: none"> <li>• No morphological analysis of microglia termed dark.</li> <li>• Dark microglia were found wrapped around the synaptic terminals, synaptic terminals were engulfed by microglia.</li> </ul>
<b>Dystrophic</b> Spheroidal, beaded, de-ramified, or fragmented.	Degenerating/senescent associated with production of chronic inflammatory mediators. Iron accumulating	Human ages 10-99 years.	Human tissue sections of hippocampal area CA1 and frontal cortex <sup>56</sup>	Age and neuropathology	<ul style="list-style-type: none"> <li>• Age related increase in microglia in areas CA1 and frontal cortex. Proportion of dystrophic microglia remains the same.</li> <li>• The number of dystrophic microglia was significantly greater in age-matched cases with either AD, Lewy body dementia or LATE neuropathological change</li> <li>• Iron accumulating. Increased expression of Ferritin light chain (FLC)</li> </ul>

<p><b>Honeycomb</b> “retract their ramified processes and form a highly connected honeycomb network” visually similar to hypertrophic</p>	<ul style="list-style-type: none"> <li>Form network around surviving astrocytes</li> <li>Transform into jellyfish microglia</li> </ul>	Mouse	Meningeal compression, mouse <sup>61</sup>	TBI	<ul style="list-style-type: none"> <li>No morphological measurements taken</li> <li>Honeycomb network formed 1 h post meningeal compression surrounding surviving astrocytes in the glial limitans.</li> <li>Honeycomb microglia could transform to jellyfish microglia within 5 mins, naïve require 30 mins.</li> <li>Fortify glial limitans with jellyfish microglia</li> </ul>
<p><b>Hypertrophy</b> Enlarged cells, hyper-ramified and thickened trunks and processes</p>	No activity investigated	Male rat	Coronal sections of the hippocampus <sup>58</sup>	Pilocarpine-induced SE	<ul style="list-style-type: none"> <li>Control: 19-30%</li> <li>4 h, 3 d post-SE: ‘very low %’</li> <li>2 weeks post-SE: 8-17%</li> </ul>
	Probably inflammatory	Mouse	Coronal section <sup>57</sup>	<ul style="list-style-type: none"> <li>TBI</li> <li>tMCAO</li> <li>pMCAO</li> </ul>	<ul style="list-style-type: none"> <li>Increased area, perimeter, Feret’s diameter, and number of grid crossings (tMCAO vs control) indicates increased presence of hyper-ramified microglia</li> <li>CD11b<sup>+</sup>, suggests inflammatory status</li> </ul>
<p><b>Jellyfish</b> “retract ramified processes and generate a single, flat, motile, phagocytotic process at the base of the glial limitans, resembling a jellyfish”</p>	Phagocytic	Mouse	Meningeal compression, mouse <sup>61</sup>	Traumatic brain injury	<ul style="list-style-type: none"> <li>No morphological measurements taken</li> <li>Formed a phagocytic layer with glial limitans via thin processes</li> <li>“fortify” the glial limitans with honeycomb microglia</li> </ul>
<p><b>Pseudopodic</b></p>	Phagocytic	Primary human resected tissue (intractable epilepsy)	<i>In vitro</i> cell culture (>90% microglia) <sup>62</sup>	E.coli bio-particle exposure (1 h; no controls)	<ul style="list-style-type: none"> <li>9% of microglia were pseudopodic</li> <li>Increased in phagocytic activity, similar to amoeboid.</li> </ul>
<p><b>Ramified</b> Small soma with many long reaching processes</p>	Surveillant unactivated microglia	Primary human resected tissue (intractable epilepsy)	<i>In vitro</i> cell culture (>90% microglia) <sup>62</sup>	E.coli bio-particle exposure (1 h; no controls)	<ul style="list-style-type: none"> <li>71% of microglia ramified</li> <li>Lowest phagocytic activity</li> </ul>
		Male rat	Coronal sections of the hippocampus <sup>58</sup>	Pilocarpine-induced SE	<ul style="list-style-type: none"> <li>Control: 50-74% ramified</li> <li>SE: Very low number at 4 h and 3 d</li> <li>2 weeks post-SE: 2-10%</li> </ul>

<b>Rod</b> Narrow body with few planar processes	Neuro-protective. Provide scaffolding for diseased neurons.	Rat diffuse brain injury model	Individual cryosections mounted on glass slides. Present in the cortex and thalamus <sup>63</sup>	Midline fluid percussion injury (mFPI), mice euthanized 1, 2, 7, 28 days post treatment.	<ul style="list-style-type: none"> <li>• Narrow post injury</li> <li>• No changes to soma length, soma width increased</li> <li>• Planar primary branches retracted post injury. Reduction in primary branch number and length</li> <li>• No changes in polar branches</li> <li>• Decrease in both planar and polar secondary branches post injury. Increase with increasing days post-treatment.</li> </ul>
		Male rat	Coronal sections of the hippocampus <sup>58</sup>	Pilocarpine-induced SE	<ul style="list-style-type: none"> <li>• Control: 0%</li> <li>• Increased number 14 d post-SE</li> </ul>
A $\beta$ : amyloid beta; AD: Alzheimer's disease; NPC1: Niemann Pick Type-C disease; SE: status epilepticus; TBI: traumatic brain injury; tMCAO: transient middle cerebral artery occlusion; pMCAO: permanent cerebral artery occlusion.					

**Table 1.1** indicates that various pathological conditions (actual and simulated) cause changes to microglial morphology. Some of these changes/morphologies were associated with molecular markers for pro-inflammatory microglial responses. However, for many of the described morphologies, no assays were performed to assess whether any particular microglial functions (inflammatory or anti-inflammatory) were associated with that morphology <sup>62</sup>. Potential associations between microglial morphology and activation status/function are being investigated. For example, amoeboid forms of microglia appear more phagocytically active than the also-present pseudopodic and ramified morphotypes <sup>62</sup>.

In a study where Sprague-Dawley rats were treated with pilocarpine to induce status epilepticus, researchers noted that alterations in morphology happened as early as 4 h post-intervention. The 5 morphotypes identified were; ramified, hypertrophic, bushy, amoeboid, and rod. Morphotypes had varying distribution across the CA1, CA3, and dentate gyrus areas of the hippocampal formation, with ramified being most abundant in control hippocampi. Pilocarpine induced time-dependent morphological changes, with a significantly increased abundance of bushy microglia at 4 h, then increased amoeboid microglia at 3 days and 2 weeks post-treatment. Increased numbers of rod microglia were only evident at 2 weeks post-treatment (Table 1.1, Table 1.2, Appendix) <sup>58</sup>. However, these were subjective categorisations, with no objective morphometrics <sup>58</sup> i.e. no numerically derived values such as area, perimeter, circularity etc. (Table 1.3) <sup>58</sup>.

Researchers use mostly qualitative methods such as descriptive terms to identify morphologies. The lack of objective measures when describing microglial morphology has led to confusion as it is unclear whether researchers are referring to the same morphologies. For example, rod-like microglia are described as being bipolar and narrow

bodied,<sup>64</sup> however this also resembles the pseudopodic morphology<sup>65</sup>. In a separate report, microglia are described as having honeycomb and jellyfish morphologies, but no morphometric analysis was used<sup>61</sup>. Visually, honeycomb microglia look like hypertrophic microglia that have formed a honeycomb-like network, and jellyfish microglia resemble large amoeboid microglia.

This demonstrates the difficulty in reconciling microglia morphology across studies and calls for a standardized objective method of measuring morphology which researchers can use to accurately compare/contrast findings. Objective numerical measures of morphological features, include area/volume, length, number of processes/extent of ramification etc. have been performed in some studies.

**Table 1.2 (Appendix)** indicates the wide variety of morphological features and calculations that are being applied to microglial studies, and the range of techniques, including automated software analysis, and 3D reconstructions of cells, sometimes even to the level of individual processes. **Table 1.3** summarises definitions some of the morphometric values that have been derived from microglial cells, while **Tables 1.4, 1.5, and 1.6** compare some of the reported values for microglial measurements.

<b>Table 1.3: Definitions for morphological descriptors and how they pertain to cell shape</b>			
<b>Measurement</b>	<b>Units</b>	<b>Definition</b>	<b>Relevance to cell shape</b>
<b>Area</b>	$\mu\text{m}^2$	Number of pixels in selected cell area, transformed to $\mu\text{m}^2$	Likely differs in 2D (flattened) vs 3D
<b>Branch points</b>		Number of nodes per concentric ring area.	More branch points indicates more complex branching/ramifications
<b>Cell volume</b>	$\mu\text{m}^3$	Volume of whole cell including soma and processes.	
<b>Circularity index (cell circularity, form factor)</b>		$(4\pi \times \text{cell area}) / (\text{cell perimeter})^2$ .	Value of 1 is perfectly circular. Decreasing value indicates decreasing circularity
<b>Convex Hull Span Ratio (CHSR)</b>		Ratio of major to minor axes of the convex hull.	
<b>Convex Hull Circularity (CHC)</b>		How circular the convex hull is $(4\pi \times \text{convex hull area}) / (\text{convex hull perimeter})^2$	Value of 1 is perfectly circular, decreasing with decreased circularity.
<b>Convex Hull Area (CHA)</b>		Convex hull is the smallest convex polygon containing the whole cell shape.	
<b>Feret's aspect ratio</b>		Feret's maximum divided by Feret's minimum	1 indicates circular, increases as cell is more elongated.
<b>Feret's maximum</b>	$\mu\text{m}$	The distance between the two furthest points of an object	Indicates greatest distance across cell
<b>Feret's minimum</b>	$\mu\text{m}$	Perpendicular distance between the closest-possible two parallel lines, that touch the object edge while the entire object is between them	Indicates narrowest distance across cell
<b>Grid crossings</b>		A grid is superimposed over image of cells, the number of crossings between the cells and the grid is calculated.	Ramified (highly processed) cells are expected to have higher instance of grid crossing than amoeboid (spherical) cells.
<b>Lacunarity</b>	$\Lambda$	Measures heterogeneity, or translational and rotational invariance in a shape.	Low $\Lambda$ value indicates homogeneity, high $\Lambda$ value indicates heterogeneity (size may have differently sized gaps or lacunas)
<b>MSACH</b>	$\mu\text{m}$	Maximum span across convex hull, similar to Feret's maximum.	
<b>Number of processes</b>		Membrane extensions leaving soma	Number of primary processes tends to remain consistent across activation states <sup>40</sup> , branching (secondary and tertiary nodes) is an indication of ramification.
<b>Perimeter</b>	$\mu\text{m}$	Distance of cell outline ( $\mu\text{m}$ )	
<b>Process length</b>	$\mu\text{m}$	Length of process	Typically shorter for amoeboid cells.
<b>Process volume</b>	$\mu\text{m}^3$	Volume of process	Typically higher in larger and ramified cells.
<b>Sholl interactions (intersections)</b>		From centre of soma, concentric rings are placed at 10 $\mu\text{m}$ intervals. Intersections are points where cell process crosses the concentric ring.	Gives an indication of the complexity of processes.
<b>Solidity</b>		Also termed density, calculated by $(\text{area of the cell}) / (\text{CHA})$	More ramified the cell, the lower solidity value.
<b>Territory</b>	$\mu\text{m}^3$	Index of 3D territory determined via convex hull analysis, as indicated by convex hull area.	

Table 1.4: Summary of length and perimeter morphometrics applied to microglia							
Model/cell culture	Treatment conditions		Summary effect vs control	Perimeter ( $\mu\text{m}$ )	MSACH ( $\mu\text{m}$ ; Maximum span across the convex hull)	Average length of process ( $\mu\text{m}$ )	Feret's max ( $\mu\text{m}$ )
Mouse coronal brain slice <sup>57</sup>	Naïve			61.46			17.10
	tMCAO		↑elongation, ↑perimeter, may indicate hypertrophic microglia	75.27*			20.10*
	pMCAO			47.69			14.92
	TBI			58.26			17.73
Mice, postnatal 1-2 days. <i>In vitro</i> primary microglia <sup>66</sup>	2 DIV	Control	Amoeboid	140			46.4
	2 DIV	A $\beta$	Amoeboid	148			45.6
	16 DIV	Control	Ramified, bipolar, rod	216+			74.4+
	16 DIV	A $\beta$	Enlarged soma with 2-1 large processes	160* vs 16 DIV control			52.8*
NPC1 mouse model. Sagittal slice <sup>67</sup>	WT	WK4				300	
	Npc1	WK4				280	
	Npc1	WK12	Retracted processes			160**	
Primary rat brain sections <sup>30</sup>	Cluster 1.1	Sal, Hyp	Large soma, small process length but thick in volume, mostly primary processes with few secondary. <b>Surveillant.</b>		52		
		NA, Hpc	Small round soma, few short thick primary processes, with few short secondary processes. <b>Activated.</b>				
	Cluster 1.2	Sal, Sept	Large soma, similar ramification but thicker branches. <b>Surveillant.</b>		63		
	Cluster 3.1	NA, Hpc	Smaller soma, similar ramification, thinner branches, longer secondary processes.		60* (compared to cluster1)		
	Cluster 3.2	Sal, Hyp	Smaller soma, more ramified, more secondary branches, thicker branches than 3.1		82* (compared to cluster1)		
N9 microglia cell line <sup>68</sup>	Control		Oval /round	80.0			26.4
	LPS		Amoeboid	34.4*			34.4*



\*significant difference versus respective control; + significant difference compared to 2DIV Control; A $\beta$ : amyloid beta; DIV: days *in vitro*; Hpc: hippocampus; Hyp: Hypothalamus LPS: lipopolysaccharide; pMCAO: permanent middle cerebral artery occlusion; tMCAO: transient middle cerebral artery occlusion NA: neuroaminidase; Npc1: Niemann-Pick disease, type C1; Sal: saline, control; TBI: traumatic brain injury; WK: weeks; WT: wild type

Table 1.5: Summary of area and volume morphometrics applied to microglia								
Model/cell culture	Treatment conditions		Summary effect vs control	Area ( $\mu\text{m}^2$ )	Cell volume ( $\mu\text{m}^3$ )	Average soma volume ( $\mu\text{m}^3$ )	Average volume of process ( $\mu\text{m}^3$ )	Microglial territory ( $\mu\text{m}^3$ )
Primary human, resected tissue (intractable epilepsy) <sup>65</sup>	<i>E. coli</i> bio-particle exposure			Pseudopodic $\sim 90^* \pm 10$ Amoeboid $\sim 190^* \pm 10$ Ramified $\sim 305^* \pm 30$ *all diff vs each other				
Mouse coronal brain slice <sup>57</sup>	Naïve			54.57				
	tMCAO		Larger cell. Hypertrophic microglia	85.78***				
	pMCAO			57.13				
	TBI			71.90				
Mice, postnatal 1-2 days. In vitro primary microglia <sup>66</sup>	2 DIV	C	Amoeboid	600				
		A $\beta$	Enlarged cell, remaining ovoid	1231*				
	16 DIV	C	Enlarged cell, accounted for by 1-2 large processes or large lamellipodia.	1297+				
		A $\beta$	Increase soma volume	1467+				
NPC1nmf164 mouse model. Sagittal section <sup>67</sup>	WT	Wk4			700		6	
	NPC1	Wk4	Increased size, increasing process vol		1500**		9**	
		Wk12	No sig dif size, increasing process vol		1000		14***	
Rat coronal section <sup>69</sup>	PL	C			1700	400		60,000
		CIE	Smallest cell, lowest # branch points		1000*	480		64,000
		LPS	Largest cell, largest soma, highest # branch points, most radially arranged		2100**	700***		58,000
	NA	C			1510	350		44,000
		CIE			1480	390		50,000
		LPS	Largest cell, largest soma.		1570	600**		58,000
N9 microglia cell line <sup>68</sup>	Control		Oval/round	230				
	LPS		Amoeboid	466*				
Ex vivo spinal slice segment <sup>70</sup>	Control		Smaller cells, more spherical	$\sim 850$	$\sim 1300$ ***			
	Niacin		Larger cells, less spherical	$\sim 1350$ ***	$\sim 2200$ ***			

\*significant difference versus control; A $\beta$ : amyloid beta; CIE: Chronic intermittent ethanol; DIV: days in vitro; LPS: lipopolysaccharide; pMCAO: permanent middle cerebral artery occlusion; tMCAO: transient middle cerebral artery occlusion NA: nucleus accumbens, NPC1: Niemann-Pick disease type C1; PL: prelimbic cortex, TBI: traumatic brain injury; WK: weeks; WT: wild type

Table 1.6: Summary of cell circularity measurements applied to microglia							
Model/cell culture	Treatment conditions	Summary effect vs control; other observations	Convex hull span ratio (CHSR; ratio of major axes; increasing above 1 indicates reducing circularity)	Circularity index (CI; decreases from 1 with reducing circularity)	Convex hull circularity (CHC; decreasing from 1 indicates reducing circularity)	Sphericity	
Mouse coronal slice <sup>57</sup>	Naïve	Ramified		0.26			
	tMCAO	Ramified		0.25			
	pMCAO	More circular		0.38**			
	TBI	More circular		0.37**			
<i>In vitro</i> primary mouse microglia <sup>66</sup>	2 DIV	C		0.448			
		Aβ		0.416			
	16 DIV	C	More ramified (vs 2 DIV)		0.380+		
		Aβ	More circular		0.456*		
Primary microglia <sup>71</sup>	Control			~0.48			
	BHB 1 mM			~0.40			
	BHB 3 mM	Less circular		~0.33**			
	BHB 5 mM	Less circular		~0.23**			
	BHB 0 h, 5 mM			~0.42			
	BHB 1 h, 5 mM			~0.36			
	BHB 4 h, 5 mM	Less circular		~0.28**			
	BHB 8 h, 5 mM	Less circular		~0.21**			
	Control			~0.41			
	BHB+	Less circular		~0.19**			
	LPS+			~0.43			
	LPS+ BHB+	Less circular		~0.21** (vs LPS)			
	Niacin 0 h, 1 mM	No impact on morphology		~0.41			
	Niacin 6 h, 1 mM	No impact on morphology		~0.38			
Niacin 12h, 1mM	No impact on morphology		~0.37				
	Niacin 24h, 1mM	No impact on morphology		~0.35			
<i>In vivo</i> <sup>71</sup>	Control			~0.44			
	BHB+	Less circular		~0.21**			
	LPS+			~0.41			
	BHB+LPS+	Less circular		~0.23** (vs LPS)			
Ex vivo spinal segment <sup>70</sup>	Control					~0.66	
	Niacin	Less spherical				~0.62*	

Rat post mortem fixed slice culture hippocampus, hypothalamus, septofimbrial nucleus <sup>30</sup>	Cluster 1.1	Sal, Hyp	Large soma, small process length but thick in vol, mostly primary processes with few secondary. <b>Surveillant.</b>	<1.35	>0.0145		
		NA, Hpc	Small round soma, few short thick primary processes, with few short secondary processes. <b>Activated.</b>	1.35 - 1.93			
	Cluster 1.2	Sal, Sept	Large soma, similar ramification but thicker branches. <b>Surveillant.</b>	<1.35	>0.0145		
				1.35 - 1.93			
	Cluster 2.1	Sal, Sept	Small round soma, highly ramified, thin processes, secondary and tertiary branches. <b>Surveillant.</b>	<1.35	0.0035-0.0145	0.80	
	Cluster 2.2	Sal, Hpc	Small round soma, highly ramified arranged radially, thin processes, secondary and tertiary branches. <b>Surveillant.</b>	<1.35	0.0035-0.0145	0.88	
	Cluster 3.1	NA, Hpc	Small round soma, similar ramification, thinner branches, longer secondary processes. <b>Activated.</b>	<1.35	<0.0035		
				1.35 - 1.93			
	Cluster 3.2	Sal, Hyp	Small round soma, more ramified, more secondary branches, thicker branches than 3.1. <b>Surveillant.</b>	<1.35	<0.0035		
				1.35 - 1.93			
	Cluster 4.1	NA, Hyp	Large soma, thick short retracted processes, multidirectional. <b>Activated.</b>		> 1.93		0.73
		NA, Sept	Small round soma, Unipolar long thin primary processes. <b>Activated.</b>				
Cluster 4.2	NA, Hyp	Large soma, thick retracted processes, overall flattened in shape. <b>Activated.</b>		> 1.93		0.85	
	NA, Sept	Large soma, thick retracted processes, overall circular in shape. <b>Activated.</b>					

(Table 1.6 continued...)

)Table 1.6 continued...)

<b>Rat post-mortem fixed slice, IHC</b> <sup>72</sup>	Cluster 1	(treated as 'control')	1.52	0.011		
	Cluster 2	Most circular according to CHSR but least according to CI, most heterogeneous, indicative of ramification	1.43	0.007		
	Cluster 3	Least circular (CHSR); greater CI than Clusters 1+2	2.55*	0.016*		
	Cluster 4	Most circular according to CI	1.57	0.031*		
*significant difference versus control; A $\beta$ : amyloid beta; BHB: $\beta$ -hydroxybutyrate; Cluster: experimenter-identified grouping of cells, based on morphological features; CHSR: convex hull span ratio; CI: Circularity Index; DIV: days <i>in vitro</i> ; Hpc: hippocampus; Hyp: Hypothalamus ;IHC: immunohistochemistry; LPS: lipopolysaccharide; NA: neuroaminidase; pMCAO: permanent middle cerebral artery occlusion; tMCAO: transient middle cerebral artery occlusion; TBI: traumatic brain injury; WK: weeks; WT: wild type						

Table 1.7: Summary of cell process complexity measurements applied to microglia										
Model/cell culture	Treatment/ conditions		Summary effect vs control	Branch points	Grid crossings	Number of intersections	Lacunarity	Solidity	Sholl interactions, intersections, or analysis	
Mouse coronal slice <sup>57</sup>	Naïve				3.80			0.55		
	tMCAO				4.39			0.55		
	pMCAO		More amoeboid		2.66			0.68**		
	TBI		More amoeboid		3.22			0.65**		
NPC1 mouse model. Sagittal slice <sup>67</sup>	WT	Week 4				190				
		Week 4				190				
	NPC1	Week 12	Fewer processes less ramified			80****				
Primary rat sections <sup>72</sup>	Cluster 1						0.40			
	Cluster 2		Heterogeneity in structure, indicative of ramification.				0.60*			
	Cluster 3						0.38			
	Cluster 4						0.37			
Rat coronal section <sup>69</sup>	PL	CIE	Smallest volume, Fewest branch points	0.0012**					0.009	
		LPS	Largest cell/soma, Most branch points, most radially arranged	0.0024**					0.014	
		C		0.0018					0.011	
	NA	CIE			0.0170					0.014
		LPS	Largest soma volume, highest number of branch points		0.0190					0.013
		C			0.0210					0.015
*statistically significant compared to control, CIE: Chronic intermittent ethanol; Cluster: microglial categorisation based on morphology; NPC1: Niemann-Pick disease, type C1; pMCAO: permanent medial cerebral artery occlusion; tMCAO: transient middle cerebral artery occlusion; WT: wild type										

**Tables 1.4, 1.5, and 1.6** collate numerical morphometric data across studies for comparison. Blank sections in the tables illustrate the high frequency with which data were not collected/reported. **Table 1.2** highlights the lack of standardisation in the approach to assess microglial morphology, with researchers using different morphological measures. This makes comparison between studies difficult as there is no direct comparison of microglial morphology. Even when some studies assess the same measure, there is usually not the same combination of measures.

One study measured area, perimeter, Feret's (maximum) diameter, circularity, aspect ratio, and the number of grid crossings (superimposed gridlines, crossed by cells) <sup>57</sup>. However, another *in vitro* cell culture study assessed area as the sole morphological feature <sup>62</sup>. Morphologies were often based on subjective descriptions (confocal microscopy, x65 objective lens), such as 'amoeboid' (described as having an area of about  $190 \pm 10 \mu\text{m}^2$ ), 'ramified' ( $\sim 305 \pm 30 \mu\text{m}^2$ ) and 'pseudopodic' ( $\sim 90 \pm 10 \mu\text{m}^2$ ), rather than providing repeated and accurate measurements.

The largest area values reported were  $600 - 1,467 \mu\text{m}^2$  <sup>66</sup>. These measurements might be an underestimate, as their methods do not take account of 'membrane sheets', which they describe as membrane overlapping and/or obscured by neighbouring cells <sup>66</sup>. Their methods however do not define what a membrane sheet is, nor the boundary between what is considered the cell and the membrane sheet. Additionally, they refer to an image showing how ImageJ software was used to delineate the cell boundary, indicating that this measurement included membrane which appeared to be overlapping with neighbouring cells, contradicting the described method. Elsewhere, the authors state that ramified microglia were static and their processes did not move. However, despite these inactivated

microglia often being described as “resting”, this surveillant microglia phenotype is increasingly recognised as having highly active processes.

Overall, cell area values showed a wide range of variation from 54.57 to 1,467  $\mu\text{m}^2$ . Smaller values were typically associated with 3D culture methods, e.g. organotypic brain slices. The same trend (smaller values) was apparent for perimeter and Feret’s maximum diameter. A possible explanation for this is that when microglia are in a 3D environment, some of the cell will project towards and away from the imaging lens (z directions), and so not contributing to measurements of area etc. (xy plane); whereas microglia cultured on coverslips restrict growth in this z axis, with more of the cell being visible to 2D imaging (more of the cell is visible within the xy plane). This means that the cellular environment may impact (restrict) morphology, although it is unclear whether or to what extent this enforced morphological change may influence activity of microglia. For example, does promoting a more amoeboid morphology drive more inflammatory cell behaviours? Or, can promoting greater ramification of microglial processes, result in reduced inflammatory responses?

#### **1.6. Microglial activation and its role in neurodegenerative disease**

Mounting evidence indicates the importance of microglial activation status in the onset, progression, and resolution of neural injury/disease. In patients with AD (n = 10), PD (n = 11), or mild cognitive impairment (MCI; n = 10), researchers used MRI to investigate whether there were correlations between microglial activation and the extent of neurodegeneration seen in these diseases<sup>73</sup>. In AD and MCI there was a significant negative correlation between increased microglial activation and mini mental state examination



(MMSE), an assessment of cognitive function based on orientation, concentration, attention, verbal memory, naming, and visuospatial skills. However, there are limitations to its use. MMSE was not originally established to “identify early stages of dementia, distinguish between different types of dementia, or to predict the development of dementia in the long term” and studies have shown that “sociocultural variables, age and education, among other factors, could affect individual scores”, calling its use into question<sup>74</sup>.

The correlation between neuroinflammation and declining score on MMSE indicates potential for increasing microglial activation leading to neural degeneration, though a direct causal effect could not be demonstrated from these data.

This was built upon more recently, in 2017 and 2020, by Parbo *et al.*<sup>75,76</sup>. Using 11C-PK11195 PET imaging of patients, brain inflammation was shown to accompany amyloid beta deposition in cases of AD and MCI, with 22 of 26 amyloid-positive MCI cases showing increased cortical microglial activation. This activation was found in the frontal, parietal, and temporal lobes. Parbo *et al.* do not conclude if this effect was associated with lesser or greater pathology, only that neuroinflammation accompanies amyloid deposition, concluding it must be a part of the neurodegenerative process.

Parbo *et al.* 2020<sup>77</sup>, demonstrated that microglia could act to protect neurons during prodromal AD. Using 11C-PK11195 PET imaging Parbo *et al.* identified raised cortical beta amyloid levels in patient cases of MCI and AD. To measure neuroprotective effects, Parbo *et al.* measured the plasma concentrations of neurofilament light protein which has been reported to be a marker of axonal degeneration (although non-specific for this). Lower levels of plasma neurofilament light were associated with greater levels of microglial activation in the precuneus, occipital, and sensorimotor cortices. If this inverse correlation

indicates that reduced microglial activation results in greater levels of axonal degeneration, then perhaps robust microglial activation is desirable, at least in the early stages of disease. Parbo *et al.* are restricted in their definition of microglial activation as they confirm microglial activation by using <sup>11</sup>C-PK11195 PET imaging monitoring expression of the Translocator protein (TSPO) marker (18kDa). A marker that is unable to distinguish between M1 pro-inflammatory and M2 anti-inflammatory states.

It has been demonstrated that TSPO is expressed on activated microglia, astrocytes, and other infiltrating immune cells such as macrophages, however it is microglia with the highest expression<sup>78-80</sup>. Using immunohistochemistry of post mortem samples of brain and spinal cord from MS patients, Nutma *et al.*<sup>81</sup> conclude that TSPO expression is increased within active and chronic MS lesions, associated with microglial cell numbers, but should not be over-interpreted as indicative of microglial activation status. Whilst TSPO can give an indication of neuroinflammation (increased numbers of glial cells due to microgliosis and astrocytosis) it cannot reliably indicate whether microglia or astrocytes are pro-inflammatory or anti-inflammatory. Therefore, investigating therapeutic interventions modulating microglia activity from pro-inflammatory to anti-inflammatory TSPO may not be helpful and a behavioural assay such as cognitive performance may be more beneficial. Immunohistochemical analysis of post-mortem tissue obtained from PD patients (Braak stage 4-6) and patients with incidental Lewy body disease (Braak stage 1-3), shows an increased number of CD68 positive amoeboid microglia in the hippocampus and substantia nigra (SN) compared to age matched healthy controls<sup>82</sup>. They also show that increase in amoeboid CD68<sup>+</sup> microglia correlates with an increased  $\alpha$ -synuclein deposition in the hippocampus and SN, and dopaminergic neuronal cell loss SN. Studies have demonstrated a presence of inflammatory microglia in AD and PD patients<sup>73,82</sup>. They do not, however,

show that microglia are responsible for neuronal loss, beyond showing a positive correlation between the presence of microglia and  $\alpha$ -synuclein and dopaminergic neuronal cell loss in the SN of Parkinson's patients <sup>82</sup>.

**Table 1.8 (Appendix)** summarises evidence for microglial involvement in human neurological conditions. This covers a range of pathologies, both early and late onset, sudden onset, and progressive degenerative conditions. Imaging studies of live patients, and post-mortem histological analyses, indicate neuroinflammation, and inflammatory microglia specifically.

### **1.7. Microglial activation in models of neurodegenerative disease**

Although many human neurological conditions do not occur naturally in other species, various animal models have been developed, particularly utilising rodents. These models frequently exhibit similar neuroinflammatory events to those seen in humans, including microglial responses and behaviours.

In a macaque model of PD, immunohistochemical analysis of brain tissue shows direct interaction between microglia and dopaminergic neurons at 1, 2, and 5 years post-administration of 1-methyl-4-phenyl-1,2,3,6-tetrahydropyridine (MPTP; specifically toxic to dopaminergic neurons) <sup>83</sup>. In the substantia nigra pars compacta (SNpc), loss of dopaminergic neurons happens alongside persistent microglial activation. Whilst the total number of microglia did not change, the proportion of activated microglia increased, alongside an increase in microglia phagocytic activity. Microglia activation was indicated by morphometric analysis where microglia show an increase in cell body size and number of

terminal tips. This study showed direct interaction between microglia and DA neurons, but not direct microglial neurotoxic effects.

In a rat model of PD<sup>84</sup>, neuron: astrocyte co-cultures (without microglia) were treated with 50  $\mu$ M MPP<sup>+</sup> which induced ~50% loss of SN dopamine neurons. In SN astrocyte: SN neuron: microglia (N:A:M) co-cultures, MPP<sup>+</sup> neurotoxicity was amplified, with cultures experiencing ~75% neuron loss. The exacerbation of neuron loss in co-cultures with microglia, compared to without microglia, highlights the potential of microglia to amplify toxicity. This exacerbation of neuronal toxicity occurred whether microglia were derived from the cortex, SN, or the ventral tegmental area (VTA). Microglia were only pro-inflammatory in the presence of MPP<sup>+</sup>, with control cultures showing no neuronal cell death, and pro-inflammatory effects dealt by activated microglia could be reversed by treatment with a TLR4 antagonist.

VTA astrocytes were able to partially reverse the neurotoxic effects in either SN neuron or VTA neuron N:A:M co-cultures, with both cultures experiencing only ~20% neuron loss. VTA astrocyte protection was abolished by doubling the number of microglia, with SN and VTA neurons experiencing ~40% and 50% loss respectively. Doubling the amount of astrocytes with respect to neurons had no impact. This shows that microglia are not only influenced by each other, but also by astrocytes, with potentially important consequences for disease progression and therapeutic interventions.

Only microglia derived from the cortex were used in these N:A:M co-cultures due to experimental limitations (cell yield). Difficulties in interpreting this study arise as there are clear regional differences in the activities of astrocytes. Microglia derived from different regional areas display different cytokine transcriptomic profiles under both treated and

control conditions. The use of cortical microglia was justified by the authors as, despite transcriptomic differences, microglia from all areas displayed similar neurotoxic properties.

**Table 1.9 (Appendix)** summarises evidence for microglial roles in animal models of neural injury/disease.

### **1.8. Immunomodulatory targets for therapy**

Microglial behaviours are critical to the onset, progression and resolution of neural disease and injury, whether their contributions are beneficial or detrimental. Potential therapies could seek to attenuate microglial inflammation, or perhaps promote neuroprotective/neurorestorative processes. However, individuals are often only diagnosed with neurodegenerative illness once a large amount of damage has occurred, and interventions may need to occur early in the pathology. Diagnostic tools such as PET scans offer the ability to detect early stage neuroinflammation, and may aid future preventative neuroimmunomodulatory treatments<sup>77,85,86</sup>.

An ideal therapy would also avoid invasive delivery to the CNS, perhaps using peripheral injection or even oral delivery. For example, immune effects of vitamin B3 are attracting interest in PD (which may involve Gpr109a activation) and the Gpr109a ligands DMF/MMF in MS; further details will be discussed in greater detail in the next section, 1.9

### 1.9. Evidence for microglial expression of GPR109a

Microglia have been reported to express GPR109a, but to varying extent, and with inconsistent evidence (**Table 1.10**)<sup>87,88,89</sup>. Wakade *et al.* 2014<sup>87</sup> studied the effects of niacin supplementation on PD patient GPR109a expression. Patterns of Gpr109a expression were reported in post mortem SN (n = 4 patients), comparing with age matched controls (n = 4). Western blot analysis showed greater expression of Gpr109a in PD SN, compared to age matched controls. Using CD11b as a microglial marker, confocal microscopy showed the majority of CD11b<sup>+</sup> cells in PD samples were co-localised with Gpr109a staining. This contrasted with control samples, where the majority of CD11b<sup>+</sup> cells were Gpr109a<sup>-</sup>. No comment was offered on potential reasons for these differences in Gpr109a expression. Increased numbers of microglia and increased microglial expression of GPR109a were reportedly evident in PD patients<sup>87</sup>. The reliability of these data is unclear, as no numerical/statistical data were reported to support these claims and the cohort was very small (n = 4), with one patient showing an absence of Gpr109a expression within the SN which Wakade *et al.* were unable to account for. Wakade *et al.* assumed that the increased expression of Gpr109a in the SN was due to increased numbers of microglia and also increased microglial expression of Gpr109a (each cell), however evidence supporting this claim is not presented.

<b>Table 1.10: Evidence for microglial expression of Gpr109a</b>			
Species	Source	Methods	Findings
Human	Post-mortem PD patient Age-matched healthy controls <sup>87</sup>	Gpr109a immunostaining Confocal microscopy	PD: CD11b co-localised with GPR109a (no numbers reported) Control: Fewer CD11b cells Not all GPR109a+ cells are co-localised with CD11b
Mouse	BV-2 cell line <sup>90</sup>	PCR Western blot	BV-2 cells express Gpr109a. No investigations in up/down regulation of Gpr109a.
Mouse	BAC-transgenic mouse strain Hca2mRFP <sup>88</sup>	Immunohistochemistry Coronal slice	CD11b+ microglia in control sample express Gpr109a.
Rat	Whole brain. Primary microglia cultures. >98% purity <sup>89</sup>	PCR Western blot	Gpr109a is expressed by microglia
		qRT-PCR LPS treatment: 0.5, 1, 10 ng/ml 4 hr, 12 hr, 24 hr	Gpr109a mRNA expression significantly increased upon LPS treatment in a concentration and time dependent manner. Dose-response curve, but no statistical analysis. Greatest expression of Gpr109a: LPS 10 ng/ml at 24 hr.
Rat	Post-fixed RVLM section (n = 4-6) <sup>91</sup>	Confocal dual-labelled fluorescence microscopy	~20% of CD11b/c+ cells are Gpr109a +

Abbreviations; LPS: Lipopolysaccharide; PCR: Polymerase Chain Reaction, qRT-PCR: Real-Time quantitative reverse transcription PCR; RVLM: Rostral Ventrolateral Medulla ; SN: Substantia nigra.

During this study Wakade *et al.* was also interested in the potential role of the peripheral inflammatory response in PD. They demonstrated elevated GPR109a expression in white blood cells (WBCs; type not specified) of Parkinson's patients compared to their age matched controls (no PD diagnosis). A densitometry scan (relative densities of the Western blot bands) showed 20 of 22 patients had upregulation of GPR109a, with a significant difference between Parkinson's patients and controls,  $p = 0.033$ . This demonstrated GPR109a's potential importance in the CNS and peripheral immune response, supporting the idea that these two systems are closely interlinked. This led to them emphasising the importance of investigating GPR109a expression in neuroglia. In particular they emphasised the interest of the possible role of GPR109a in recruiting microglia to the SN.

In 2015, Wakade *et al.* conducted a clinical trial of GPR109a ligand supplementation <sup>92</sup> in a 65 year old Parkinson's patient (45 d, oral niacin, 250 mg). The aim was to study the effect of niacin on GPR109a expression and patient symptoms. The patient underwent. *Wakade et al* monitored GPR109a expression levels in the patient's WBCs and measured Beta Hydroxybutyric acid (BHBA) expression levels in plasma. Symptomology was assessed at 2 weeks, 6 weeks, and 3 months. To determine GPR109a levels a western blot of WBCs was assessed. WBCs were used as obtaining microglia would be highly invasive, although the researchers comment that GPR109a expression in WBCs cannot be correlated with levels within the SN. However the purpose was to assess GPR109a ligand use on inflammation bearing in mind that systemic inflammation has also been implicated in Parkinson's pathology. Symptomatology was assessed using the Unified Parkinson's Disease Rating Scale (UPDRS) handwriting test, and quality of sleep. UPDRS is used by clinicians and researchers to measure the impairment and disability associated with PD. There are four sections: the first considering mental activity, behaviour, and mood, the second the ability for the patient to carry out activities of daily living independently, the third the ability to carry out motor skills, and the fourth more general complications as a result of the PD <sup>93</sup>. The patient saw improvements in aforementioned parameters without side effects and this was abolished in the absence of niacin supplementation. Wakade comments that there was a reduction of Gpr109a in patients' WBCs with niacin treatment. BHB levels and NAD/NADP ratio was normalised with niacin treatment and reverted back to previous levels after the treatment had stopped. Normalised BHB levels and NAD/NADP ratio correlated with improvement in symptoms.

This is an important finding in that it is the first clinical case of treating a PD patient with Niacin and the study shows promising results. However, it is restricted in that their sample



size was only one patient. In addition, niacin is also known to act via non-GPR109a mechanisms (e.g. Nrf2, discussed later) and they do not explore the potential mechanism beyond assessing GPR109a expression and NAD/NADP ratio.

## **1.10. How do microglia respond to GPR109a ligands?**

### **1.10.1. Microglial response to BHBA**

Fu *et al.* (2015)<sup>89</sup> showed in a rat model that subcutaneous treatment with the GPR109a ligand BHBA improved functional recovery from intranigral LPS-induced lesions, indicated by better scores in the amphetamine induced rotation test. Fu *et al.* investigated the effect of LPS intranigral injection on microglial activation and injury to dopaminergic neurons by using RT-PCR and western blots of post-mortem rat tissue. Increased GPR109a mRNA expression was detected 4 h post-LPS stimulation. Further, mRNA expression increased significantly in both a dose- and time-dependent manner, highlighting a potential connection between GPR109a expression and the inflammatory response.

In studies conducted by Rahman *et al.* 2014<sup>88</sup> in a mouse middle cerebral artery occlusion (MCAO) model of ischemic stroke, both niacin and BHBA elicited a neuroprotective response, with reduced infarct size compared to control. Mice received subcutaneous injections of BHBA pre-MCAO, with beneficial effects abolished in a Gpr109a<sup>-/-</sup> knockout mouse. Niacin is a known agonist of the Gpr109a receptor and mice received a 100 mg/kg dose pre-MCAO (10 mins) and post-MCAO (4 h, 8 h, 24 h, 28 h, 32 h). As with BHBA, protective effects were abolished in Gpr109a<sup>-/-</sup> knockouts. This confirmed the hypothesis that BHBA was activating the Gpr109a receptor to deliver its effects.

Rahman *et al.* investigated which cells in the brain were Gpr109a positive using fluorescence microscopy to analyse a BAC-transgenic mouse line Gpr109a mRFP where the Gpr109a locus directs the expression of the monomeric red fluorescent protein. When Gpr109a mRFP<sup>+/+</sup> mice were not undergoing any treatment staining revealed the exclusive staining for Gpr109a<sup>+</sup> to CD11b<sup>+</sup> microglia, no Gpr109a expression was detected in neurons or astrocytes. Rahman *et al.* assumed the CD11b<sup>+</sup> cells to be microglia as in MCAO control the blood brain barrier is thought to remain unperturbed, hence no infiltration of bone marrow derived cells. In Gpr109a mRFP<sup>+</sup> mice post MCAO Rahman *et al.* found an increased presence in CD11b<sup>+</sup> and Iba1<sup>+</sup> cells surrounding the infarct, of which 87.5 ± 14.6% and 98.7 ± 18.0% were also Gpr109a<sup>+</sup>, respectively, showing that Gpr109a is expressed by microglia and/or infiltrating monocytes/macrophages.

Using bone marrow transplantations in a chimeric mouse model, three populations were established:

Gpr109a <sup>+/+</sup> >Gpr109a <sup>+/+</sup>	Gpr109a <sup>+/+</sup> receiving bone marrow from Gpr109a <sup>+/+</sup> mice
Gpr109a <sup>+/+</sup> > Gpr109a <sup>-/-</sup>	Gpr109a <sup>-/-</sup> receiving bone marrow from Gpr109a <sup>+/+</sup> mice
Gpr109a <sup>-/-</sup> >Gpr109a <sup>+/+</sup>	Gpr109a <sup>+/+</sup> receiving bone marrow from Gpr109a <sup>-/-</sup> mice

Each population received either niacin or saline vehicle (sham) pre- and post-MCAO. Gpr109a<sup>+/+</sup>>Gpr109a<sup>+/+</sup> mice saw a protective effect by niacin treatment: reduced infarct diameter compared with control (~15 mm<sup>3</sup> vs ~29 mm<sup>3</sup>). For Gpr109a<sup>-/-</sup>>Gpr109a<sup>+/+</sup>, decreased infarct volume was seen in niacin-treated mice. This protective effect was abolished in Gpr109a<sup>+/+</sup>> Gpr109a<sup>-/-</sup>, suggesting that it is Gpr109a<sup>+</sup> bone marrow-derived cells that are mediating the protective effects. They report that macrophages are delivering the beneficial effects as they assume microglia cannot develop from hematopoietic cells (at least in adult organisms).

Some studies suggest hematopoietic cells can differentiate into microglia-like cells. Getts *et al.* (2008)<sup>94</sup> suggest that infiltrating inflammatory monocytes can differentiate into a new microglial population, with the phenotype CD45<sup>int</sup>CD11b<sup>+</sup>GFP<sup>+</sup>Ly-6c<sup>+</sup> (intermediate levels of CD45 expression). In addition, Lund *et al.* (2018)<sup>95</sup> showed that infiltrating macrophages alter their gene expression profile, such that they more closely resemble microglia and adopt microglia-typical DNA methylation signatures whilst retaining a distinct expression signature (although not identical to microglial expression). Their results suggest that infiltrating macrophage/monocytes are imprinted by the CNS microenvironment to become a functionally distinct niche of microglia-like cells.

The cells reported by Rahman *et al.* were of two populations of monocytes/macrophages CD11b<sup>+</sup>/CD45<sup>+</sup>/Ly-6G<sup>-</sup>/Ly-6C<sup>-</sup> and CD11b<sup>+</sup>/CD45<sup>+</sup>/Ly-6G<sup>-</sup>/Ly-6C<sup>+</sup>. Ly-6c is not an effective marker to distinguish between peripherally derived monocytes/macrophages and microglia; as, microglia can be Ly-6c<sup>+</sup> or Ly-6c<sup>-</sup>, likewise expression is seen in monocytes/macrophages<sup>94</sup>. Monitoring CD45 expression might be a more effective way of distinguishing between macrophages and microglia<sup>96</sup>. Whilst Rahman *et al.* used flow cytometry for identification of CD45 they did not monitor its levels of expression, not allowing them to distinguish between microglia and macrophages.

Rahman's findings might not be translatable to other neurodegenerative disease such as AD where there is not such drastic alteration to blood brain barrier integrity. By using an *in vivo* stroke model, responses cannot be monitored independent of infiltrating macrophages. The microglial response may be present but insufficient in the case of stroke, and may require peripheral immune system input. Where the microglial response may be lacking in the case of stroke, there may perhaps be a greater response in disease states

such as AD, PD, or TBI (with perhaps limited peripheral immune cell involvement). This is beyond the scope of this discussion but an important factor to consider.

### **1.10.2. Microglial response to Niacin**

Rawji *et al.*<sup>70</sup> screened a library of 1,040 generic medications, and identified niacin's capability to enhance microglia/macrophage cytokine secretion and phagocytosis *in vitro*.

Rawji *et al.* investigated the potential of niacin treatment to alter lesional microglia/macrophages to promote remyelination. Delayed recruitment of microglia into lesions, and reduced phagocytic clearance of debris, inhibits this remyelination. Myelin debris activates microglia (pro-inflammatory phenotype), which upregulate IL-1 $\alpha$  and TNF $\alpha$ . Myelin phagocytosis requires the scavenger receptor CD36 and overexpression of the receptor lead to a significant increase in microglia phagocytic activity. Lower level expression of the CD36 receptor was seen in aged microglia, which are reportedly less effective at clearing debris.

Treatment with niacin lead to an enhanced capability of microglia to uptake myelin debris in both young and age mouse microglia. This effect was seen in primary young and aged rat microglia as well as adult human microglia obtained via biopsy. This was attributed to elevated CD36 levels.

In primary microglia obtained from Gpr109a<sup>-/-</sup> knockout mice Rawji sought to identify Gpr109a's involvement. Wild type microglia saw an enhancement in phagocytosis with niacin treatment whereas this was abolished in Gpr109a<sup>-/-</sup> microglia. Rawji suggests that niacin upregulates CD36 via activation of the Gpr109a receptor.

### **1.10.3. Dimethyl fumarate (DMF) and its metabolites: Dimethyl Fumarate-glutathione conjugate (DMF-GSH) and Monomethyl fumarate (MMF)**

Delayed-release DMF is an approved treatment for MS. Microglial involvement is central to MS pathology, however the effects of DMF, and DMF's primary metabolite MMF, on microglia still remains unclear.

DMF has a short half-life and is rapidly converted to its primary metabolite MMF. MMF has been shown to cross the BBB, penetrating into the brain parenchyma<sup>97-99</sup>. It was previously believed that DMF could not enter portal circulation as it does not survive absorption through the gut. However, some studies show DMF-GSH, a glutathione conjugate of DMF, present in portal circulation of rodents after receiving oral DMF, with Peng *et al.*<sup>100</sup> suggesting the presence of MMF and DMF-GSH in portal circulation. Peng *et al.*<sup>100</sup> demonstrated that both are detected in plasma and brain parenchyma, with MMF present in greater quantities.

It is still unclear which substance DMF or MMF is biologically active after oral DMF dosing. DMF likely exerts broader ranging biological activity. These affected signalling pathways are largely correlated with nuclear factor erythroid-2-related factor 2 (Nrf2) and NF- $\kappa$ B pathways. DMF activates a larger number of NRF2 target genes in comparison to MMF. Nrf2 is independent of Gpr109a. DMF also suppressed transcriptional responses associated with NF- $\kappa$ B.

In a study of HIV-induced neuroinflammation and neurotoxicity<sup>101</sup> MMF treatment (100  $\mu$ M) of microglia-HIV vector infected monoculture shows a 4.6 fold reduction in CXCL10 (~2000 pg/ml to ~400 pg/ml). This was seen in both HMC3 cell line and human primary microglia. Supernatant (conditioned media) from microglia monocultures and microglia-

monocyte co-cultures (+/- MMF treatment) was applied to human foetal neurons. MMF treatment of microglia-monocyte co-cultures at concentrations 10  $\mu$ M and 30  $\mu$ M led to significantly enhanced neuronal viability.

In a 6 week old albino BALB/c mouse model of LIR (light induced retinopathy), Jiang *et al.*<sup>102</sup> demonstrated the ability of MMF to protect the retinal structure and function. Assessing the thickness of the photoreceptor layer in the retina, a single dose of MMF before light exposure preserves layer thickness in a dose-dependent manner, while this layer is thinned in the retinopathy group. 100 mg/kg MMF showed greatest protective effect with the photoreceptor layer being indistinguishable from naive mice. The functional protective effect of MMF was assessed by electroretinography (ERG). Again, MMF improved ERG responses in a dose-dependent manner, with greatest effect being seen in mice treated with 100 mg/kg, shown by amplitudes indistinguishable from naïve mice.

LIR increased expression of Gpr109a and the pro-inflammatory marker CD14 3-24 h post treatment, with highest level at 12 h. LIR initially decreased the expression of the anti-inflammatory marker Mrc1 expression but increased its expression at 12 h. MMF treatment pre-LIR limited this increase in expression of Gpr109a and CD14, but had no impact on Mrc1 expression. Depletion of microglial numbers using PLX5622 demonstrated that these changes in expression were primarily occurring in retinal microglia.

Jiang *et al.* (2019)<sup>103</sup> did not explore the mechanisms behind MMF's effects. They did however note LIR upregulation of genes associated with NF- $\kappa$ B and Nrf-2, and that this upregulation was mitigated by MMF. They cannot say definitively from this data whether MMF is acting through Gpr109a or Nrf-2 or both. Further experiments involving Gpr109a and Nrf-2 knockouts would be required. **Table 1.11** summarises reported *in vitro* effects of Gpr109a ligands on cultured microglia.

<b>Table 1.11: Effects of Gpr109a ligands on primary microglia</b>			
<b>Source</b>	<b>Experimental details</b>	<b>Gpr109/ Nrf2 mediated?</b>	<b>Outcome</b>
Mice (6-8 wks)	demyelinating toxin lysolecithin  phagocytosis assay  fluorescence microscopy <sup>70</sup>	Gpr109a	Myelin debris activates microglia and myelin phagocytosis requires the scavenger receptor CD36.
Human  Young, and aged.	phagocytosis assay  fluorescence microscopy <sup>70</sup>		Niacin significantly enhances the microglial phagocytosis of myelin debris in both young and aged mice as well as human cells.
HCA2 <sup>-/-</sup> knockout mice	phagocytosis assay  fluorescence microscopy <sup>70</sup>		Niacin's enhancement in phagocytosis is abolished in Gpr109a <sup>-/-</sup> microglia.
Rat	Pre-treatment: MMF, DMF 10 $\mu$ M 24 h.  Treated with LPS or IL-4 for 3, 6, 24 h.  qPCR to measure gene expression <sup>104</sup>	Not determined	Neither DMF nor MMF affected phagocytic activity of untreated, LPS treated, or IL-4 treated microglia.  MMF had no impact on microglia treated with either LPS or IL-4.  DMF upregulated M1 inflammatory markers: TNF $\alpha$ , iNOS, and anti-inflammatory markers; IGF-1, Tgf-1 $\beta$ , Mrc-1, in microglia treated with LPS (6 h). Effects not seen for other time points.  DMF pre-treatment of M0 or LPS (M1) microglia increased expression in MCR1 at 6 h only and IGF-1 at 3 h and 6 hr.
Rat	Transcriptional microarray  LPS 100 ng/ml for 24 h <sup>100</sup>	Not determined	<ul style="list-style-type: none"> <li>• DMF: DMF exerts a wide range of biological activity</li> <li>• Alteration in 1,822 genes (naïve microglia), 2,672 genes (classically activated microglia induced by LPS + IFN-<math>\gamma</math>)</li> <li>• Suppressed transcriptional activity of NF-<math>\kappa</math>B-associated genes</li> <li>• Reduced expression: IL-1<math>\beta</math>, TNF<math>\alpha</math>, Il-22b, Stat-1, CD40</li> <li>• DMF acted both via and independently of Nrf2, whereas MMF thought to act through Nrf2 only.</li> <li>• DMF and MMF: upregulated <i>Gclm</i>, <i>Srxn1</i>, <i>Gsta3</i>, <i>Txnrd1</i>, <i>Cat</i>, and <i>Osgin1</i> (all associated with Nrf2)</li> <li>• MMF: no suppression of NF-<math>\kappa</math>B-associated genes</li> <li>• Naïve microglia: transcriptional modification in 198 genes,</li> <li>• Classically activated microglia: only 19 genes modified</li> <li>• DMF not MMF: decreased inflammatory responses in classically activated (LPS or IFN-<math>\gamma</math> treated) microglia</li> <li>• DMF is present in the brain as its metabolites DMF-GSH or MMF, with MMF being present in greatest amount.</li> <li>• The effect of DMF-GSH was not studied</li> </ul>
Abbreviations: DMF: Dimethyl Fumarate, DMF-GSH: DMF-glutathione conjugate			

#### 1.10.4. How do DMF and MMF affect gene expression and inflammatory response in primary microglia?

The fumarate drugs DMF and MMF have both been shown to alter microglial gene expression, with DMF affecting the greater number of individual genes (**Table 1.12**)<sup>100</sup>. Modified gene expression was investigated in untreated *in vitro* cultures (naïve microglia) and LPS treated *in vitro* cultures (microglia pre-treated with LPS). Interestingly, DMF treatment of LPS-activated microglia altered expression in the greatest number of genes, while MMF treatment of LPS-activated microglia had the most limited effects.

Drug Treatment	Microglial activation	Upregulated genes	Downregulated genes	Total genes with altered expression
DMF	Naïve	783	1039	1822
DMF	LPS activated	1458	1214	2672
MMF	Naïve	94	104	94
MMF	LPS activated	5	14	19

DMF: dimethyl fumarate; MMF: monomethyl fumarate. Ref<sup>100</sup>

The mechanism of DMF and its metabolite MMF is still largely unclear. Using a NRF2 knockout mouse model, DMF's anti-inflammatory activity was maintained, demonstrating DMF activity to be independent of Nrf2. However, using transcriptional profiling DMF was able to activate Nrf2 target genes *Gclm*, *Srxn1*, *Csta3*, *Txnrd1*, *Cat*, and *Osgin1*, which together offer various protective functions<sup>100</sup>.

*Gclm* codes for the glutamate-cysteine ligand (GCL) modifier subunit. Gclm and GCLC are catalytically-active heavy subunits of GCL. GCL functions in the production of glutathione, which is an important antioxidant<sup>105</sup>.

Sulfiredoxin 1 (*Srxn1*) is one of the endogenous antioxidant proteins that maintain cellular redox homeostasis. Upregulation of *Srxn1* decreased high glucose (HG)-evoked apoptosis,



ROS generation, and pro-inflammatory cytokine release in retinal ganglion cells (RGCs). *Srxn1* enhances Nrf2 signalling in HG-exposed RGCs by up-regulating phosphorylation of Akt and glycogen synthase kinase-3 $\beta$  (GSK-3 $\beta$ )<sup>106</sup>.

In human astrocytes, MMF-mediated cyto-protection is OSGIN1 dependent (specifically the OSGIN1-61 kDa isoform). MMF treatment promoted Nrf2-dependent OSGIN1 expression which induced p53 nuclear translocation resulting in cell-cycle inhibition and cell protection against oxidative damage.

DMF is reported by tang *et al.* (2008)<sup>107</sup> to be inactive with regards to Gpr109a activity, with an IC<sub>50</sub> of ~10  $\mu$ M (MMF IC<sub>50</sub> ~70 nM; niacin IC<sub>50</sub> ~16 nM). MMF effects were suspected to be Nrf2-dependent, with Peng *et al.* 2016<sup>100</sup> stating that no inhibitory effects were seen in Nrf2<sup>-/-</sup> primary microglia cultures treated with MMF. It seems likely that MMF effects are mediated by Gpr109a and Nrf2, as Tang *et al.*<sup>107</sup> report MMF to have high affinity for Gpr109a (10 fold higher than niacin) and Peng *et al.*<sup>100</sup> demonstrates MMF's effects to be abolished in Nrf2<sup>-/-</sup> knockout primary microglia. However, it is still unclear whether MMF requires activation of both Gpr109a and Nrf2. Additionally, there was no investigation into whether MMF's effects were dependent on the route taken. MMF's impact on microglial behaviour could differ depending on whether it activates Gpr109a or Nrf2.

#### **1.10.5. Evidence for astrocyte expression of GPR109a**

Astrocytes treated with DMF or MMF have shown a reduction in inflammatory behaviours<sup>108,109</sup>. It has been suggested that this action is independent of Gpr109a, and may be mediated by Nrf2, which was shown to undergo nuclear translocation. However, as DMF and MMF are Gpr109a ligands, there could still be concurrent Gpr109a activation, along with Nrf2 mediated effects.

Investigations into the expression of GPR109a in astrocytes is limited (**Table 1.13**). Rezaq *et al.*<sup>91</sup> studied rat RVLM histological sections, reporting that TH<sup>+</sup> neurons, microglia, and astrocytes express GPR109a. NeuN<sup>+</sup> and TH<sup>+</sup> neurons showed a greater percentage of cells expressing GPR109a, than did other cell types, reporting approx. 90% of TH<sup>+</sup> cells expressing Gpr109a, and approx. 70% of NeuN<sup>+</sup> cells being Gpr109a<sup>+</sup>. Microglia and astrocytes showed a low percentage of cells expressing GPR109a: approx. 27% of CD11b/c<sup>+</sup> microglia, and approx. 7.5% of GFAP<sup>+</sup> astrocytes.

Species	Source	Methods	Findings
Mouse <sup>88</sup>	BAC-transgenic mouse line Hca2mRFP Middle cerebral artery occlusion (MCAO)	Immuno-histochemistry Coronal slice, with MCA	GFAP <sup>+</sup> cells were negative for Gpr109a, before and after MCAO
Rat <sup>91</sup>	Post-fixed RVLM section (n = 4-6)	Confocal dual-labelled immunofluorescence microscopy	~7.5% of GFAP <sup>+</sup> cells were Gpr109a <sup>+</sup>

There are few direct studies of Gpr109a expression in microglia or astrocytes. Evidence suggests some human microglia express Gpr109a, and that this percentage can be altered by pathology. However, there is still limited understanding of the extent of Gpr109a expression in glia, and what the direct effects of Gpr109a activation may be. A thorough understanding of these aspects could be beneficial in understanding neuroinflammatory responses and exploring therapeutic exploitation of Gpr109a.

Current ideas for immunomodulatory therapeutic targets are summarised in **Table 1.14**; with research targeting inflammatory and anti-inflammatory transcription factors, and the pathways and receptors/ion channels upstream of these transcription factors.<sup>110</sup>

<b>Table 1.14: Summary of experimental data for potential therapeutic targets NF-κβ, Nrf2, and the JAK-STAT3 pathway</b>				
<b>Name of target</b>	<b>Treatment</b>	<b>Model/ Culture conditions</b>	<b>Treatment details</b>	<b>Results</b>
<b>NF-κβ</b>	Baicalein <sup>111</sup>	Rat cerebral I/R injury model of ischemia: MCAO.	Daily baicalein (200 mg/kg) for 7 days.  Does not distinguish microglia from (peripheral) macrophages.	<ul style="list-style-type: none"> <li>• Reduced neurobehavioral deficits.</li> <li>• Reduced brain infarct volume from 18.99% to 7.41%.</li> <li>• Suppressed NF-κβ signaling by reducing IκBα phosphorylation and nuclear translocation of NF-κβ-p65 which reduced release of pro-inflammatory cytokines: IL-6, IL-18, and TNF –α.</li> </ul> Immunofluorescence of ischemic penumbra: <ul style="list-style-type: none"> <li>• Reduction in microglia/macrophage expression of M1 markers CD16 and CD86</li> <li>• Increased expression of M2 markers CD163 and CD206</li> </ul>
<b>Nrf2</b>	ALGERNON2 <sup>112</sup>	Male mice, 8/9 wks.  MPTP injection or LPS injection	Intraperitoneal injection. MPTP four times 20 mg/kg (10 ml/kg) 2 h intervals  LPS once daily 4 days 1 mg/kg	<ul style="list-style-type: none"> <li>• ALGERNON2 rescues neurodegeneration following MPTP and LPS administration.</li> <li>• ALGERNON2 suppresses cytokine production upon LPS stimulation via Nrf2. Proven by knockdown studies with siRNA.</li> <li>• ALGERNON2 increases the Nrf2 pool for nuclear translocation proposed to be sufficient to rescue neurodegeneration <i>in vivo</i>.</li> </ul>
<b>JAK2-STAT3</b>	SC99 <sup>113</sup>	Cerebral ischemia  MCAO <i>in vivo</i>  Oxygen-glucose deprivation <i>in vitro</i> (OGD)	Intracerebro-ventricular injection 10 mmol/L, 15 uL	<ul style="list-style-type: none"> <li>• Phosphorylated JAK2-STAT3 (p-JAK2-P-STAT3) upregulated in acute phase of cerebral ischemia.</li> <li>• During acute phase SC99 reduced levels of p-JAK2-p-STAT3 in the penumbra cortex as shown by western blotting.</li> <li>• Downregulated p-JAK2-p-STAT3</li> <li>• Prevented nuclear translocation in primary microglia OGD cultures.</li> <li>• Inhibiting JAK2-STAT3: reduced infarct volume, ameliorated neurological deficit, decreased brain edema, reduction in neural apoptosis and neural degeneration.</li> <li>• SC99 promoted M1-&gt;M2.</li> <li>• MCAO induced M1 (CD16<sup>+</sup>), but also M2 (CD206<sup>+</sup>) to a lesser proportion.</li> <li>• SC99, <i>in vitro</i> microglia: reversal of M1 markers.</li> <li>• SC99: M2 proteins (iNOS, TNF-α, IL-1β) increased, M1 (arginase1, IL-4, and IL-10) cytokines decreased.</li> <li>• Same effect for <i>in vitro</i> OGD microglia</li> </ul>
ALGERNON2: Altered generation of neurons 2; IκBα:nuclear factor of Kappa light polypeptide gene enhancer in B cells inhibitor, alpha; JAK2-STAT3: Janus Kinase signal transducer and activator of transcription pathway; MCAO: middle cerebral artery occlusion; MPTP: 1-Methyl-4-phenyl-1,2,3,6-tetrahydropyridine, Nrf2:Nuclear Factor Kappa Beta; OGD: oxygen-glucose deprivation, simulating ischaemia; SC99: a novel specific inhibitor targeting JAK2-STAT3 pathway.				

NF- $\kappa$ B is a transcription factor shown to activate microglia to M1 phenotype <sup>114,115</sup>. NF- $\kappa$ B translocates to the nucleus where it triggers an inflammatory response, releasing inflammatory cytokines: IL-18, IL-6, TNF $\alpha$  <sup>111</sup>. Inhibitors of the NF- $\kappa$ B pathway include baicalein and glycine. In a rat model of ischemic stroke, baicalein was shown to significantly reduce neurobehavioral deficits and brain infarct volume <sup>111</sup>. Baicalein suppresses NF- $\kappa$ B signalling through reducing I $\kappa$ B $\alpha$  phosphorylation and the nuclear translocation of NF- $\kappa$ B-p65. Suppressing the NF- $\kappa$ B signalling pathways reduced the release of pro-inflammatory cytokines IL-6, IL-18, and TNF $\alpha$ . Immunofluorescence treatment of the ischemic penumbra after baicalein treatment shows a significant reduction in microglia/macrophage expression of the M1 markers CD16 and CD86, whilst increasing M2 markers CD163 and CD206. A limitation to this investigation was that they did not distinguish between microglia and peripheral macrophages.

The Janus Kinase signal transducer and activator of transcription (JAK-STAT) is part of an inflammatory pathway, amongst many that lead to the NF- $\kappa$ B pathway, and as such is a target for therapies. Signal transducer and activator of transcription (STAT) proteins are a family of proteins of which the pro-inflammatory transcription factor STAT3 belongs.

STAT3 can be targeted by therapeutics. STAT3 inhibitors, such as SC99, have been suggested to promote microglial transition from M1 to M2 <sup>116</sup>. During the acute phase of cerebral ischemia the levels of phosphorylated JAK2-STAT3 (p-JAK2-p-STAT3) were upregulated. During this acute phase, SC99 treatment reduced levels of p-JAK2-p-STAT3 in the penumbra cortex as shown by decreased protein expression by western blotting. SC99 downregulated levels of p-JAK2-p-STAT3 and prevented translocation from cytoplasm to the nucleus in primary microglia OGD cultures. Inhibiting the JAK2-STAT3 pathway reduced

infarct volume, ameliorated neurological deficit, decreased brain oedema, and reduced neuronal apoptosis and neural degeneration (**Table 1.14**).

In addition, SC99 reduced overall levels of inflammation by promoting the transformation of microglia from M1 to M2. Whilst MCAO reliably induced M1 (CD16<sup>+</sup>) microglia, it also induced M2 (CD206<sup>+</sup>) cells, although to a lesser extent. When *in vitro* microglia were treated with SC99 there was a reversal in this expression of M1 markers. In addition, upon SC99 treatment the levels of M1-associated proteins (iNOS, TNF- $\alpha$ , IL-1 $\beta$ ) increased and M2-associated proteins (Arg1, Il-4, and Il-10) decreased. The same effect was mimicked *in vitro* for OGD-treated microglia.

The Nrf2 is also a target for immunomodulatory agents. Nrf2 is considered to be a “master regulator of endogenous cytoprotective antioxidant and anti-inflammatory signalling pathways <sup>117</sup>”. In a mouse model of chronic cerebral hypoperfusion, induced by bilateral carotid artery stenosis (BCAS), more extensive white matter pathology was evident in Nrf2 knockout mice (Nrf2<sup>-/-</sup>) compared to wild-type. Alongside the more extensive white matter pathology, increased levels of microgliosis and astrogliosis were also seen in Nrf2<sup>-/-</sup> <sup>117</sup>.

Altered generation of neurons 2 (ALGERNON2) is a proposed therapeutic targeting the Kelch-like ECH-associated protein 1 (Keap1)-Nrf2 pathway (**Table 1.14, Figure 1.3**). ALGERNON2 rescued degenerating neurons (neuroinflammation-induced) by increasing the pool of cytoplasmic Nrf2. This increased Nrf2 cytoplasmic pool was thought to suppress cytokine production by inflammatory (LPS activated) microglia. A Nrf2 siRNA knockout mouse model was used to demonstrate these effects were Nrf2-mediated <sup>118</sup>.

Like ALGERNON1 Gpr109a agonists act upstream of the Keap1-Nrf2 pathway except with the addition of the NF- $\kappa$ B-I $\kappa$ B $\alpha$  complex (Fig 1.3) Gpr109a ligands have been shown to reduce NF- $\kappa$ B-mediated inflammation. These ligands include beta hydroxyl butyric acid

(BHBA), niacin, monomethyl fumarate (MMF) and dimethyl fumarate (DMF). All ligands have been shown to induce anti-inflammatory effects in peripheral immune cells *in vitro*. Vitamin B3 includes both niacin and its amide form nicotinamide and both are candidates for the treatment of neurodegenerative disease. Niacin acts independently of the Nrf2 pathway; whilst nicotinamide acts independently of the Gpr109a. Activation of Nrf2 has potential to affect the NF- $\kappa$ B pathway indirectly by increasing anti-oxidant defence and decreasing the rate of degradation of the I $\kappa$ B- $\alpha$  complex. These molecules may be acting synergistically when taken in the oral form of vitamin B3 <sup>119</sup>.

### **1.11. Neuroimmunomodulatory agents in clinical trials**

There are relatively few drugs in the pipeline for neurodegenerative conditions. The World Health Organisation (WHO) states there are 170 drugs in the pipeline for AD worldwide compared with 433 for diabetes and 6,833 for malignant neoplasms. This disparity is attributed to the high risk of failure in AD drug development programmes. This is largely because drug targets are less well defined for neurodegenerative diseases. Using the U.S. Food and Drug Administration (FDA) ClinicalTrials.gov website, Cummings *et al.* <sup>120</sup> noted that of those 170 drugs in development, 121 are in clinical trials. Of those in phase 2 or phase 3, the proportion targeting inflammation/infection/immunity is: 11/55 (20%) and 3/17 (18%), respectively.

The naturally occurring Gpr109a ligand niacin has attracted interest as an immunomodulatory therapeutic. Niacin skewed macrophage polarisation from M1 to M2 phenotype in both *in vitro* (RAW264.7 mouse peripheral macrophage cell line) and *in vivo* experiments (Patients with Parkinson's disease). Microglia would be predicted to respond similarly to peripheral macrophages, although this is not fully established. Niacin is in

widespread use clinically, reducing the necessity and cost of drug development programmes.

Two neuroimmunomodulatory compounds of particular interest are ALZT-OP1 a co-formulation of cromolyn + ibuprofen and Azeliragon a RAGE antagonist <sup>121,122</sup>. Both target microglial activation to attenuate inflammation and modulate microglial activation to clear A $\beta$  plaques. They have progressed to phase 3 clinical trial after success in phase 1 and 2 trials (**Table 1.15**). Of particular interest is ALZT-OP1 as both formulations are NICE and FDA approved non-invasive medications repurposed for the treatment of AD. This reduces the cost of drug development, as safety data are already in place.

<b>Table 1.15: Potentially neurotherapeutic agents in clinical trials, with suspected neuroimmunomodulatory action</b>			
<b>Agent</b>	<b>Phase, target</b>	<b>Mechanism of action, rationale</b>	<b>Previous findings</b>
<b>ALZT-OP1 (cromolyn + ibuprofen)</b>	Phase3 – active  Alzheimer's disease (AD)	Cromolyn (mast cell stabiliser): a repurposed asthma drug  Ibuprofen: anti-inflammatory drug  Modulation of microglial activation to promote clearance of A $\beta$ plaques and reduce inflammation.	<ul style="list-style-type: none"> <li>• Pre-clinical <i>in vivo</i> data, mouse: cromolyn alone (or +ibuprofen) reduced A<math>\beta</math> and induced neuroprotective microglial activation state favouring clearance of A<math>\beta</math> via phagocytosis <sup>121</sup></li> <li>• Phase 1 clinical trial showed cromolyn+ibuprofen is safe and well tolerated</li> <li>• CSF levels of cromolyn and ibuprofen are sufficient to clear the estimated daily amyloid production of 17.7 ng and the associated inflammatory response <sup>122</sup></li> </ul>
<b>Azeliragon</b>	Phase3 – recruiting  AD	RAGE antagonist.  RAGE is expressed on the surface of astrocytes and microglia  Aim is to reduce amyloid transport in the brain and to reduce inflammation	<ul style="list-style-type: none"> <li>• Phase 2b, Burstein <i>et al.</i> <sup>123</sup>: mild to moderate AD</li> <li>• Azeliragon slowed cognitive decline</li> <li>• Higher plasma levels of Azeliragon saw slower rate of cognitive decline, with even low doses being favoured over placebo</li> </ul>
<b>Gpr109a ligands</b>	Phase2  Parkinson's disease (PD)	Activation of Gpr109a, preventing activation of NF- $\kappa$ B, thereby skewing phenotypic switching from M1 to M2	<ul style="list-style-type: none"> <li>• Post-mortem PD samples: GPR109a expression increased in substantia nigra</li> <li>• Microglia were co-localised with this GPR109a stain <sup>87</sup></li> <li>• RAW264.7 , LPS-treated: niacin reduced translocation of NF-<math>\kappa</math>B</li> <li>• RAW264.7 pre-treated with niacin before LPS: reduced pro-inflammatory cytokine release (1L-16, IL-6, TNF-<math>\alpha</math>) and rise in anti-inflammatory cytokine IL-10 <sup>124</sup></li> <li>• Randomised controlled trial, Parkinson's disease (n = 42): low dose niacin skewed macrophage polarisation from M1 to M2 through Gpr109a activation <sup>125</sup>.</li> </ul>
A $\beta$ : amyloid beta; ALZT-OP1: co-formulation of cromolyn+ibuprofen; CSF: cerebral spinal fluid; Gpr109a: G-coupled protein receptor 109a; NF- $\kappa$ B: Nuclear Factor kappa-light-chain-enhancer of activated B cells, RAW264.7: mouse peripheral macrophage cell line			



### 1.12. Ligands of the Gpr109a receptor may have therapeutic potential

Gpr109a ligands have been shown to have therapeutic potential for both non-neurological and neurological diseases. Two clinically used ligands for Gpr109a exist; niacin and DMF with its metabolites; DMF-GSH and monomethyl fumarate (MMF). Niacin is a clinically recognised therapy for the treatment of the autoimmune disorder psoriasis and the nutrient deficiency disorder pellagra. Pellagra is the result of severe niacin and/or Tryptophan deficiency which has three characteristic clinical symptoms; diarrhoea, dermatitis, and dementia. Pellagra is most commonly seen in malnourished patients, however other risk factors for niacin deficiency are nervous anorexia, AIDS, cancer, chemotherapy, Crohn's disease, and alcoholism <sup>126–128</sup>. Patients with Pellagra may show psychiatric symptoms such as depression, paranoia, suicidal and aggressive behaviours that are resolved with niacin supplementation <sup>129</sup>.

These claims have limited supporting evidence, as they are taken from only a handful of cases that were successfully treated with niacin (**Table 1.16**). In 2006 a suspected case of alcoholic induced pellagra with reduced niacin serum concentration was resolved with nicotinamide therapy <sup>130</sup>. Similar case was reported in 2008 when a malnourished 45 year old man who showed delusional parasitosis (mistaken strongly held belief that parasites have infested one's own body), skin lesions, and recent history of persistent diarrhoea was diagnosed with pellagra. This man was treated with B-complex capsule at 50 mg of niacin per day. After 4 days the patient's delusional parasitosis had improved, over 2 weeks the man's skin lesions had also improved <sup>131</sup>. More recently in 2012 a case report showed a 45 year old patient displaying the classical symptoms of dermatitis, dementia, and diarrhoea making a full recovery 75 days post niacin treatment <sup>132</sup>. In 2013 <sup>133</sup> a 56 year old male

showed mild confusion, memory disturbances, apathy, spastic quadriparesis, myoclonic jerks, and myoclonus. He was found to have low serum levels of niacin. The cause of these symptoms was thought to be alcoholic induced pellagra encephalopathy. Doctors treated the patient with niacin at 300 mg/day through a nasogastric tube. Myoclonic jerks were diminished within 4 days and a month later weakness and ataxia had fully improved. The realisation that pellagra was a disorder of niacin deficiency and that psychiatric symptoms could be ameliorated with niacin treatment inspired researchers to consider niacin and other Gpr109a ligands in the treatment of neurological disease. DMF/MMF is an approved treatment for MS and was shown to reduce peripheral immune cell damage on the central nervous system, although whether there is any activity on microglial cells remains unclear

134–138

<b>Table 1.16: Clinical use of Gpr109a ligands</b>				
<b>Date and ref</b>	<b>Treatment</b>	<b>Disease</b>	<b>Clinical details</b>	<b>Outcome</b>
<b>2006</b> <sup>130</sup>	Niacin	Pellagra encephalopathy	Alcoholism for 30 years, Decreased serum concentration of niacin.	Full recovery
<b>2008</b> <sup>131</sup>	Niacin	Pellagra	Malnourishment, delusional parasitosis, skin lesions, diarrhoea, 45 year old male, treatment with B-complex capsule 50 mg/day.	Full recovery. Delusional parasitosis improved after 4 days, Over 2 weeks skin lesions improved, No diarrhoea post niacin treatment.
<b>2012</b> <sup>139</sup>	Niacin	Pellagra	45 year old, dermatitis, diarrhoea, dementia.	Recovery 75 days after niacin therapy
<b>2013</b> <sup>140</sup>	Niacin	Alcoholic pellagra encephalopathy	Alcoholism 30+ years, 56 year old male, mild confusion, memory disturbances, apathy, spastic quadriparesis, myoclonic jerks, serum niacin levels low.	Dramatic improvement 3-4 days post niacin therapy, with myoclonic jerks disappearing. A month later weakness and ataxia improved.
<b>2018</b> <sup>137</sup>	DMF/MMF (dimethyl fumarate, monomethyl fumarate)	Multiple sclerosis		Reduce peripheral immune cell damage
Abbreviations; DMF: Dimethyl Fumarate, MMF: Monomethyl Fumarate				

Although there is a lack of evidence for Gpr109a ligands generating therapeutic benefits through microglial activation, there are some preclinical data from rodents indicating that these ligands can directly activate microglia, altering their behaviour and/or phenotype (**Table 1.17**).

<b>Table 1.17 Experimental evidence for Gpr109a ligands directly affecting microglia</b>				
<b>Gpr109a ligands</b>	<b>Target</b>	<b>Disease</b>	<b>Source/ disease model/ culture/ clinical details</b>	<b>Impact</b>
<b>Niacin</b>	Gpr109a	MS <sup>70</sup>	Primary mouse (6-8 wks).  HCA2 <sup>-/-</sup> knockout mice.  Young and adult/ aged human microglia.	Enhanced microglial phagocytosis of myelin debris.  Effects seen in both aged and young human microglia as well as mouse microglia.
<b>MMF</b>	not declared (nd) <sup>104</sup>	nd	Primary rat microglia, <i>in vitro</i>	<ul style="list-style-type: none"> <li>• No effect on phagocytic activity of untreated, LPS treated, or IL-4 treated microglia.</li> <li>• MMF had no impact on the regulation of inflammatory or anti-inflammatory markers in either LPS or IL-4 treated microglia.</li> </ul>
	nd <sup>100</sup>	nd	Primary rat microglia, <i>in vitro</i>	<ul style="list-style-type: none"> <li>• Greater levels of MMF in the brain after oral dosing.</li> <li>• MMF increased expression of Nrf2 associated response genes similar to DMF however fewer overall genes.</li> <li>• MMF did not suppress genes associated with NF-<math>\kappa</math>B signalling.</li> <li>• MMF did not alter cytokine profile or NO levels, suggesting it had no impact on microglial activation.</li> </ul>
<b>DMF</b>	nd <sup>141</sup>	nd	Primary rat microglia, <i>in vitro</i>	<p>No effect on phagocytic activity of untreated, LPS treated, or IL-4 treated microglia.</p> <p>6 h post-LPS treatment:</p> <ul style="list-style-type: none"> <li>• Upregulation of M1 inflammatory markers; TNF<math>\alpha</math> and iNOS</li> <li>• Upregulation of anti-inflammatory markers; IGF-1, Tgf-1B, Mrc-1.</li> </ul> <p>DMF pre-treatment of surveillant (M0) and LPS activated (M1) microglia lead to increased expression in MCR1 (6 h only), and IGF-1 (3 h and 6 h)</p>
	nd <sup>100</sup>	nd	Primary rat microglia, <i>in vitro</i>	<ul style="list-style-type: none"> <li>• The conjugate DMF-GSH not DMF itself is present in the brain.</li> <li>• DMS-GSH is present in lower amounts than MMF.</li> <li>• Expression of IL-1<math>\beta</math>, TNF-<math>\alpha</math>, IL-22b, STAT-1, and CD40 was reduced.</li> <li>• DMF acted independently of Nrf2.</li> <li>• It is thought that DMF exerts a wider range of biological activity.</li> </ul>
Abbreviations; DMF: Dimethyl Fumarate, DMF-GSH: DMF-glutathione conjugate, IGF-1: MCR:1MMF: Monomethyl Fumarate, nd: not declared (no explicit declarations that intended effects are solely mediated by activation of Gpr109a, or otherwise), NO:				

Gpr109a (hydroxycarboxylic acid receptor 2, Hcar2) is a G protein-coupled receptor within the nicotinic acid receptor family. Gpr109a activation produces anti-inflammatory effects

through reducing NF- $\kappa$ B activity which has strong association with pro-inflammatory activation. In addition, Gpr109a activation elevates levels of Pparg which is associated with M2-activation and neuroprotection in neurological diseases as demonstrated in a Parkinson's model <sup>142</sup>.

**Fig 1.3** is a schematic of Gpr109a and Nrf2 pathways and mediated effects. It has been shown in peripheral immune cells that Gpr109a ligands may induce (i) Gpr109a-dependent anti-inflammatory effects, and (ii) Gpr109a independent anti-oxidative and cytoprotective effects through Nrf2. Although both mechanisms are not fully understood they hold the potential to reduce damage to neurons and offer clinical benefit. It has been shown that microglia express Gpr109a <sup>87</sup> however it is not clear whether microglia respond to Grp109a ligands in similar manner to how peripheral immune cells respond.

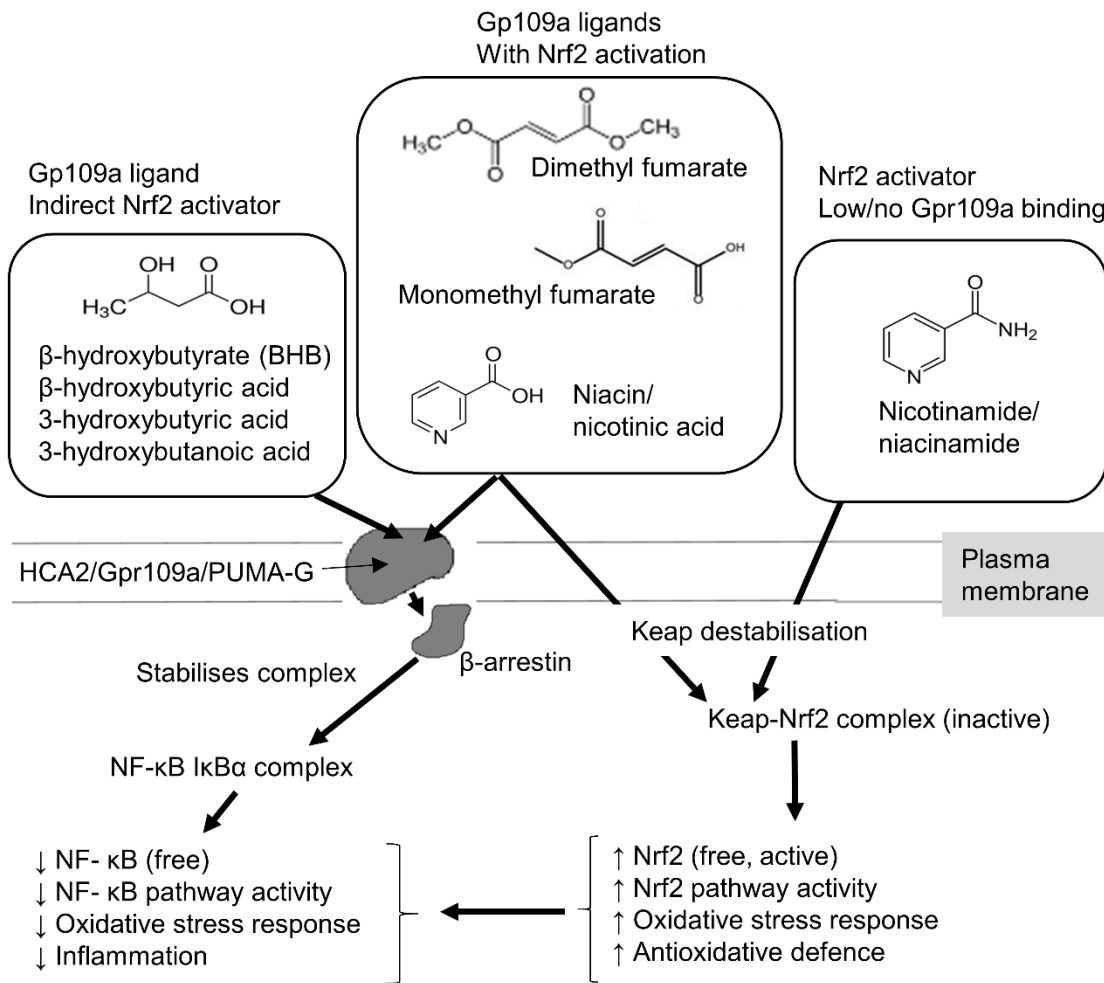


**Figure 1.3: Schematic showing Gpr109a and Nrf2 mediated effects.** Gpr109a ligands bind Gpr109a (AKA HCA2, PUMA-G), producing multiple effects, including release of  $\beta$ -arrestin.  $\beta$ -arrestin stabilises the NF- $\kappa$ B-I $\kappa$ B $\alpha$  complex, reducing levels of free NF- $\kappa$ B, and therefore reducing activity of the NF- $\kappa$ B pathway. This reduces oxidative stress and inflammation. Nrf2 is inactivated by Keap1, and Keap1 can be degraded by monomethyl fumarate (MMF), dimethyl fumarate (DMF), niacin, or nicotinamide (amongst others), releasing active Nrf2<sup>143</sup>. Free Nrf2 promotes anti-oxidative defences. The Nrf2 pathway can indirectly reduce the activity the NF- $\kappa$ B by its anti-oxidative defence coupled with its ability to reduce the degradation of the NF- $\kappa$ B-I $\kappa$ B $\alpha$  complex<sup>119</sup>. Nicotinamide destabilises Keap1, with little to no Gpr109a activation. BHB activates Gpr109a, but can also be metabolised to generate

fumarate, which can then activate Nrf2. BHB, niacin and nicotinamide are all naturally occurring in mammals with normal diets; high concentrations may be used therapeutically. DMF and MMF are synthetic, and used as drugs.

---

Treatment of neurodegenerative disease with Gpr109a ligands would be promising therapy as medications are already in clinical use, hence they are recognised as safe for use, easily obtained, and low cost. There are however outstanding questions on how Gpr109a ligands would be delivered to the brain. Ligands would need to cross the blood brain barrier if they are to target the neurodegenerative process, and this has been shown to be possible for Gpr109a ligands.<sup>136</sup> If oral doses were prescribed, then once ingested they will have an impact on the peripheral tissues potentially causing unwanted side effects that may reduce a patients adherence to treatment, and requiring doses sufficient to raise CNS concentrations to therapeutic levels.

As part of the continued investigation into Gpr109a ligands as neurotherapeutics, fundamental research will be required to establish which neural cells express the Gpr109a receptor, and how they respond to activation. There may be a requirement to develop novel ligands, which lack the broader activities induced by niacin, and MMF, for example. The hypotheses for this study are (i) that Grp109a is expressed by neural immune cells, and (ii) that neural immune cell activity can be modulated by Gpr109a ligands.

### **1.13. Aims and Objectives**

The aim of this thesis is to assess whether Gpr109a ligands affect neural immune cells in ways that could be of therapeutic benefit.

The objectives are:

- Determine whether neural immune cells express the niacin receptor (Gpr109a)
- Assess whether neural immune cells respond to clinically-relevant Gpr109a ligands



## Chapter 2: Materials and Methods

The care and use animals was in accordance with the Animals Scientific Procedures Act of 1986 (UK) with approval by the local ethics committee.

### 2.1. Rationale for experimental design

*In vitro* investigations of microglial behaviour allow for greater experimental control including multiple experimental factors (doses, time-points) being investigated with cells derived from the same source, reducing noise due to biological variation, compared to *in vivo* studies<sup>144</sup>. *In vitro* studies are more cost effective, with ethical benefits from reducing animal usage, as well as reducing suffering inherent to many *in vivo* procedures<sup>145</sup>.

Rodents were chosen, as their genetic and biological characteristics closely resemble those of humans<sup>146</sup>, with the rat immune system sharing many characteristics with humans<sup>147</sup>. Multiple rat models exist for metabolic and neurodegenerative diseases, so hypotheses developed from rat cell culture systems could be translated to *in vivo* models

Several Gpr109a ligands are approved for clinical usage (**Table 2.1**) including niacin (nicotinic acid, NA) and MMF, and so could readily be translated to CNS therapeutic purposes.

<b>Drug</b>	<b>Details</b>	<b>Gpr109a ligand activity</b>	<b>Nrf2 activation</b>	<b>Clinical use</b>
<b>DMF, dimethyl fumarate</b>	Drug names: Tecfidera, BG-12	Reported as inactive. IC <sub>50</sub> :10 µM <sup>107</sup> K <sub>i</sub> is lower than NA and MMF <sup>107</sup>	Yes, via Keap1  Toxicity concerns, including GSH depletion <sup>148</sup>	Relapsing remitting Multiple Sclerosis (2013) <sup>149</sup>  Acts on peripheral immune cells
<b>Fumaderm</b>	Combination: DMF, MEF and MMF	Various, but high affinity	Yes, via Keap1  Toxicity concerns <sup>150</sup>	Psoriasis (1959) <sup>151</sup>  Acts on peripheral immune cells, without immunosuppression
<b>MEF, mono-ethyl fumarate</b>		High affinity EC <sub>50</sub> :26 µM <sup>107</sup> IC <sub>50</sub> :160 nM <sup>107</sup> K <sub>i</sub> :1.3 µM <sup>107</sup>	Yes, via Keap1  Less activity than DMF  Fewer toxic off-target effects than DMF  No GSH depletion <sup>150</sup>	
<b>MMF, mono-methyl fumarate</b>		High affinity EC <sub>50</sub> :9.4 µM <sup>107</sup> IC <sub>50</sub> :70 nM <sup>107</sup> K <sub>i</sub> : 980 nM Greater than DMF <sup>107</sup>	Yes, via Keap1; fewer toxic off-target effects than DMF <sup>150</sup>	
<b>Niacin (NA)</b>	Nicotinic acid  Vitamin B3	Yes EC <sub>50</sub> : ~1 µM <sup>152</sup> 2 µM <sup>107</sup> , ~0.25 µM (HEK-293) <sup>153</sup> ~0.4 µM (rat HM74A) <sup>153</sup> ~0.53 µM  IC <sub>50</sub> :16 nM <sup>107</sup>  K <sub>i</sub> :160 nM <sup>107</sup>  Activates Pparg, which is associated with neuroprotection <sup>154</sup>	Yes	500-2000 mg/day activates Gpr109a  Dietary requirements are 15-20 mg daily
<b>Nicotinamide (Nm)</b>	Niacinamide  Vitamin B3	Very low affinity EC <sub>50</sub> >1000 µM <sup>153</sup> IC <sub>50</sub> ~75.3 µM <sup>153</sup> Does not activate Pparg <sup>154</sup>	Yes	
<b>B-hydroxybutyrate</b>	B-D-hydroxybutyric acid  A ketone body	High affinity	Yes, although seemingly indirectly, after conversion to fumarate <sup>155</sup>	

EC<sub>50</sub>: concentration of drug that produces half the maximal response; IC<sub>50</sub>: half-maximal inhibitory concentration; GSH: glutathione, an anti-oxidant (neutralises reactive oxygen species); Keap1: Kelch-like ECH associated protein 1  
K<sub>i</sub>: inhibitory constant; Pparg: peroxisome proliferator-activated receptor gamma, associated with neuroprotection in Parkinson's Disease; Psoriasis: immune-related skin condition; Relapsing-Remitting Multiple Sclerosis: disease in which peripheral immune cells invade from the blood into the central nervous system, damaging nerve cells.

NA has various other biological effects, besides being a Gpr109a ligand. Nicotinamide (Nm) shares these biological effects, but has very limited Gpr109a ligand activity, as shown by Wise *et al.* (2003); Nm half maximal effective concentration (EC<sub>50</sub>) values were >1,000 μM (~4,000-fold greater than NA) and half maximal inhibitory concentration (IC<sub>50</sub>) was 75.3 (~1,000-fold greater than NA; tested using human adipocyte membranes) <sup>156</sup>.

- EC<sub>50</sub> – Concentration of drug or agonist required to stimulate half-maximal response
- IC<sub>50</sub> – concentration of inhibitory substance (e.g. drug) that is required to inhibit a biological process or response *in vitro* by 50%

Therefore, Nm was included as a control to possibly distinguish Gpr109a-mediated effects from other biological activity.

Biological activity of Gpr109a ligands varies. Tang *et al.* 2008 <sup>157</sup> conducted a head to head comparison of DMF, MEF, MMF, and NA in an A9 cell line transfected to express Grp109a. They used an aequorin assay (measures Ca<sup>2+</sup> signal via luminescence) as a proxy for Gpr109a activation to determine EC<sub>50</sub>. To determine IC<sub>50</sub> a cAMP assay was used (ligands measured according to inhibition of forskolin-induced cAMP synthesis). Tang *et al.* 2008 measured efficacy (expressed as EC<sub>50</sub> value) and affinity (expressed as IC<sub>50</sub> value). Efficacy was used to measure the amount of drug required to elicit the desired effect and affinity to measure how strongly the drug bound its active site. In order of efficacy:

NA            EC<sub>50</sub>    2μM <sup>107</sup> (similar to reports of an EC<sub>50</sub> of 1 μM <sup>158</sup>),

MMF        EC<sub>50</sub>    9.4 μM,

MEF        EC<sub>50</sub>    26 μM,

with DMF reported to be inactive.

In order of affinity:

NA	IC <sub>50</sub>	16 nM,
MMF	IC <sub>50</sub>	70 nM,
MEF	IC <sub>50</sub>	160 nM,
and DMF	IC <sub>50</sub>	10 μM (10,000 nM).

To measure whether MMF and NA interacted at the same binding pocket of the Gpr109a receptor they monitored the displacement of <sup>3</sup>H-labeled NA. K<sub>i</sub> (dissociation constant) values were determined: NA K<sub>i</sub> 160 nM, MMF K<sub>i</sub> 980 nM, and MEF 1,300 nM. DMF showed minimal displacement of <sup>3</sup>H-labeled NA. They concluded that NA, MMF, and MEF all bind to the same binding pocket of Gpr109a receptor, likely explaining their similarities in efficacy and binding affinities.

There is some variation in EC<sub>50</sub> and IC<sub>50</sub> values of NA amongst cell types, with Wise *et al.* 2003<sup>153</sup> reporting EC<sub>50</sub> values of 0.25 μM in human embryonic kidney 293T (HEK 293T) cells and 0.4 μM in rat HM74A cells, and another report of values approximately x4-5 fold less than in a mouse cell line A9<sup>107</sup>. Shen *et al.*<sup>159</sup> demonstrated in Chinese hamster ovary cells (expressing Human Gpr109a) EC<sub>50</sub> values of 0.53 μM, approximately half of that reported by Tang *et al.*<sup>107</sup>. IC<sub>50</sub> values obtained for NA in human adipocytes was slightly higher at 79 nM, being closer to MMF IC<sub>50</sub>: 70 nM<sup>107</sup>. Variation amongst EC<sub>50</sub> values for NA were within 10 fold, ranging from 0.25 μM to 2 μM. These values were comfortably within the concentration range tested for each ligand: 0.015, 0.15, 1.5, 15, 150 μM.

These variations may be due to the different species, cell types, and source organs being used. Effective concentrations may vary between cell types, and therapeutic dosages should be determined experimentally for each target cell type.

## 2.2. Antibodies, equipment, and reagents used

Antibodies and reagents are summarised in **Tables 2.2, 2.3 and 2.4.**

Primary antibody	Antigen/marker	Supplier	Product code	Dilution	Species, type
Arg1	Arginase 1	SLS	SAB4200508-200UL	1:400	Mouse
GFAP	Glial fibrillary acidic protein	Dako	Z0334	1:500	Rabbit
Puma gamma (Gpr109a)	G-coupled protein receptor 109a	abcam	ab180642	1:200	Rabbit
Iba1	Iba1	abcam	ab5076	1:1000	Goat
Nox2 (gp91 phox)	Nox2	abcam	ab180642	1:400	Rabbit

Fluorophore	Target species	Host species	Manufacturer	Product code	Dilution
Cy3	anti-Goat	Donkey	Stratech	705-165-147-JIR	1:200
Cy3	anti-Rabbit	Donkey	Stratech	711-165-152-JIR	1:200
Cy3	anti-Rabbit IgG	Goat	Stratech	111-165-144-JIR	1:200
Cy3	anti-Rat	Goat	Stratech	112-165-167-JIR	1:200
FITC	anti-Mouse	Goat	Stratech	115-545-166-JIR	1:200
FITC	anti-Rabbit	Goat	Stratech	111-095-144-JIR	1:200
FITC	anti-Rat	Goat	Stratech	112-095-167-JIR	1:200
FITC	anti-Mouse	Donkey	Stratech	715-095-151-JIR	1:200
FITC	anti-Rat	Donkey	Stratech	712-095-153-JIR	1:200

Primary antibody	Dilution	Species, type	Fluorophore	Target species	Dilution
Arg1	1:400	Mouse	FITC	anti-mouse	1:200
GFAP	1:500	Rabbit	FITC	anti-rabbit	1:200
Puma gamma (Gpr109a)	1:200	Rabbit	Cy3	anti-Rabbit	1:200
Iba1	1:1000	Goat	Cy3	anti-goat	1:200
Nox2 (gp91 phox)	1:400	Rabbit	Cy3	anti-rabbit	1:200

Product name	Manufacturer	Code	Solvent/Diluent	Storage
Dulbecco's modified Eagle's medium (DMEM) 4.5 g/L glucose (no L-glutamine or sodium pyruvate)	Lonza	12-733f		4°C
Fetal bovine serum (FBS)	Corning	35-079-CV		-20°C
Monomethyl fumarate (MMF)			Neurobasal or D10	1 M, -20°C
Neurobasal	Gibco	21103049		
Niacin			Neurobasal or D10	1 M, -20°C
Nicotinamide	Sigma	N0636-100G	Neurobasal or D10	1 M, -20°C
Paraformaldehyde	Fisher Scientific	11473704	PBS	4% at -20°C
Penicillin streptomycin (PenStrep)	Lonza/SLS	LZDE17-602E		-20°C
Poly-D-Lysine (PDL)	Corning/SLS	354210	PBS	-20°C
Sodium Pyruvate	Lonza	LZBE13-115E		4°C
Triton X-100	Sigma	X100	PBS	
Trypan Blue 0.4%	Fisher Scientific	15250061		
TyrpLE™ Express Enzyme (1X), no phenol red	Fisher Scientific	10573283 (New code – 12604013)		

### **2.3. Preparation of cell adhesion surfaces**

Under aseptic condition using a laminar flow hood coverslips were sterilised within culture plates, by being left in 70% ethanol (20-30 mins). Ethanol was aspirated and the coverslips were washed three times with double distilled water (ddH<sub>2</sub>O). Cell culture plastics and sterile coverslips were coated in poly-d-lysine (PDL) to promote adherent monolayer growth. PDL was incubated on surfaces for 30 mins, aspirated, then surfaces washed with (ddH<sub>2</sub>O) three times. Coverslips were stored in ddH<sub>2</sub>O at room temperature for up to 8 h, or at 4 °C for up to 1 week, with ddH<sub>2</sub>O removed before use.

### **2.4. Dissection, establishing, and maintenance of primary mixed glial, microglial, and astrocyte cultures**

#### **2.4.1. Dissection**

Primary mixed glial cultures were prepared from cerebral cortices of postnatal day 0-3 Sprague-Dawley rats based on an established protocol <sup>160</sup>. The rat brain was dissected into ice-cold Hank's balanced salt solution (HBSS), then, under sterile conditions, the olfactory

bulbs, cerebellum and mid-brain were removed. The cerebral cortices were isolated and rolled gently on an autoclaved hand towel to remove meninges. Cerebral cortices were then mechanically dissociated, and a single cell suspension generated by trituration (Pasteur pipette x30; gauge needle x3; gauge needle x3). This was then sieved (70  $\mu\text{m}$  then 40  $\mu\text{m}$ ), pelleted by centrifugation, and seeded as explained below.

#### **2.4.2. Establishing mixed glial culture protocol**

All three cell types were cultured together under sterile conditions in D10 medium. Usually oligodendrocyte precursor cells (OPCs) are cultured in chemically defined medium (OPC-MM), however pilot experiments show microglia and astrocytes do not tolerate this medium. Mixed glial cultures were grown on PDL coated flasks and maintained in D10 medium (Dulbecco's modified Eagle's Medium (DMEM) supplemented with 10% Fetal Bovine Serum (FBS), 2 mM glutaMAX-1, 1 mM sodium pyruvate, 50 U/ml penicillin, and 50  $\mu\text{g}/\text{ml}$  streptomycin) at 37°C in 5% CO<sub>2</sub>/95% humidified air for 8-10 d, with 50% D10 refresh every 2-3 d. Mixed glial cultures were allowed to reach confluence for 2-3 d, allowing for the stratification of cell layers, with oligodendrocyte precursor cells (OPCs) and microglia being above a bedlayer of astrocytes.

#### **2.4.3. Enriched microglia culture protocol**

After 2-3 d confluency, microglia were isolated by mechanical detachment using a rotary shaker (120 mins at 220 rpm). To maintain pH of the medium, flasks were sealed to maintain 5% CO<sub>2</sub>. Media enriched with microglia was then collected and the cells pelleted

by centrifugation at 1500 rpm, 5 mins. Cell pellet was re-suspended in warm D10 medium and cells were then counted using trypan blue and a Neubauer chamber. Cell density was then adjusted with D10 to  $6 \times 10^5$  cells/cm<sup>2</sup> and applied to PDL-coated coverslips. Cells are left to attach to the coverslips for 24 h and treated the following day.

#### **2.4.4. Enriched astrocyte culture protocol**

Mixed glial culture flasks were sealed with parafilm (to seal headspace) and shaken on a rotary shaker overnight (220 rpm; 37°C). Medium, containing mainly oligodendrocyte precursor cells, was discarded and replenished with fresh D10 medium. Flasks were then placed in an incubator at 37°C in 5% CO<sub>2</sub>/95% humidified air for 1-2 h to re-gas (return to 5% CO<sub>2</sub>). These steps were typically repeated up to 4 times, to deplete non-astrocytic cells, with assessment by light microscopy. Once astrocyte purity was sufficient, flasks were rinsed with PBS then treated with 7 ml of TrypLE™ Express Enzyme (1X), returned to the shaker and observed every 5 mins. TrypLE™ treatment was restricted to 10-15 mins to avoid cellular toxicity. TrypLE™ was collected, along with a PBS rinse of the flasks, and cells pelleted by centrifugation (1500 rpm; 5 mins). Cells were seeded at  $2.0 \times 10^5$  cells/ml in D10 medium at a volume of 300 µl per well and maintained according to the microglia culture protocols.

#### **2.4.5. Cell counting**

To seed cultures at the appropriate density, cell counts were performed using a Neubauer chamber. After mechanical isolation and centrifugation the supernatant was re-suspended in warm D10. A 1:1 mixture of cells:trypan blue was established and trypan blue negative



cells were quantified. Cells were quantified by counting cells touching the top and left lines of Neubauer grid, but not the right or bottom. The number of cells was counted and then multiplied by the dilution factor to give number of cells per mL. Cells were then diluted to the appropriate concentration.

## **2.5. Experimental procedures**

Cells were seeded onto PDL coated coverslips at the appropriate cellular density using protocol mentioned earlier, and were left to incubate overnight at 37 °C in 5% CO<sub>2</sub>/95% humidified air to allow microglia to attach. LPS and Gpr109a ligands (NA, MMF) were prepared to the desired concentration in D10 or neurobasal media. The desired concentrations were based on effective concentrations reported in the literature. Cultures were treated by 100% media change then incubated for 24 h. Samples were then fixed, as described below.

## **2.6. Fixation and Immunocytochemistry**

### **2.6.1. Fixation**

Cells were washed with PBS and subsequently fixed with 4% paraformaldehyde (PFA) at room temperature for 25 mins. PFA has been shown to have minimal impact on microglial morphology compared to other fixatives <sup>161</sup>. PFA was disposed of safely and cells were washed 3 times with PBS. Samples remained in PBS at 4 °C until staining.

### **2.6.2. Staining**

Cells were incubated with blocking solution (5% normal donkey serum in PBS, 0.3% Triton X-100; room temperature; 30 mins). Primary antibody in blocking solution at appropriate

concentrations (**Table 2.2**) was applied and left overnight (4 °C). Samples were washed 3 times for 3 mins with PBS, then incubated in blocking solution (room temperature; 30 mins), then incubated in darkness (2 h) with the appropriate secondary antibody (chosen to match species of primary) in blocking solution (1:200; **Table 2.3, Table 2.4**). Samples were then washed 3 times (3 mins each), and coverslips mounted with mounting medium containing nuclear (4', 6-diamidino-2-phenylindole; DAPI) stain.

## **2.7. Image acquisition for cellular analysis**

### **2.7.1. Fluorescence microscopy**

Immunostained samples were imaged using Nikon (Eclipse 80i or Eclipse Ti) microscope. Images were taken using the Hamamatsu black and white camera and the NIS Elements software. A fixed exposure was used for experimental repeats. Images taken in channels appropriate for FITC ( $\lambda \sim 494\text{-}520$  nm), Cy3 ( $\lambda \sim 560\text{-}570$  nm), and DAPI ( $\lambda \sim 460$  nm). Images were taken at either x20 or x40 magnification, with standardised exposure settings for each channel. Fields of interest (FOI) were chosen at random (without looking down the microscope or at a monitor) while moving the objective across the cultures, taking care to not overlap fields. If an FOI was chosen with large clumps of cells, identified by nuclear DAPI staining, where cells are overlapping and difficult to differentiate, the FOI was rejected, and another chosen. A minimum of 3 micrographs/fields were taken for every treatment condition, within every culture.

Micrographs were exported raw, without alterations to brightness or contrast (NIS Elemental software, Nikon; Tag Image File Format, TIF). Separate colour micrographs were later merged and brightened, to aid identification of cell margins.

### **2.7.2. Justification of markers**

The following markers and their expression have been analysed in this study; Arginase-1, Iba1, and Nox2.

Iba1 is an ionized calcium binding adaptor molecule 1 exclusively expressed by macrophages and microglia. It is a key protein in microglial membrane shuffling and phagocytosis. Expression of Iba1 was found to be upregulated in activated microglia as seen after facial nerve axotomy, ischemia and when microglia were associated with A $\beta$  plaques<sup>162</sup>. However, its effectiveness as a marker of M1 has recently been questioned by researchers. In a diabetic retinopathy model microglial activation occurred independent of an increase in Iba-1 expression. Furthermore, in post-mortem coronal brain slices a population of microglial cells in deep subcortical lesions became Iba1<sup>-</sup>/CD68<sup>+</sup><sup>163</sup>

Iba1 was used in this study despite it potentially lacking the ability to be an effective M1 marker as it is still an effective identification marker of microglia. Additionally, it is uniformly expressed throughout microglial cytoplasm and processes allowing for clearer imaging and morphological analysis<sup>164</sup>. Due to conflicting findings regarding Iba1's effectiveness as a M1 marker this study used it in conjunction with the M1 marker Nox2.

NADPH oxidase isoform 2 (Nox2) is an isoform of the Nox family. Single cell RNA sequencing identified Nox2 as the most highly expressed isotype in human and mouse microglia<sup>165</sup>. It, however, is not microglial specific as it can be expressed by infiltrating macrophages<sup>166</sup>.

Nox2 mediates oxidative burst in response to pro-inflammatory stimuli or during phagocytosis by catalysing the production of free radicals, ROS and NOS, by oxidising nicotinamide adenine dinucleotide phosphate (NADPH) to NADP<sup>+</sup> and H<sup>+</sup>. This is typically M1 mediated. In a TBI injury mouse model Nox2 knockout saw reduced microglial M1 activity whilst increasing M2 activity. Additionally, it has been used as a marker in neuropathology; ischemic stroke, AD, PD, and HIV-induced dementia.

There is little research conducted on Gpr109a ligand impact on microglial Nox2 expression. In a heart failure with preserved ejection fraction model BHB downregulated Nox2/GSK-3 $\beta$  pathway in cardiac Treg cells improving diastolic function, fibrosis, and cardiac remodelling<sup>167</sup>. Using a human retinal pigment epithelium cell line (APRE-19) and human colonic tissue cell line (CCD-841) Gpr109a ligands 4-hydroxynonenal (4-HNE), niacin, 3-OHBA were shown to interact with Nox4 isoform of the Nox family. In APRE-19 cells high concentrations of Gpr109a ligands induced G $\beta\gamma$  mediated apoptosis increasing Ca<sup>2+</sup> and superoxide levels; which were blocked by knockdown of Gpr109a and Nox4 genes, and inhibition of G $\beta\gamma$  and intracellular Ca<sup>2+</sup>. In APRE-19 and CCD-831 cells low concentrations of Gpr109a ligands mediated G $\alpha_i$ -dependent anti-inflammatory process; down regulated expression of pro-inflammatory cytokines IL-6 and IL-8 which was inhibited by cAMP analogue<sup>168</sup>.

Nox2 was chosen as it is thought to be an effective marker of M1, and the predominant isoform expressed by microglia. Despite being the predominant isoform expressed by microglia there is limited research on Gpr109a ligand impact on microglial expression of Nox2. The promising effects of BHB on the expression of Nox2 in cardiac Treg cells and Nox4 in APRE-19 and CCD-831 cells suggests a potential for Gpr109a ligand interaction with microglial Nox2. Therefore, investigating Gpr109a ligand impact on microglial expression of Nox2 will provide novel findings.

Arginase-1 (Arg1) is widely recognised for its ability to identify M2 and in particular M2a. Arg1 is associated with cell proliferation, ion channel function, neuroprotection, and collagen formation to promote wound healing. Arg1 also has additional anti-inflammatory roles by ammonia detoxification through urea cycle and outcompeting inducible nitric oxide synthase (iNOS) inhibiting the production of NO. Microglia with greater Arg1

expression were correlated with increased A $\beta$  plaque phagocytosis and decreased deposition amyloid plaque load <sup>169</sup>

Arg1 was chosen as a marker of M2 expression due to its accepted ability to identify M2 microglia. Additionally, similar to Nox2 there is lack of research into the impact of Gpr109a ligands and Arg1 activity, therefore, conducting research in Gpr109a ligand impact on Arg1 will provide novel findings.

## **2.8. Analyses**

### **2.8.1. Cell counts**

Micrographs were analysed using open-source ImageJ software (NIH, USA). To derive cell counts and culture purity data each nucleus in the micrograph was scored positive or negative for DAPI immunostaining. Some image analyses were performed by supervised undergraduate students (named and thanked in Acknowledgements).

### **2.8.2. Morphometric analysis and antibody analysis**

Individual cells in micrographs had their outline drawn (**Fig 2.1**), and ImageJ was used to derive morphometric data (**Table 2.6**) and integrated density values, as a proxy for antibody staining intensity. Blank (background) integrated density values were derived by outlining large regions without cells, and measuring as with cells (5 regions per micrograph, per colour channel). The mean intensity of the background, multiplied by cell area, indicates

fluorescence expected if no cell was present, and this is subtracted from the cell integrated density. These data were used to calculate corrected total cell fluorescence (CTCF) values for each cell:

$$\text{CTCF} = \text{cell integrated density} - (\text{cell area} \times \text{mean fluorescence of background readings})$$

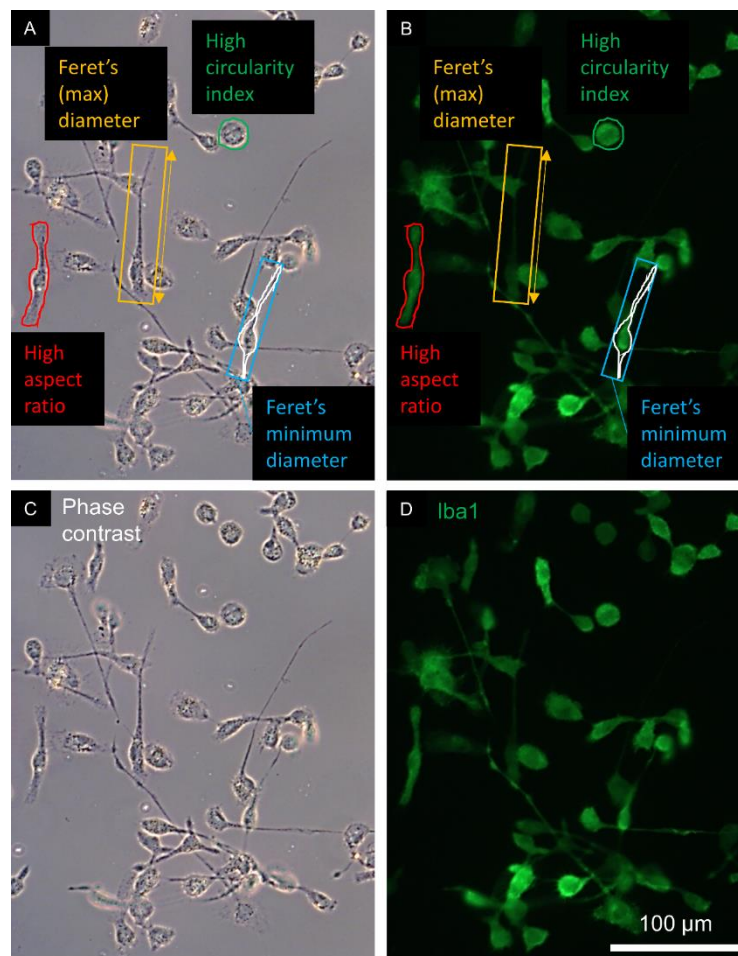


**Figure 2.1: Examples of cell morphometrics using fluorescence micrographs.**

(A) Phase contrast micrograph of microglial culture showing various morphologies. Red, green and white outlines of individual cells are representative of ImageJ delineation of cells. After delineation, ImageJ automatically determined cell area, perimeter, Feret's diameter (maximum and minimum), with aspect ratio and circularity being calculated afterwards. Red and green indicate cells with high and low aspect ratios (low and high circularity indices), respectively. Orange rectangle (longest axis) indicates how Feret's diameter would be determined. Blue rectangle (shortest axis) indicates Feret's minimum diameter. (B) Same labels on counterpart fluorescence micrograph from which integrated density values would be measured: summation of brightness for all pixels within cell outline. (C-D) Same images without labelling. Note range of morphologies and staining intensities.

<b>Measurement</b>	<b>Definition / Calculation</b>	<b>Morphometric information</b>
<b>Area</b>	Total number of pixels present in a singular cell. Expressed in square micrometres.	Indication of cell size.
<b>Circularity Index</b>	$4\pi \times (\text{area}/\text{perimeter}^2)$ . 0 (linear polygon) to 1 (perfect circular object)	Indication of how circular a cell is
<b>Feret's (Maximum) Diameter</b>	The distance between the two furthest points of an object	Greatest distance covered by cell
<b>Feret's Minimum Diameter</b>	Perpendicular distance between the closest-possible two parallel lines, that touch the object edge while the entire object is between them	Narrowest region of cell
<b>Feret's Aspect ratio</b>	Feret's Maximum divided Feret's Minimum	Shows how elongated the cell is
<b>Perimeter</b>	Outline length of cell. Measured in microns	Related to size and ramification

### **2.8.3. Statistical analyses and data presentation**

Prism software (GraphPad, USA) was used to generate graphs and perform statistical analyses. All data described within text and displayed in graphs is mean  $\pm$  SD (standard deviation) unless otherwise stated. With sufficient datapoints ( $n = 8$  or more), data were tested for normality using a D'Agostini-Pearson test (Prism statistical software, GraphPad, USA).

Morphometry normality testing, unaltered values: For 24 concentrations across 6 morphological measurements, each with 9 replicates, only 8 (of 144) individual conditions failed the D'Agostini-Pearson normality test, and these were not clustered/grouped within any particular treatment or measurement. Therefore, for all these datasets, one-way ANOVA was used, with Dunnett's multiple comparisons test.

Cell count normality testing was normalised within each culture: only 2 of 24 concentrations (9 replicates each) failed the D'Agostini-Pearson normality test. Therefore, for all these datasets, one-way ANOVA was used, with Dunnett's multiple comparisons test. CTCF normality testing, normalised within each culture: for culture-average values, only 3 or 6 replicates were available, preventing reliable normality testing. Therefore, for all these datasets, non-parametric Kruskal-Wallis tests were used, with Dunn's multiple comparisons test. For individual cell values, the majority of datasets failed the D'Agostini-Pearson normality test. Therefore, for all these datasets, non-parametric Kruskal-Wallis tests were used, with Dunn's multiple comparisons test.



# Chapter 3: Do neural immune cells express Gpr109a, and respond to Gpr109a ligands?

## 3.1. Introduction

As outlined in Chapter 1, neural immune cells may be responsive to Gpr109a ligands in ways that influence immune responses and may be exploited therapeutically. Microglia and astrocytes would be the most obvious target cells, being immunocompetent cell types. There are limited reports relating to Gpr109a expression by glial cells, and/or to glial responses to Gpr109a ligands.

Of the few studies assessing Gpr109a expression in microglia, one suggests that only 20% of microglia may be Gpr109a<sup>+</sup><sup>91</sup>, with other studies mentioning Cd11b<sup>+</sup>/Gpr109a<sup>+</sup> cells, but not indicating the percentage of Cd11b<sup>+</sup>/Gpr109a<sup>-</sup> cells<sup>87,88</sup>. Another study suggests elevated Gpr109a mRNA expression post-LPS treatment, but without detailed analysis<sup>89</sup>.

The only known studies of astrocyte-specific expression of Gpr109a indicate that GFAP<sup>+</sup> mouse cells were negative for Gpr109a, before and after simulated stroke (MCAO)<sup>88</sup>, and that only 7.5% of GFAP<sup>+</sup> rat cells in the rostral ventrolateral medulla were Gpr109a<sup>+</sup><sup>91</sup>.

Given these minimal and conflicting data, this Chapter will assess whether the immune competent glial cells of the CNS express Gpr109a, and whether clinically relevant Gpr109a ligands induce responses in these cells.

### **3.2. Objectives**

To identify Gpr109a expression in the following neural cells:

- Primary rodent microglia
- Primary rodent astrocytes

To identify rat primary microglia response to LPS, as a positive inflammatory control

To identify rat primary microglia responses to Gpr109a ligands:

- Niacin (nicotinic acid, NA)
- Monomethyl fumarate (MMF)

To assess whether microglia responses to niacin may be unrelated to Gpr109a activation, nicotinamide (Nm) was used as a control. Nicotinamide has similar metabolic functions (e.g. as vitamin B3) but has little or zero activity as a Gpr109a ligand. Therefore, differences in microglial responses to niacin and nicotinamide may be indicative of Gpr109a activation.

### 3.3. Results

#### 3.3.1. Primary rat microglia and astrocyte cultures successfully established

Mixed glial cultures were established, and high purity fractions of microglia and astrocytes derived, as judged by morphology and cell type-specific marker expression: Microglial cultures were >98% Iba1<sup>+</sup>. Astrocyte cultures were >98% GFAP<sup>+</sup>.

#### 3.3.2. Primary rat microglia expressed Gpr109a

Microglial cultures were stained using a serial dilution of a Gpr109a antibody and a null-primary control (Fig 3.1). No immunostaining was evident without Gpr109a primary antibody, but clear (nuclear-localised) immunostaining was evident at 1:200 antibody dilution, and staining intensity decreased as the primary antibody was diluted (Fig 3.2).

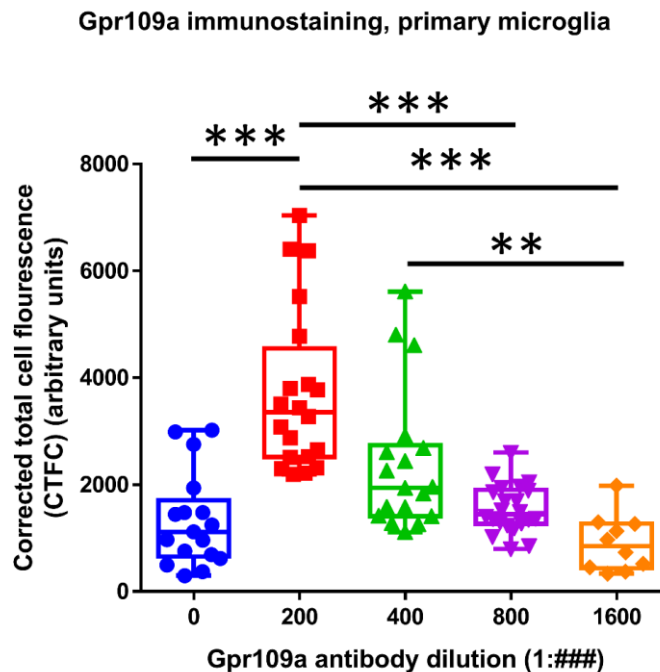


**Figure 3.1. Gpr109a immunostaining of primary microglia was dose-dependent.** Box-and-whisker plots (all datapoints displayed) of individual microglial cells measured within cultures stained for Gpr109a at different antibody dilutions. 0 dilution indicates null primary (secondary antibody only). Kruskal-Wallis ( $p < 0.0001$ ) with Dunn's post-test; \*\* $p < 0.01$ , \*\*\* $p < 0.001$ ; bars indicate groups being compared;  $n = 10-22$ .

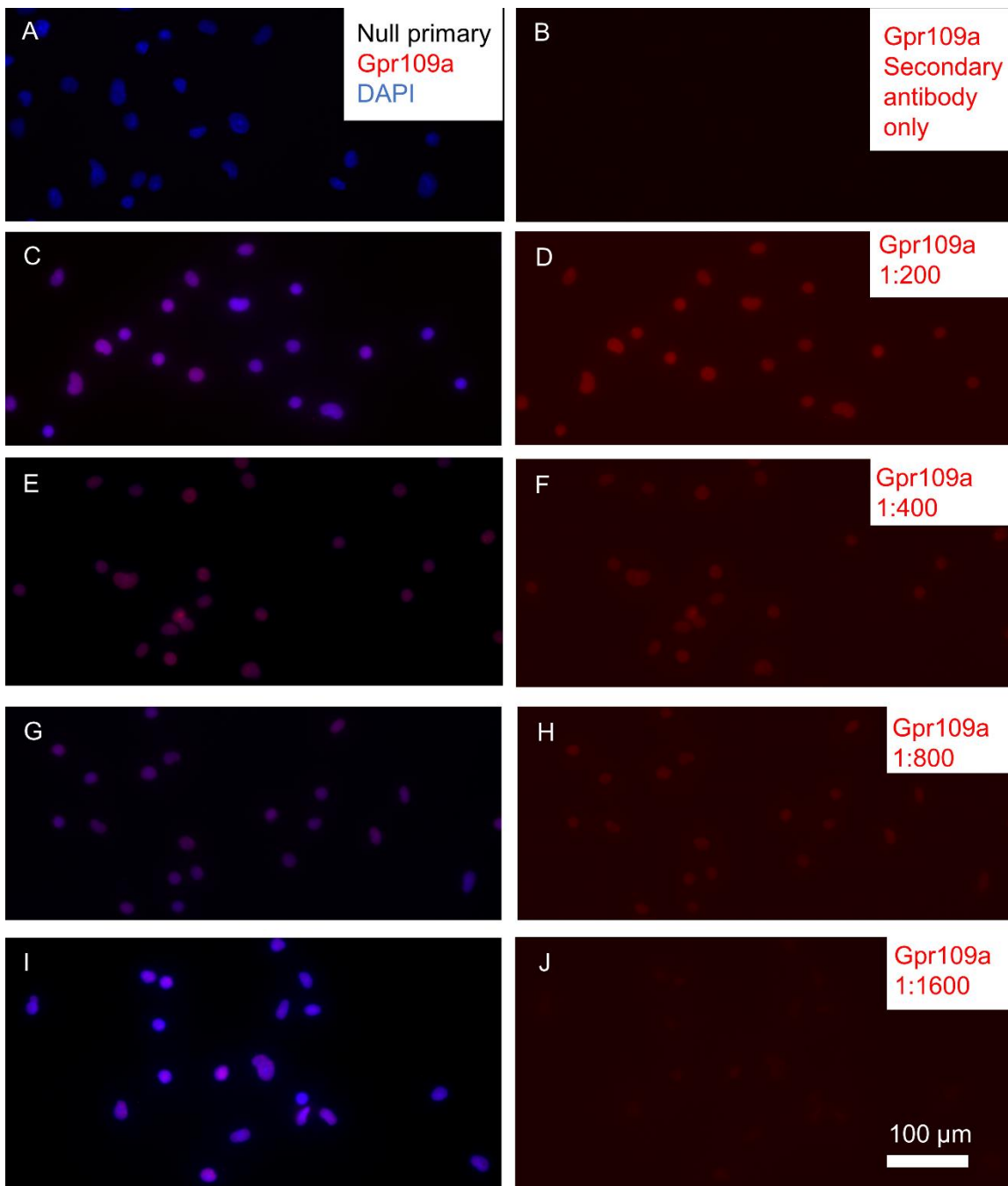


**Figure 3.2. Intensity of Gpr109a immunostaining in primary microglial cultures was antibody-dose-dependent.** Fluorescence micrographs of microglial cultures, immunostained for Gpr109a, with and without DAPI-merges. (A-B) Secondary antibody only, without Gpr109a primary antibody, showed no immunostaining. (C-D) Primary Gpr109a antibody staining was obvious at 1:200 dilution, and nuclear-localised. (E-J) Serial dilution of Gpr109a showed diminishing intensity of immunostaining. Note that Gpr109a staining is almost entirely nuclear-localised.

### **3.3.3. Impact of LPS, NA, Nm, and MMF treatment on microglial cell count**

Cell counts were normalised to untreated controls within each culture, and separate controls were included for each treatment (LPS, niacin, nicotinamide, MMF), so that they would be cultured within the same plate.

Based on statistical testing, cell counts for primary microglial cultures were unaffected by treatment with niacin, nicotinamide or MMF, but at the greatest LPS concentration tested, there was a reduction in cell number (**Fig 3.3**). Lower concentrations of LPS did not affect cell number at the level of statistical significance, though there was a downwards trend with increasing concentration.

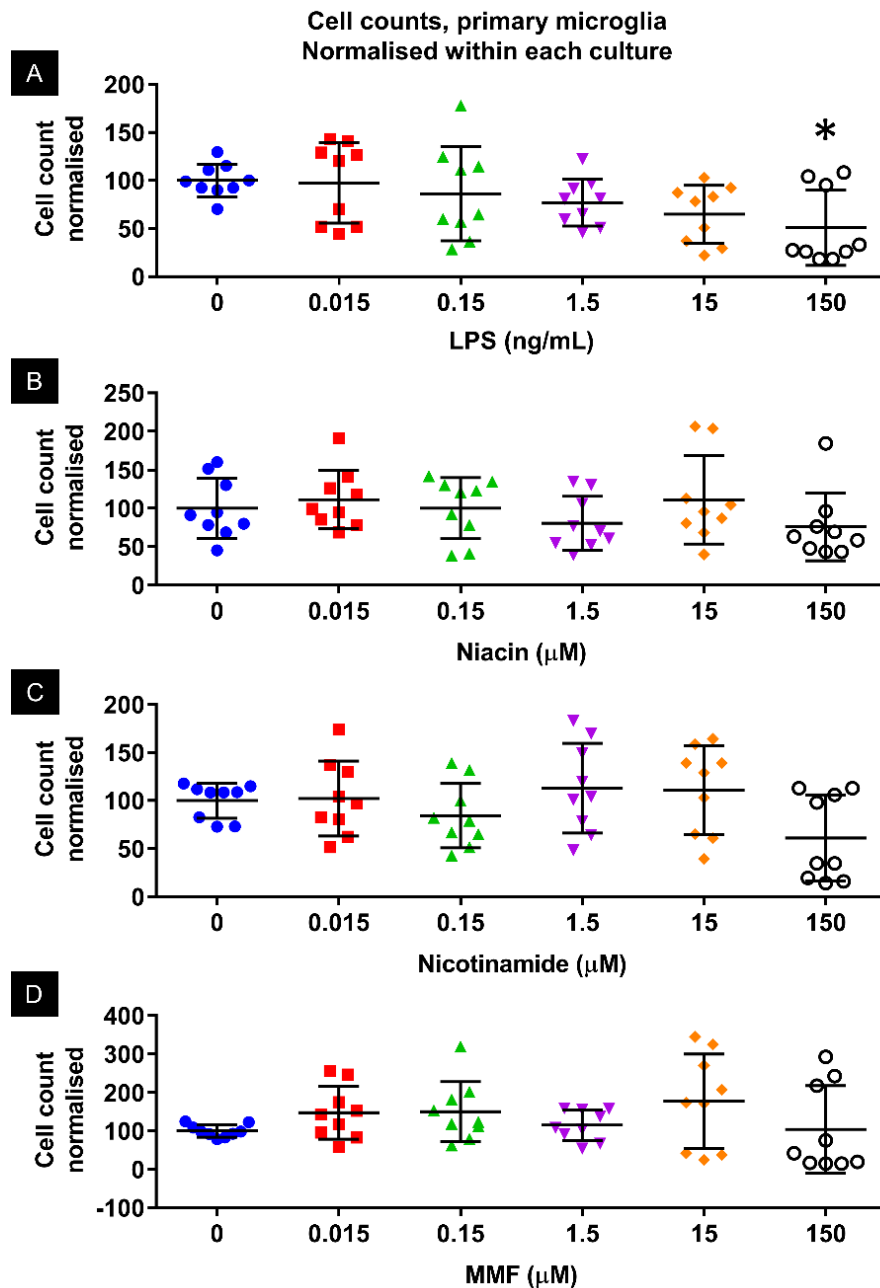


**Figure 3.3. Microglial cell counts were reduced at high LPS concentration, but unaltered by Gpr109a ligands.** Cell counts were normalised within each culture. At the greatest concentration of LPS tested, cell numbers were decreased (A;  $F_{(5, 48)} = 2.648$ ,  $p = 0.034$ ). Cell numbers were unaltered for niacin (B;  $F_{(5, 48)} = 1.115$ ,  $p = 0.365$ ), nicotinamide (C;  $F_{(5, 48)} = 2.238$ ,  $p = 0.066$ ) and MMF (D;  $F_{(5, 48)} = 1.258$ ,  $p = 0.298$ ) treated cultures. One-way ANOVA with Dunns post-test; \* $p < 0.05$  versus control;  $n = 9$ .

#### **3.3.4. Microglial response to LPS: Iba1 and Nox2 fluorescence**

The intensity of cellular immunostaining was measured using integrated density, then corrected total cell fluorescence (CTCF) was calculated. For each treatment condition, 3 cultures were stained for Iba1 plus Nox2, 3 cultures for Nox2 plus Arg1, and 3 cultures for Arg1 plus Gpr109a. Analysis was performed by collating all cell values, across all micrographs, and plotting as box-and-whisker plots: Box indicates mean, within 25th and 75th percentiles, while whiskers extend to 5th and 95th percentiles, with outliers indicated by coloured shapes (**Fig 3.4**). Iba1 was elevated at 1.5 ng/ml, while Nox2 was elevated at 1.5 and 15 ng/ml, with Iba1 and Nox2 both decreased at 150 ng/ml. Increased Iba1 and Nox2 expression (LPS 15 ng/ml) was apparent in fluorescence micrographs (**Fig 3.5**). Reduced cell numbers and small cell bodies are also seen at 150 ng/ml LPS (**Fig 3.5F**).

Iba1, Nox2; LPS; primary microglia  
 Corrected fluorescence, individual cells; whiskers show 5-95%  
 Normalised to control within each culture

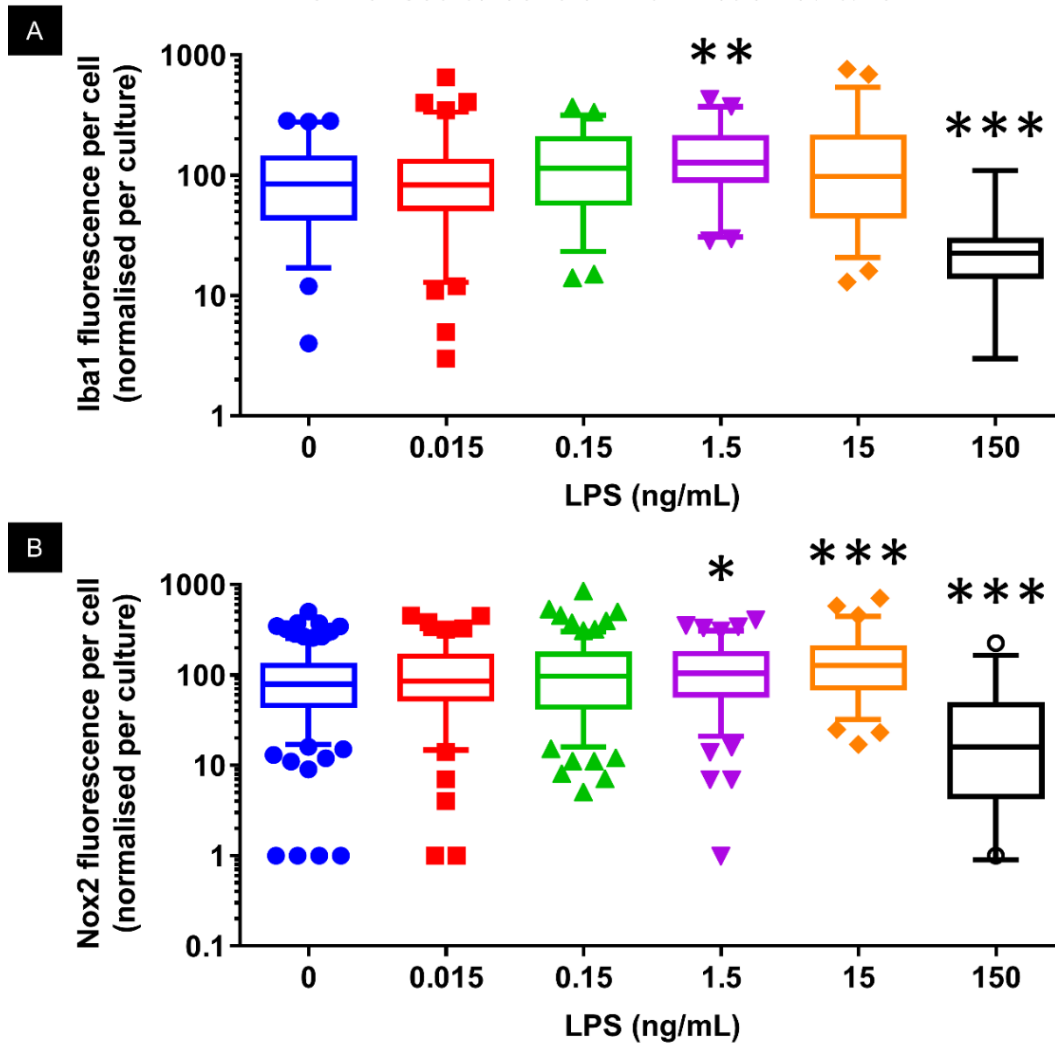


**Figure 3.4. LPS increased microglial staining intensity for Iba1 and Nox2, except at the greatest concentration, which reduced both.** Box (25-75<sup>th</sup> percentiles) and whisker plots (5-95<sup>th</sup> percentiles) show individual cell staining intensity, normalised to the average of the control within each culture, with outliers shown as symbols. Log y axis. (A) Iba1 intensity varied with LPS treatment ( $p < 0.0001$ ;  $n = 315$ ), being greater than control at 1.5 ng/ml LPS, but lower at 150 ng/ml. (B) Nox2 intensity varied with LPS treatment ( $p < 0.0001$ ;  $n = 729$ ), being greater at 1.5 and 15 ng/ml LPS, but lower at 150 ng/ml. Kruskal-Wallis with Dunn's post-test; \* $p < 0.05$ , \*\* $p < 0.01$ , \*\*\* $p < 0.001$  versus control.



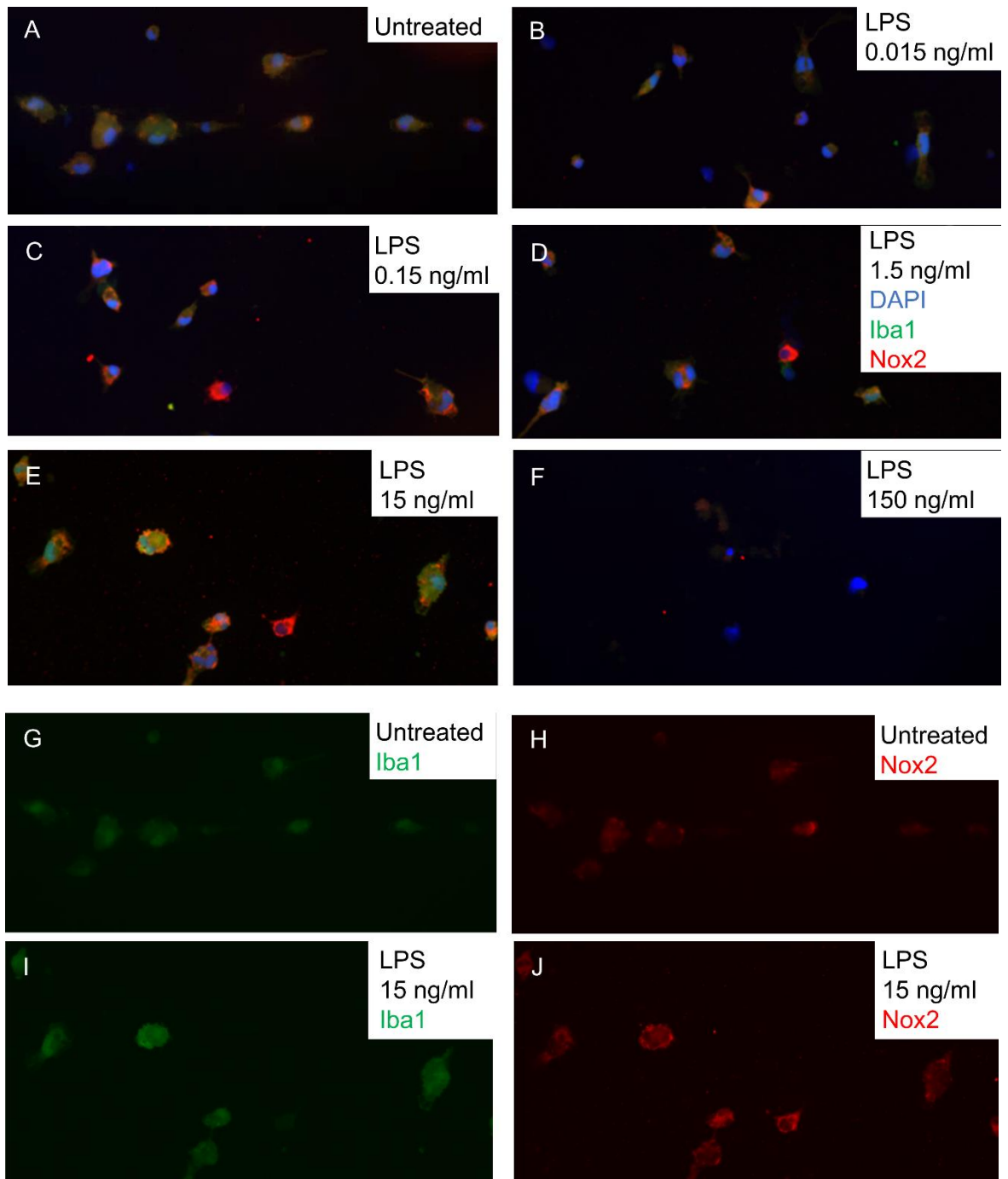


**Figure 3.5. Microglia were Iba1<sup>+</sup> and Nox2<sup>+</sup>, with and without LPS treatment.** Merged fluorescence micrographs of control (A) and LPS-treated (B-F) microglial cultures. Raw, un-brightened, unmerged micrographs show staining intensity was notably weaker in untreated control cultures (G, H) compared to LPS at 15 ng/ml (I, J). At the greatest concentration of LPS tested, Iba1 and Nox2 staining was often weak, and cells were notably smaller, and reduced in number (F).

### 3.3.5. Microglial response to LPS: Arg1 and Gpr109a fluorescence

LPS concentration (0.15 – 150 ng/mL) was associated with decreased Gpr109a expression, with Arg1 also reduced at 150 ng/mL (**Fig 3.6**). Reduced Arg1 expression is evident in micrographs, which also show that Gpr109a expression remained nuclear localised with and without LPS treatment (**Fig 3.7**).

**Arg1, Gpr109a; LPS; primary microglia**  
 Corrected fluorescence, individual cells; whiskers show 5-95%  
 Normalised to control within each culture

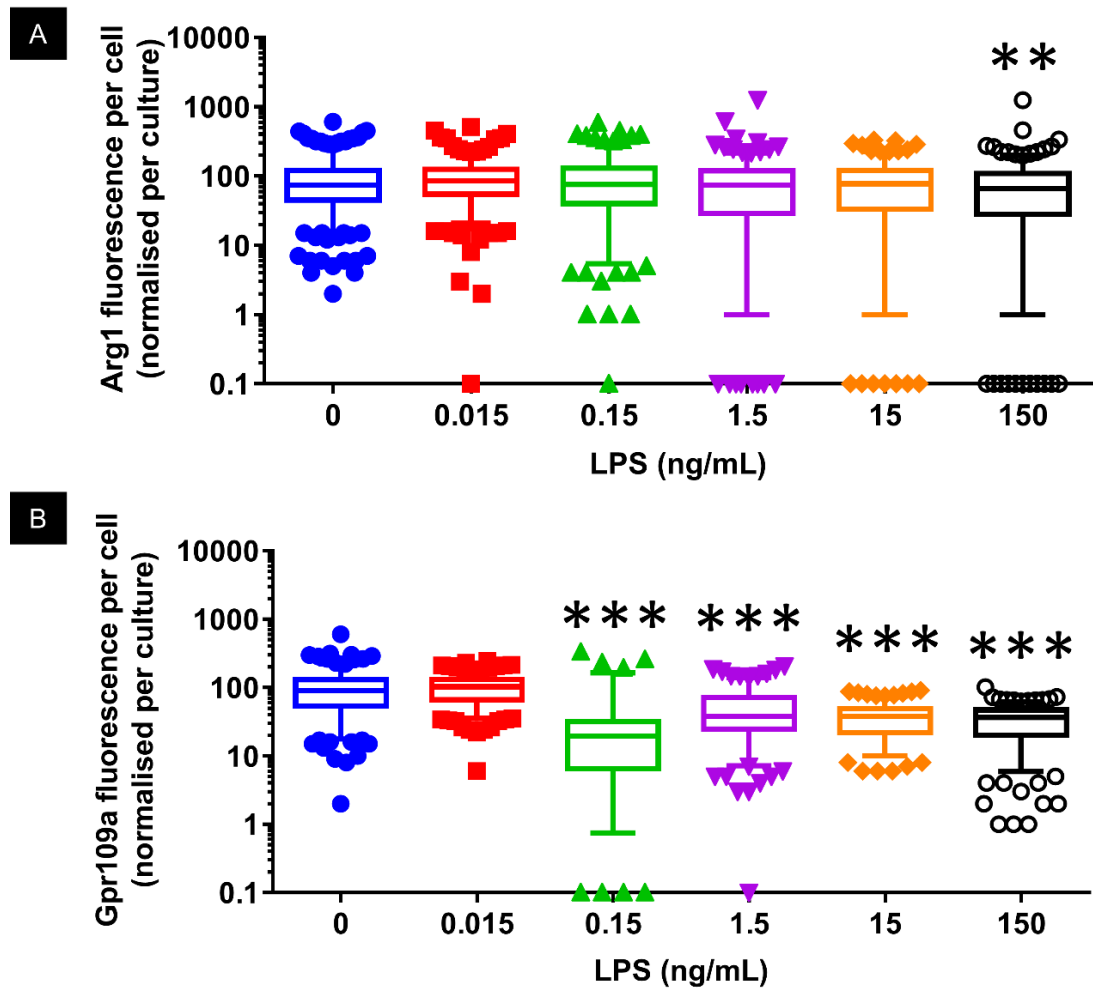


**Figure 3.6. LPS decreased microglial staining intensity for Gpr109a and Arg1.** Box (25-75<sup>th</sup> percentiles) and whisker plots (5-95<sup>th</sup> percentiles) show individual cell staining intensity, normalised to the average of the control within each culture, with outliers shown as symbols. Log y axis. (A) Versus control, Arg1 intensity decreased at 150 ng/ml ( $p < 0.0001$ ;  $n = 1,601$ ). (B) Gpr109a intensity varied with LPS treatment, decreasing at concentrations greater than 0.015 ng/mL ( $p < 0.0001$ ;  $n = 1,186$ ). Kruskal-Wallis with Dunn's post-test; \*\* $p < 0.01$ , \*\*\* $p < 0.001$  versus control.

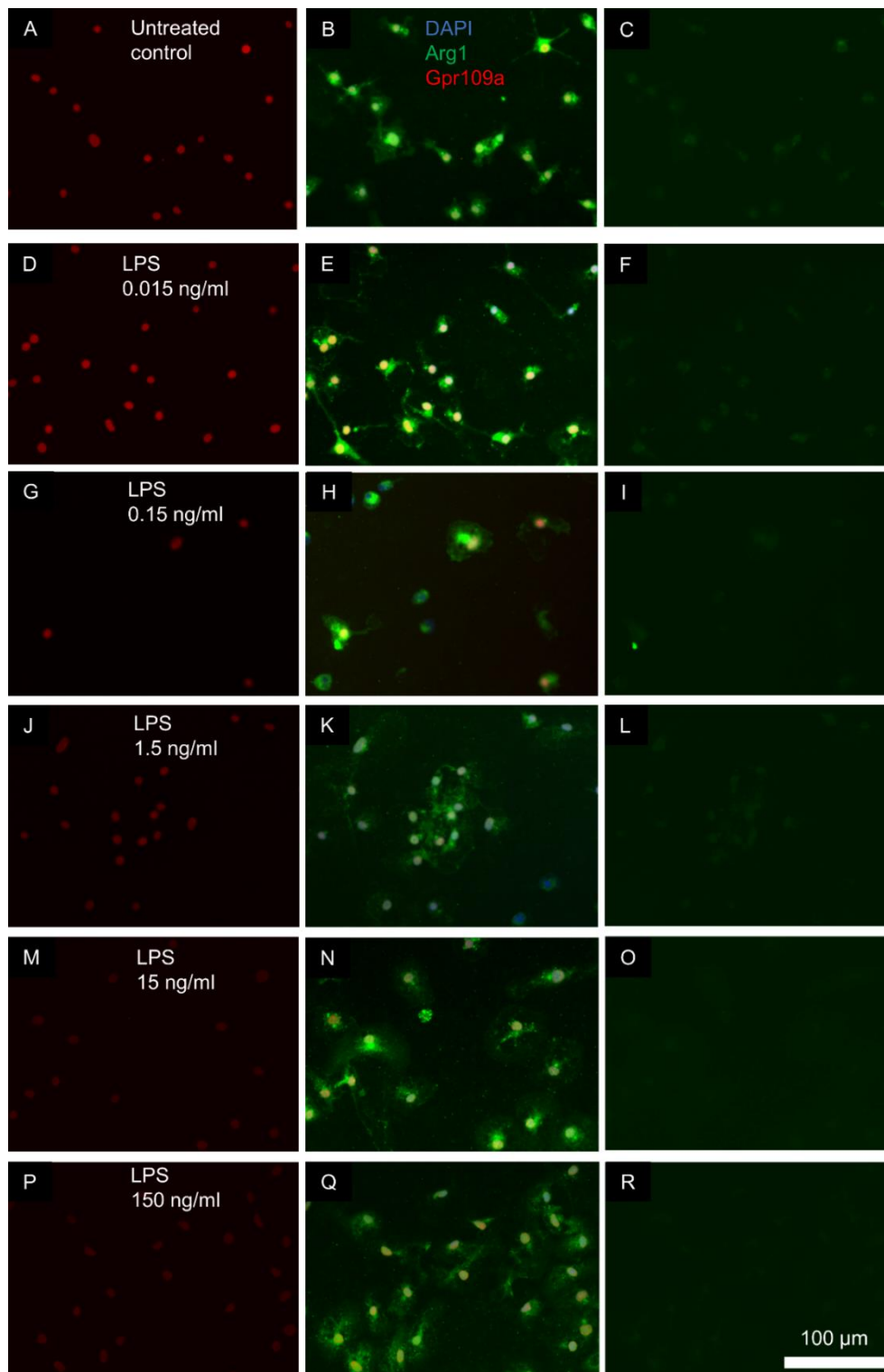


**Figure 3.7 LPS treatment of microglial cultures diminished Gpr109a and Arg1 expression.** Fluorescence micrographs of microglial cultures stained for Gpr109a, Arg1 and DAPI (left column: Gpr109a only, right column: Arg1 only, central column: both merged with DAPI). Untreated cultures (A-C) were Arg1<sup>+</sup>/Grpr109a<sup>+</sup>, with nuclear-localised Gpr109a staining. LPS-treated cultures (D-R) also showed nuclear Gpr109a expression, which was diminished at 0.15 – 150 ng/mL. Arg1 was only detectably diminished at 150 ng/mL (Q-R).

### 3.3.6. Microglia responses to niacin (NA): Iba1 and Nox2 expression

Iba1 staining intensity increased at 1.5  $\mu\text{M}$  NA, but at no other concentration (Fig 3.8). Nox2 staining intensity was greater at 0.015  $\mu\text{M}$  NA, but at no other concentration (Fig 3.8).

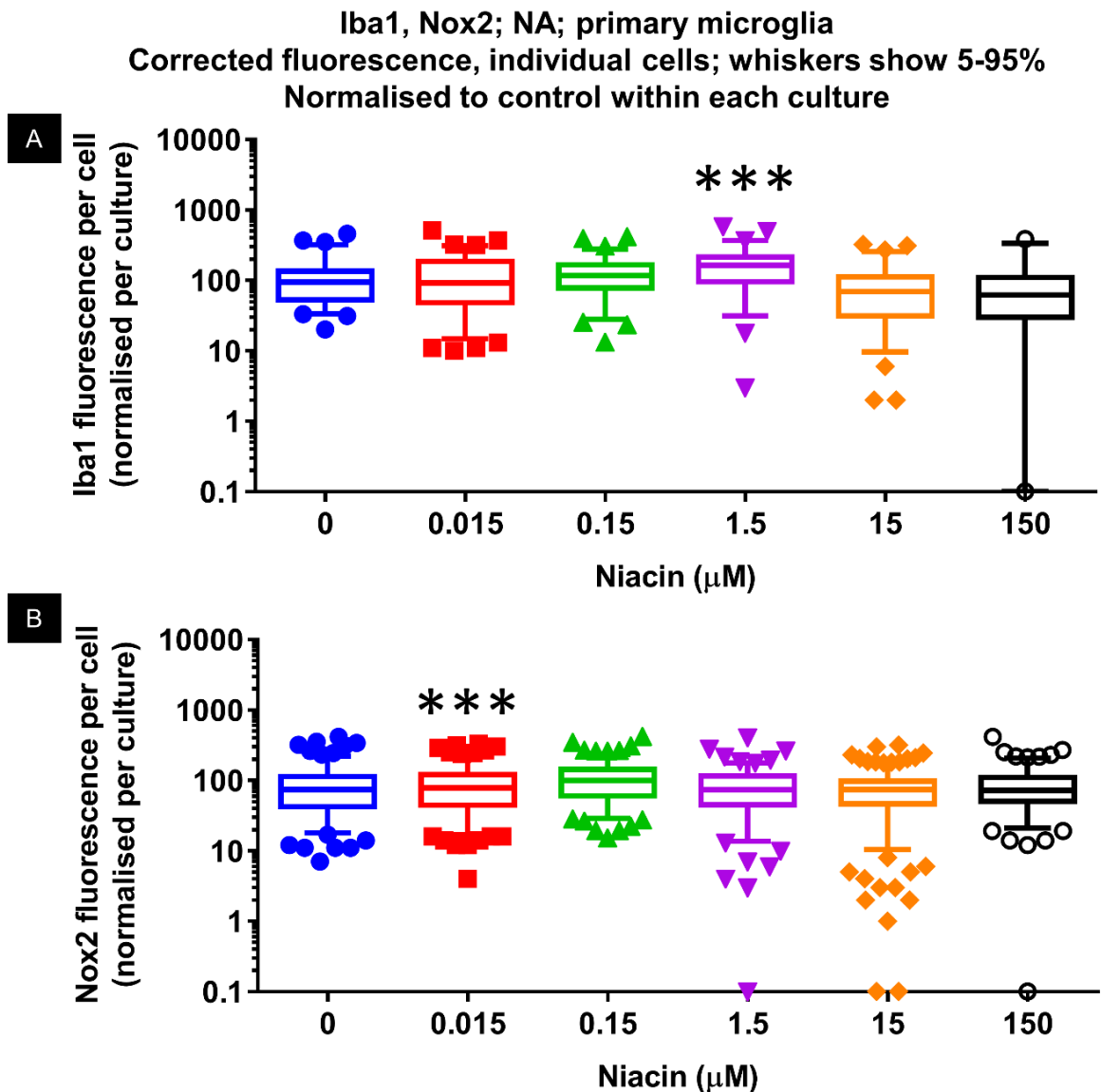


**Figure 3.8 Niacin-treated microglial cultures, staining intensity for Iba1 and Nox2.** Box (25-75<sup>th</sup> percentiles) and whisker plots (5-95<sup>th</sup> percentiles) show individual cell staining intensity, normalised to the average of the control within each culture, with outliers shown as symbols. Log y axis. (A) Versus control, Iba1 intensity was increased at 1.5  $\mu\text{M}$  niacin but at no other concentration ( $p < 0.0001$ ,  $n = 413$ ). (B) Versus control, Nox2 intensity was elevated at 0.015  $\mu\text{M}$  niacin, but not at any higher concentration ( $p = 0.0001$ ,  $n = 1,066$ ). Kruskal-Wallis with Dunn's post-test; \*\*\* $p < 0.001$  versus control.

### 3.3.7. Primary rat microglia responses to niacin (NA): Arg1 and Gpr109a

Following treatment with NA there was a slight increase in Arg1 intensity at 0.015  $\mu\text{M}$  and 0.15  $\mu\text{M}$ , but not at 1.5, 15, and 150  $\mu\text{M}$  (Fig.3.9). NA very slightly increased Gpr109a staining intensity at 0.015, 0.15, 1.5, and 15  $\mu\text{M}$ , but not at 150  $\mu\text{M}$  (Fig 3.9).

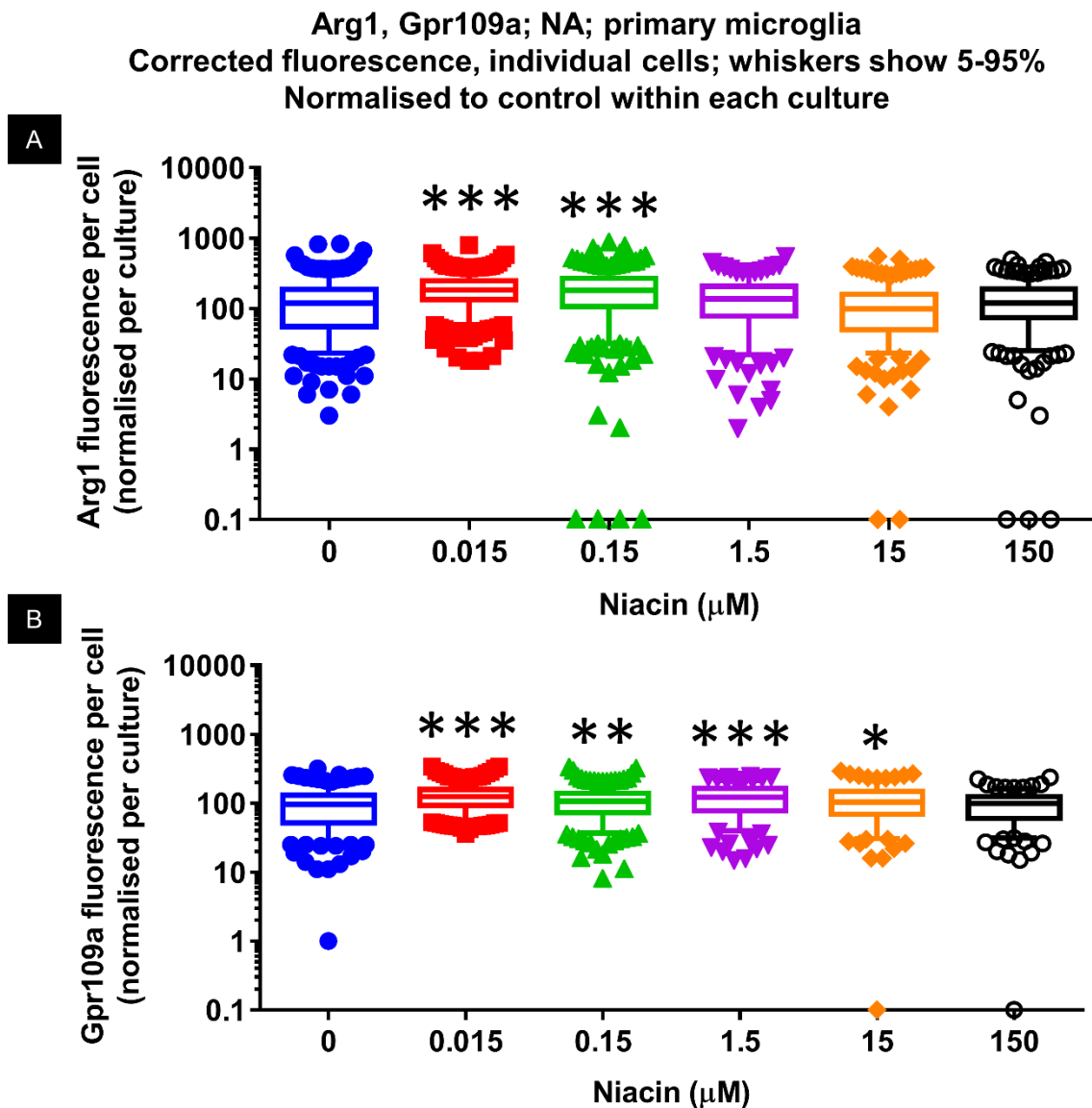


**Figure 3.9. Niacin-treated microglial cultures, microglial staining intensity for Arg1 and Gpr109a, in niacin-treated cultures.** Box (25-75<sup>th</sup> percentiles) and whisker plots (5-95<sup>th</sup> percentiles) show individual cell staining intensity, normalised to the average of the control within each culture, with outliers shown as symbols. Log y axis. (A) Versus control, niacin concentrations 0.015  $\mu\text{M}$  and 0.15  $\mu\text{M}$  niacin elicited an increase in Arg1 intensity ( $p < 0.0001$ ,  $n = 2257$ ). (B) Versus control, niacin concentrations of 0.015  $\mu\text{M}$ , 0.15  $\mu\text{M}$ , 1.5  $\mu\text{M}$ , and 15  $\mu\text{M}$  niacin elicited an increase in Gpr109a intensity ( $p < 0.0001$ ;  $n = 1609$ ). Kruskal-Wallis with Dunn's post-test; \* $p < 0.05$ , \*\* $p < 0.01$ , \*\*\* $p < 0.001$  versus control.

### 3.3.8. Microglia responses to nicotinamide (Nm): Iba1 and Nox2

There was an increase in Iba1 intensity at 1.5  $\mu\text{M}$  Nm, but not at any other concentration. Nox2 staining intensity was greater at 1.5  $\mu\text{M}$  Nm, lower at 150  $\mu\text{M}$  Nm, but unchanged at all other concentrations (Fig 3.10).

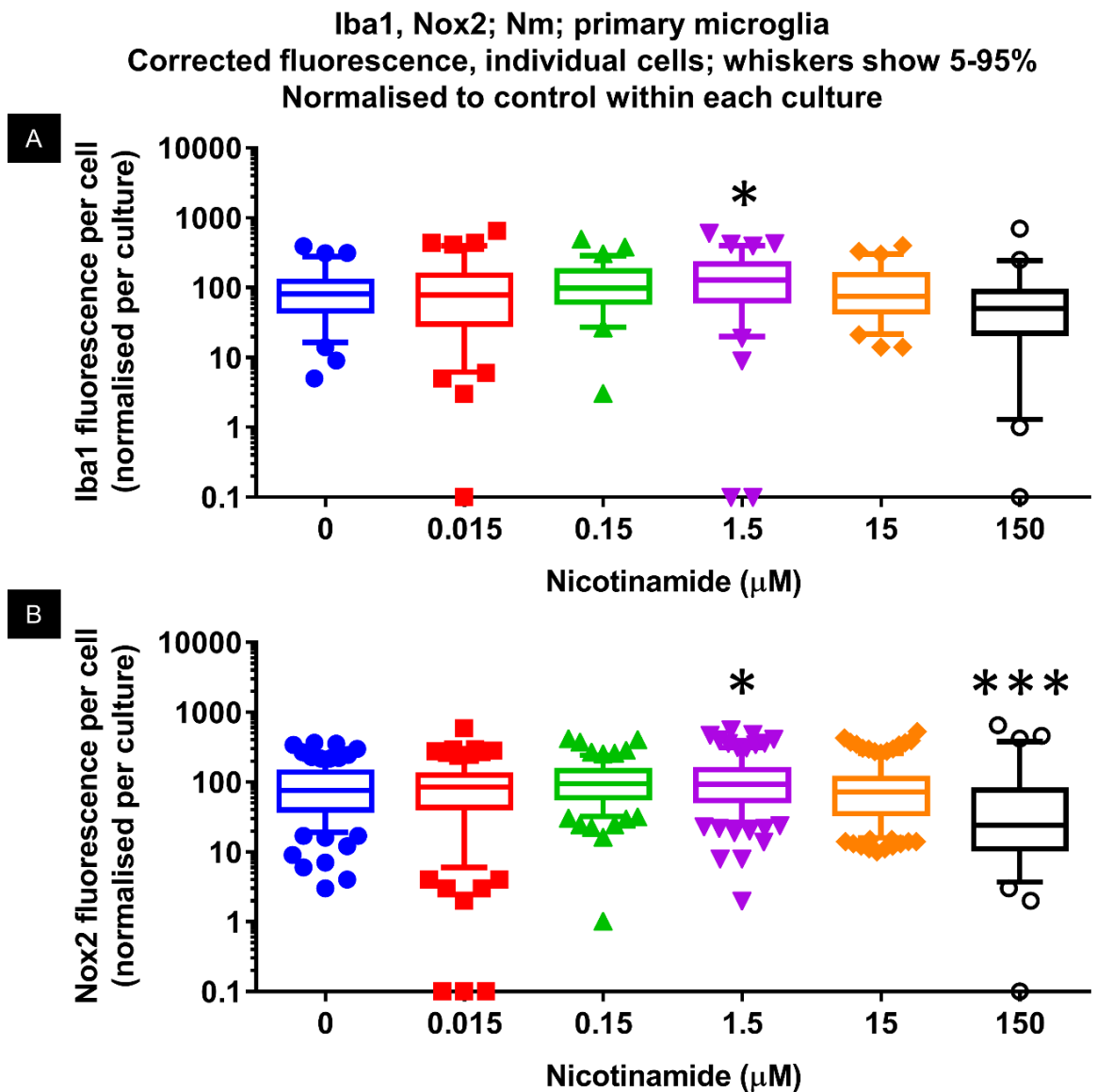


**Figure 3.10. Nicotinamide-treated microglial cultures, microglial staining intensity for Iba1 and Nox2.** Box (25-75<sup>th</sup> percentiles) and whisker plots (5-95<sup>th</sup> percentiles) show individual cell staining intensity, normalised to the average of the control within each culture, with outliers shown as symbols. Log y axis. (A) Versus control, Iba1 intensity increased only at 1.5  $\mu\text{M}$  Nm ( $p < 0.0001$ ;  $n = 408$ ). (B) Versus control, Nox2 intensity increased with 1.5  $\mu\text{M}$ , but decreased at 150  $\mu\text{M}$  Nm ( $p < 0.0001$ ,  $n = 1139$ ). Kruskal-Wallis with Dunn's post-test; \* $p < 0.05$ , \*\*\* $p < 0.001$  versus control.

### 3.3.9. Microglia responses to nicotinamide (Nm): Arg1 and Gpr109a

Following treatment with Nm statistical analysis suggested very slightly lowered expression of Gpr109a at 0.015  $\mu\text{M}$ , and very slightly elevated expression at 15 and 150  $\mu\text{M}$  (Fig 3.11).

Nm did not affect the expression of Arg1 at the concentrations 0-150 $\mu\text{M}$  (Fig 3.11).

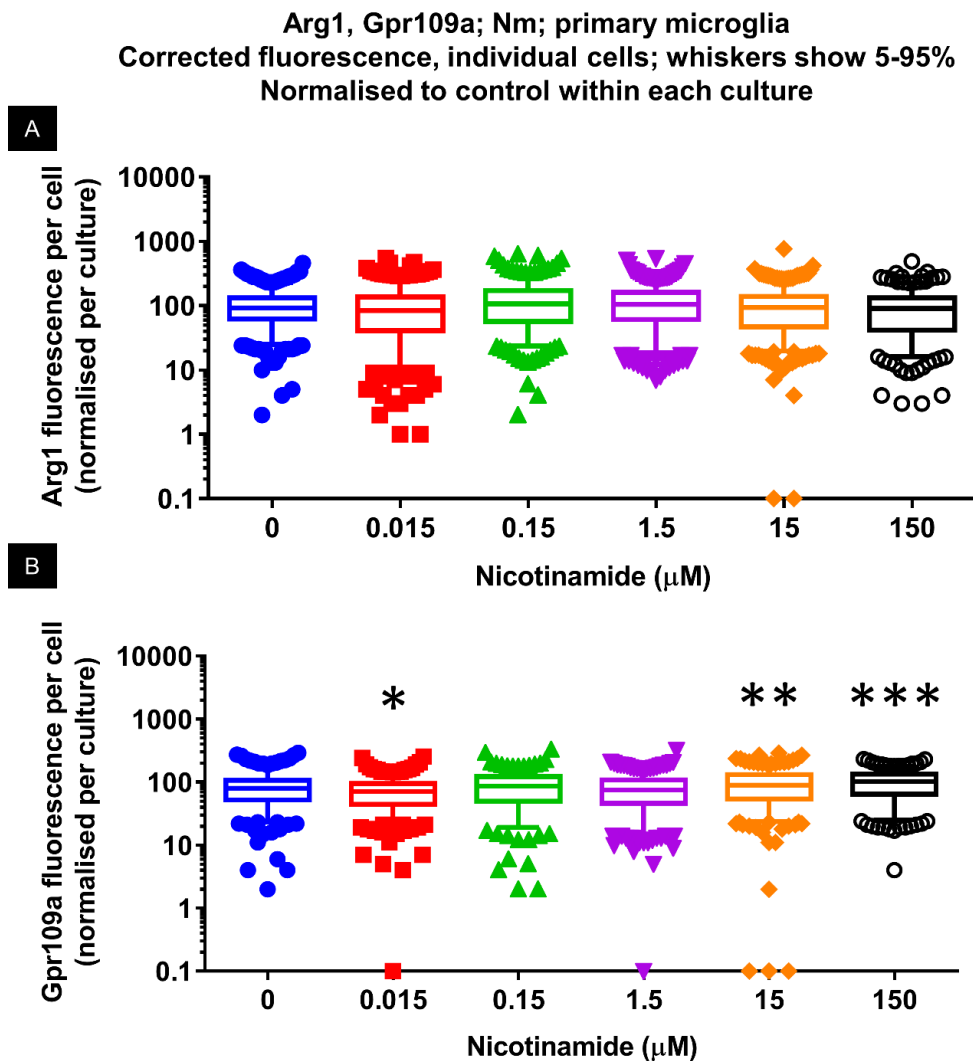


**Figure 3.11. Nicotinamide treated microglial cultures, microglial staining intensity for Arg1 and Gpr109a individual cells.** Box (25-75<sup>th</sup> percentiles) and whisker plots (5-95<sup>th</sup> percentiles) show individual cell staining intensity, normalised to the average of the control within each culture, with outliers shown as symbols. Log y axis. (A) Versus control, Arg1 intensity was unaltered (n = 2,786). (B) Versus control, Gpr109a intensity was diminished at 0.015  $\mu\text{M}$ , but elevated at 15  $\mu\text{M}$  and 150  $\mu\text{M}$  Nm ( $p < 0.0001$ , n = 2063). Kruskal-Wallis with Dunn's post-test; \* $p < 0.05$ , \*\* $p < 0.01$ , \*\*\* $p < 0.001$  versus control.



### 3.3.10. Microglia responses to monomethyl fumarate (MMF): Iba1 and Nox-2

In MMF-treated cultures, both Iba1 and Nox2 staining intensity was reduced at the highest concentration tested, 150  $\mu\text{M}$  (Fig 3.12)

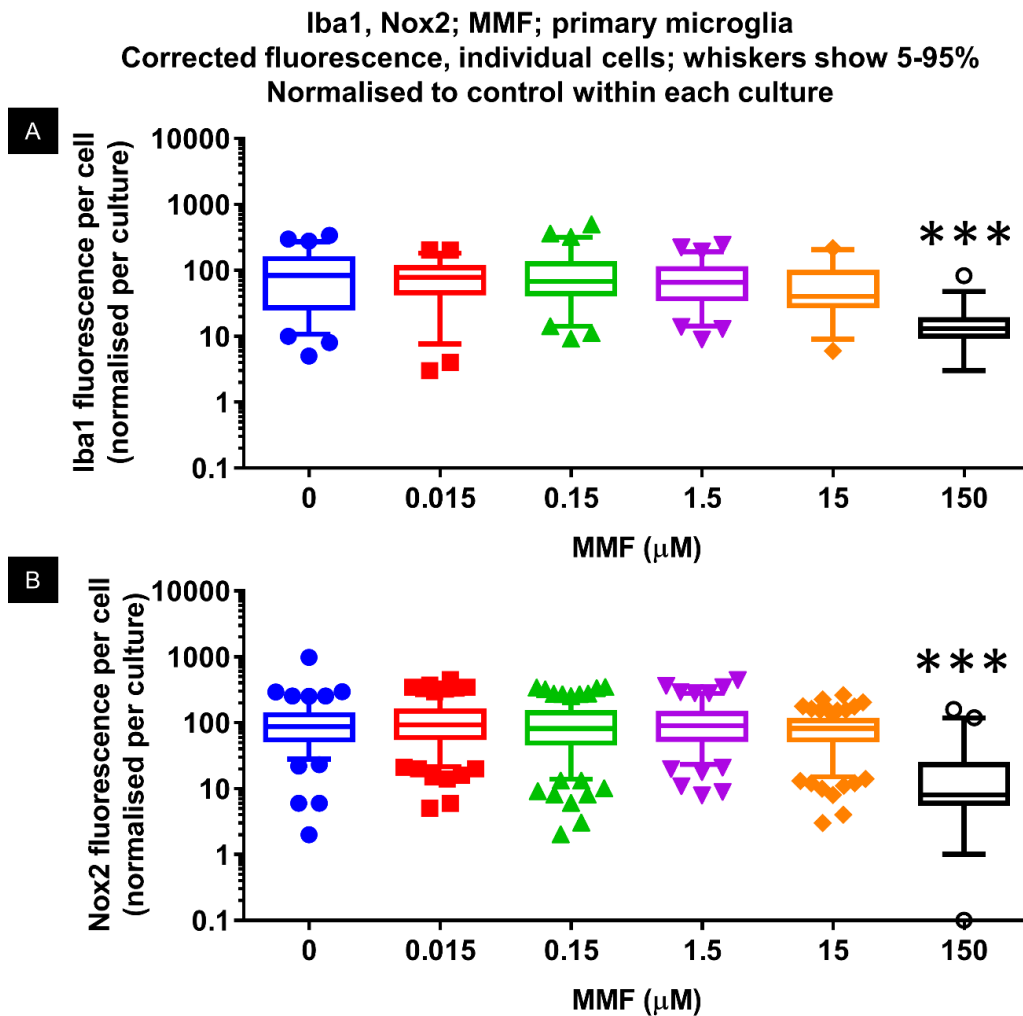


**Figure 3.12 MMF-treated microglial cultures, microglial staining intensity for Iba1 and Nox2 expression.** Box (25-75<sup>th</sup> percentiles) and whisker plots (5-95<sup>th</sup> percentiles) show individual cell staining intensity, normalised to the average of the control within each culture, with outliers shown as symbols. Log y axis. (A) Versus control, Iba1 decreased at highest concentration of MMF 150 $\mu\text{M}$  ( $p < 0.0001$ ;  $n = 311$ ). (B) Versus control, Nox2 decreased at highest concentration of MMF ( $p < 0.0001$ ;  $n = 875$ ). Kruskal-Wallis with Dunn's post-test; \*\*\* $p < 0.001$  versus control.

### 3.3.11. Microglia responses to monomethyl fumarate (MMF): Arg1 and Gpr109a

Following treatment with MMF statistical analysis suggested a very slightly increased Arg1 intensity at 0.015, 0.15, 1.5 and 15  $\mu\text{M}$ , but not at 150  $\mu\text{M}$ . For Gpr109a, staining intensity was very slightly greater at 0.015, 1.5 and 15  $\mu\text{M}$ , but unchanged at 0.15 and 150  $\mu\text{M}$  (Fig 3.13).

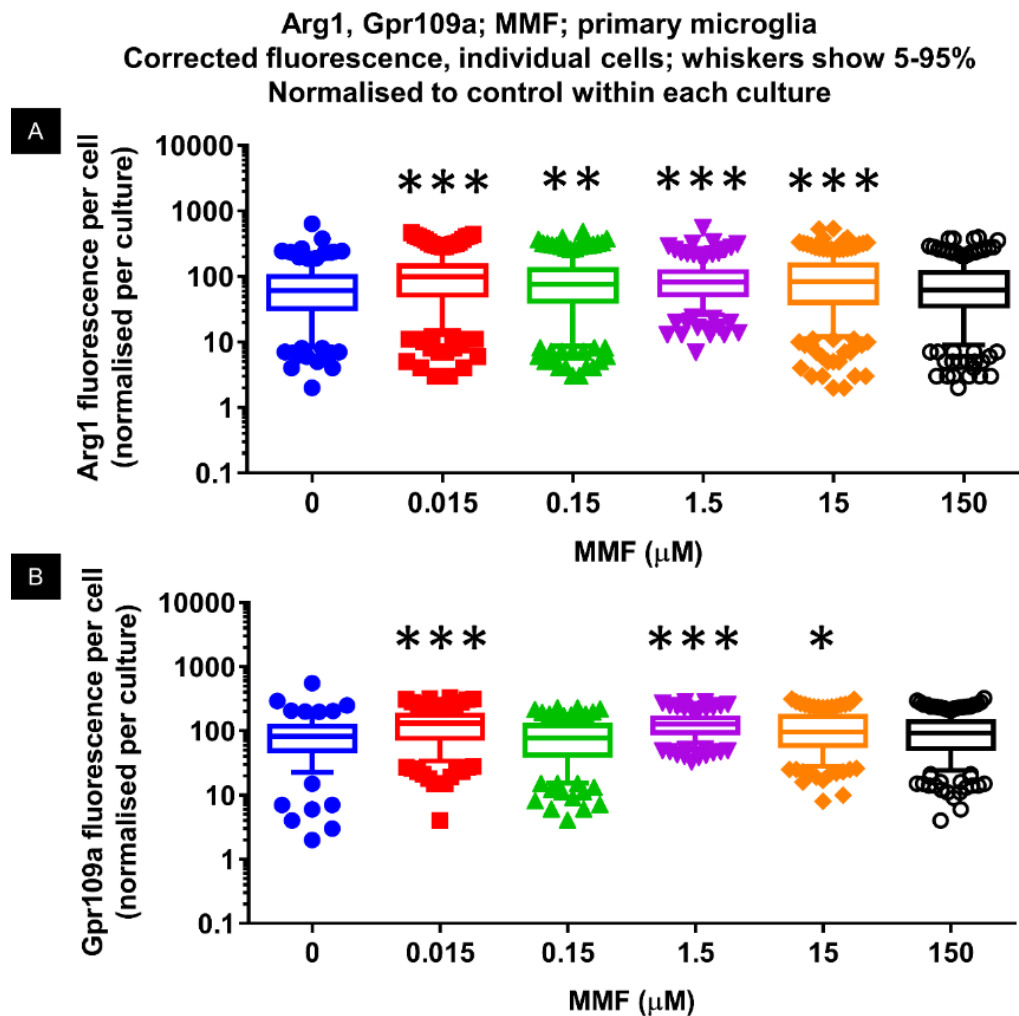


**Figure 3.13 MMF-treated microglial cultures, staining intensity for Arg1 and Gpr109a.** Box (25-75<sup>th</sup> percentiles) and whisker plots (5-95<sup>th</sup> percentiles) show individual cell staining intensity, normalised to the average of the control within each culture, with outliers shown as symbols. Log y axis. (A) Versus control, Arg1 intensity increased at concentrations 0.015  $\mu\text{M}$ , 0.15  $\mu\text{M}$ , 1.5  $\mu\text{M}$ , 15  $\mu\text{M}$  MMF ( $p < 0.0001$ ;  $n = 2,230$ ). (B) Versus control, Gpr109a intensity increased at concentrations 0.015  $\mu\text{M}$ , 1.5  $\mu\text{M}$ , 15  $\mu\text{M}$  MMF ( $p < 0.0001$ ;  $n = 1697$ ). Kruskal-Wallis with Dunn's post-test; \* $p < 0.05$ , \*\* $p < 0.01$ , \*\*\* $p < 0.001$  versus control.

### 3.3.12. Microglial morphological responses to LPS, Nm and Gpr109a ligands

#### Cell area

Each cell was delineated using ImageJ, and various morphological features measured. The average area for each culture was compared, with no differences versus control (Fig 3.14).

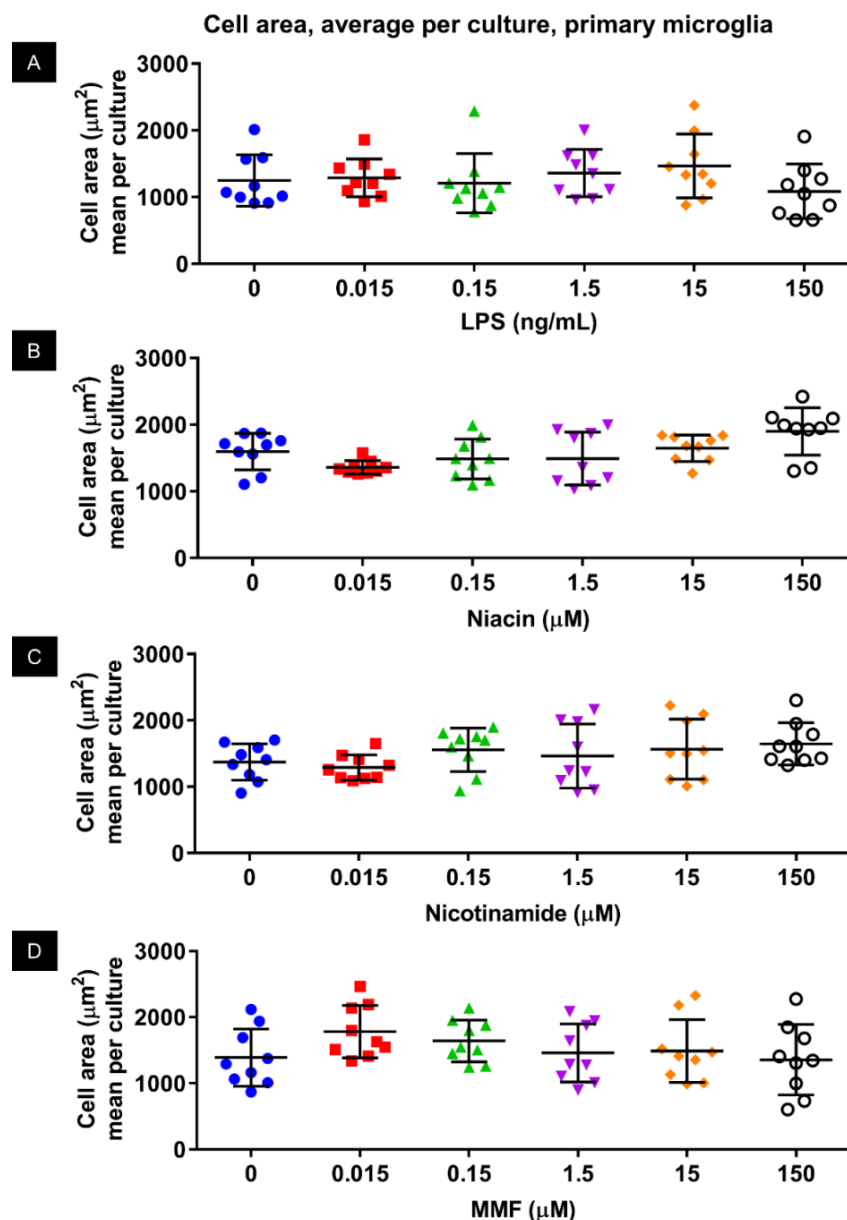


**Figure 3.14. Microglial cell area was unaffected by LPS, Nm or Gpr109a ligands.** Mean cell area within each culture was unaltered versus control for all treatments: LPS (A;  $F_{(5, 48)} = 0.9767$ ,  $p = 0.442$ ), NA (B;  $F_{(5, 48)} = 3.700$ ,  $p = 0.007$ ), Nm (C;  $F_{(5, 48)} = 1.254$ ,  $p = 0.299$ ) or MMF (D;  $F_{(5, 48)} = 1.236$ ,  $p = 0.307$ ). For NA, 0.015  $\mu\text{M}$  differed versus 150  $\mu\text{M}$  ( $p < 0.05$ ). One-way ANOVA with Dunnett's post-test;  $n = 9$ .

## Cell perimeter

The average perimeter for each culture was compared, with statistical analysis suggesting no differences induced by any treatment (Fig 3.15).

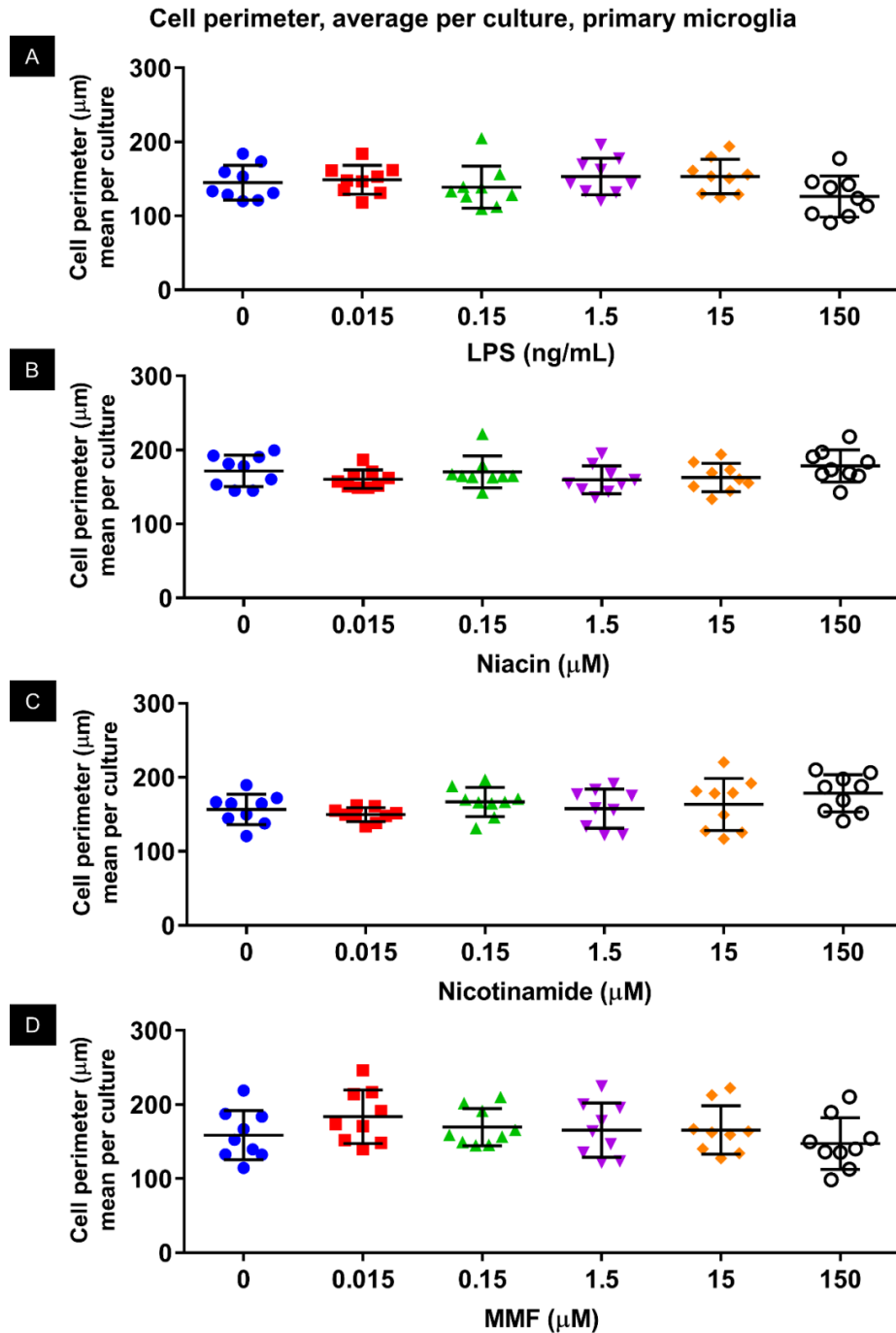


**Figure 3.15. Microglial cell perimeter was unaffected by LPS, Nm or Gpr109a ligands.** Mean cell perimeter within each culture was unaltered by any treatment: LPS (A;  $F_{(5, 48)} = 1.588$ ,  $p = 0.182$ ), NA (B;  $F_{(5, 48)} = 1.321$ ,  $p = 0.271$ ), Nm (C;  $F_{(5, 48)} = 1.543$ ,  $p = 0.194$ ) or MMF (D;  $F_{(5, 48)} = 1.154$ ,  $p = 0.346$ ). One-way ANOVA with Dunnett's post-test;  $n = 9$ .

### Cell Feret's (max)

The average Feret's (maximum) diameter for each culture was compared, with statistical analysis suggesting no differences induced by any treatment (**Fig 3.16**).

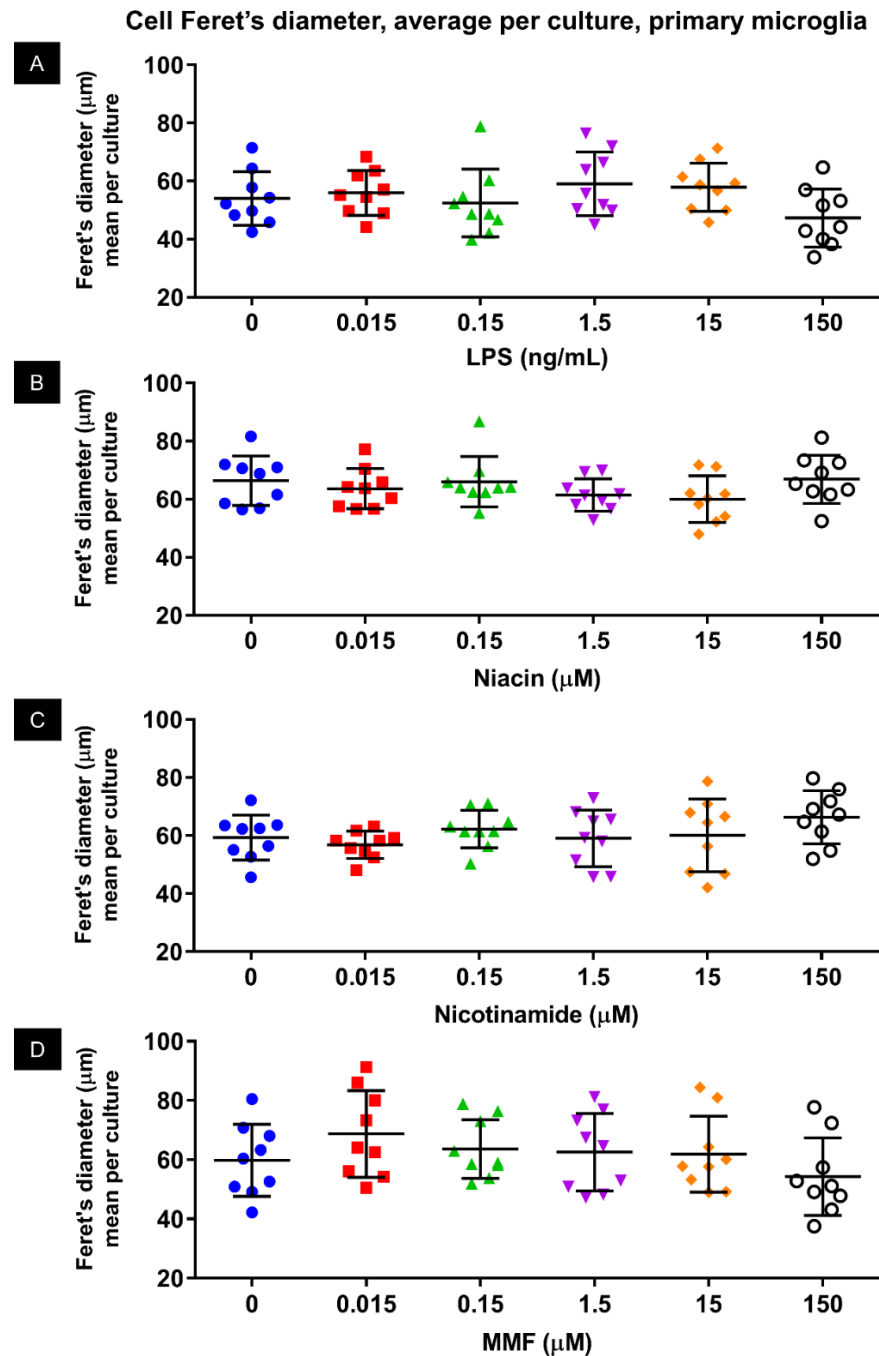


**Figure 3.16. Microglial cell Feret's maximum diameter was unaffected by LPS, Nm or Gpr109a ligands.** Mean cell Feret's diameter within each culture was unaltered by any treatment: LPS (A;  $F_{(5, 48)} = 1.725$ ,  $p = 0.147$ ), NA (B;  $F_{(5, 48)} = 1.219$ ,  $p = 0.315$ ), Nm (C;  $F_{(5, 48)} = 1.256$ ,  $p = 0.299$ ) or MMF (D;  $F_{(5, 48)} = 1.240$ ,  $p = 0.305$ ). One-way ANOVA with Dunnett's post-test;  $n = 9$ .

## Cell Feret's minimum

The average Feret's minimum diameter for each culture was compared, with statistical analysis suggesting no differences induced by any treatment (**Fig 3.17**).

Cell Feret's minimum diameter, average per culture, primary microglia

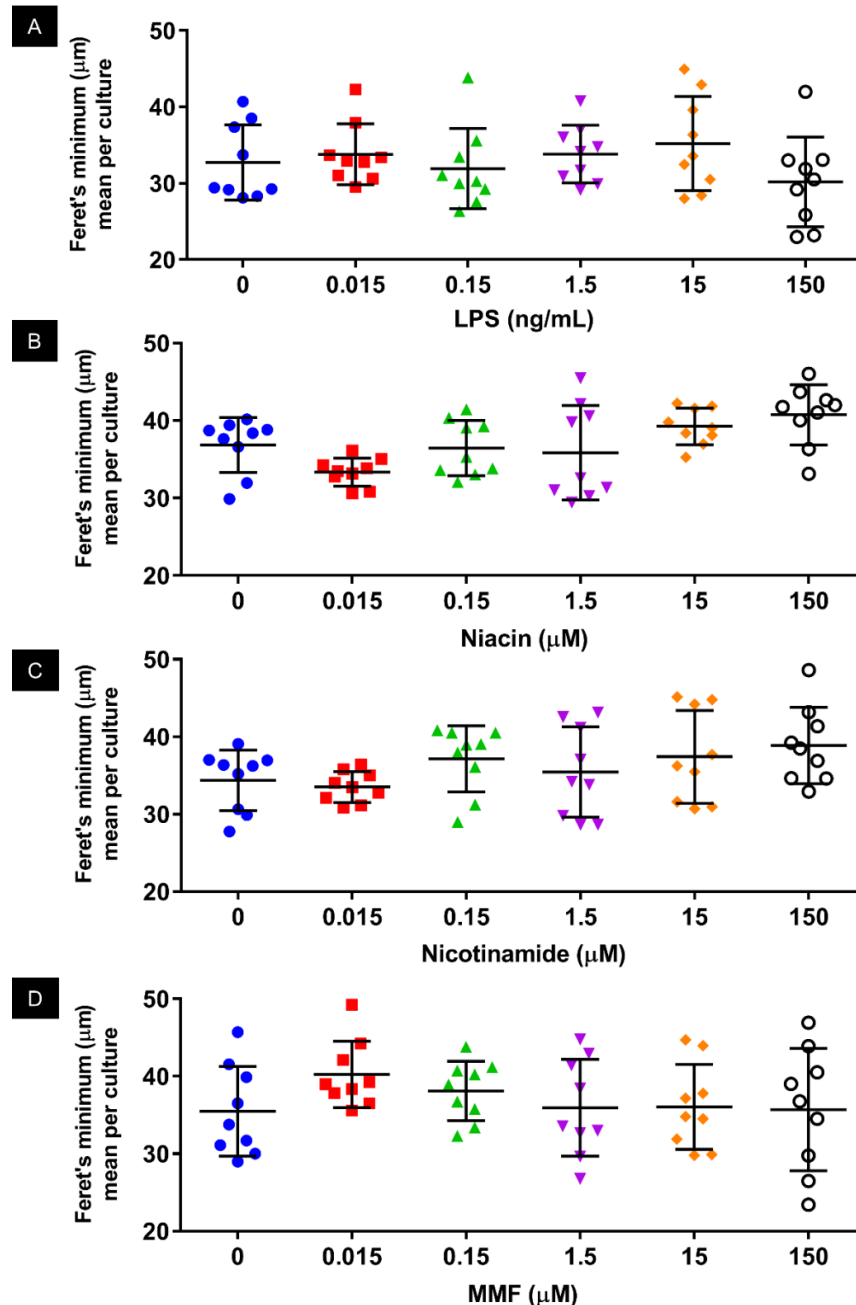


**Figure 3.17. Microglial cell Feret's minimum diameter was unaffected by LPS, Nm or Gpr109a ligands.** Mean cell Feret's minimum within each culture was unaltered by any treatment: LPS (A;  $F_{(5, 48)} = 1.062$ ,  $p = 0.393$ ), NA (B;  $F_{(5, 48)} = 4.254$ ,  $p = 0.003$ ), Nm (C;  $F_{(5, 48)} = 1.698$ ,  $p = 0.153$ ) or MMF (D;  $F_{(5, 48)} = 0.9660$ ,  $p = 0.448$ ). For NA, 0.015 µM differed versus 15 µM ( $p < 0.05$ ) and 150 µM ( $p < 0.01$ ). One-way ANOVA with Dunnett's post-test;  $n = 9$ .

## Cell aspect ratio

Average aspect ratio (Feret's maximum divided by Feret's minimum) for each culture was compared, analysis suggested no differences induced by any treatment (Fig 3.18).

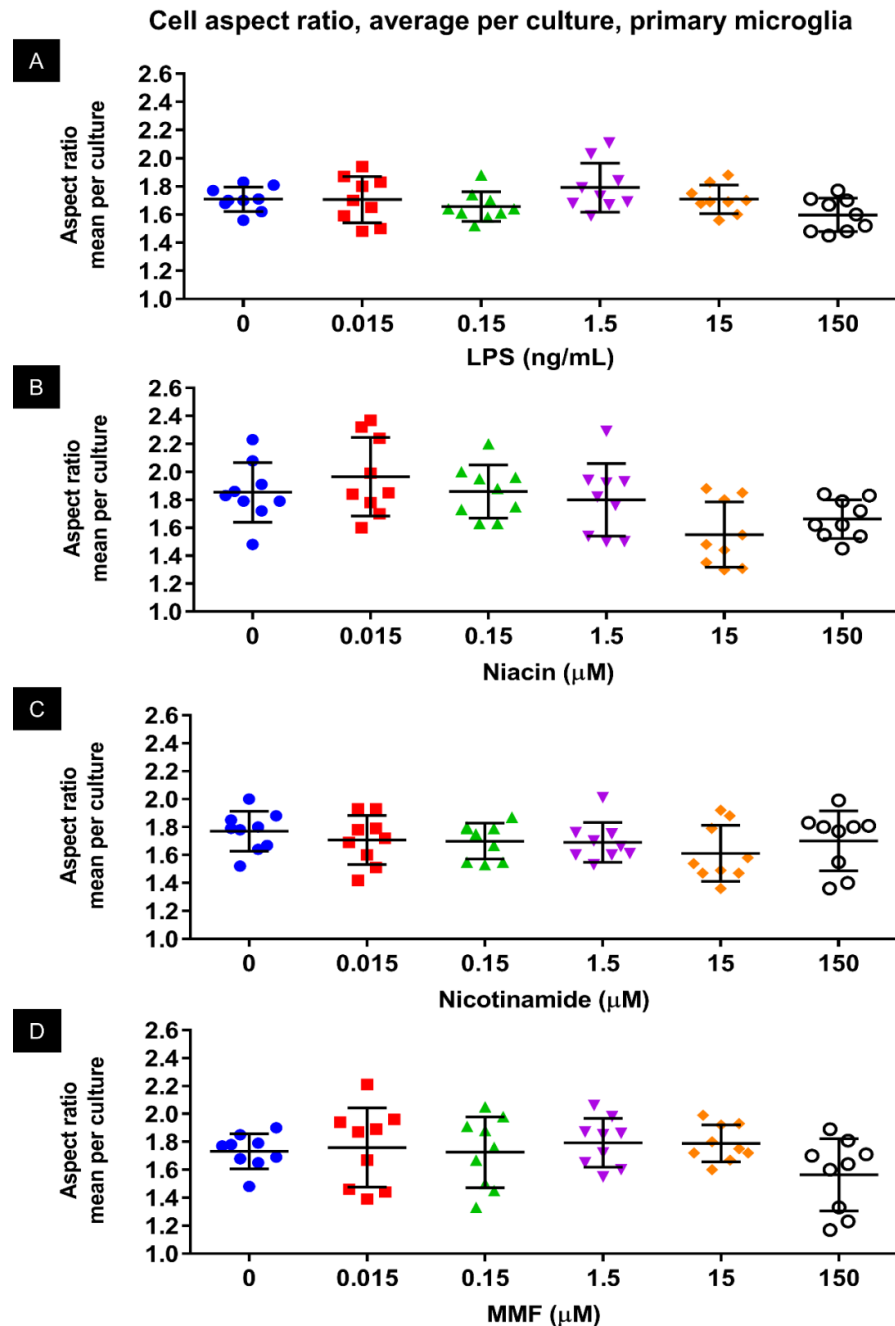


**Figure 3.18. Microglial cell aspect ratio was unaffected by LPS, Nm or Gpr109a ligands.** Mean cell aspect ratio within each culture was unaltered by any treatment: LPS (A;  $F_{(5, 48)} = 2.244$ ,  $p = 0.065$ ), NA (B;  $F_{(5, 48)} = 4.031$ ,  $p = 0.004$ ), Nm (C;  $F_{(5, 48)} = 0.801$ ,  $p = 0.554$ ) or MMF (D;  $F_{(5, 48)} = 1.404$ ,  $p = 0.240$ ). For NA, 0.015  $\mu\text{M}$  differed versus 15  $\mu\text{M}$  ( $p < 0.01$ ). One-way ANOVA with Dunnett's post-test;  $n = 9$ .

## Cell circularity index

At the greatest concentration of LPS, circularity index was greater than control (0.801 vs 0.729;  $p < 0.05$ ; **Fig 3.19A**), indicating that cells more closely resembled circles (an index of 1 being a circle). No other treatment was found to affect circularity index (**Fig 3.19B-D**).

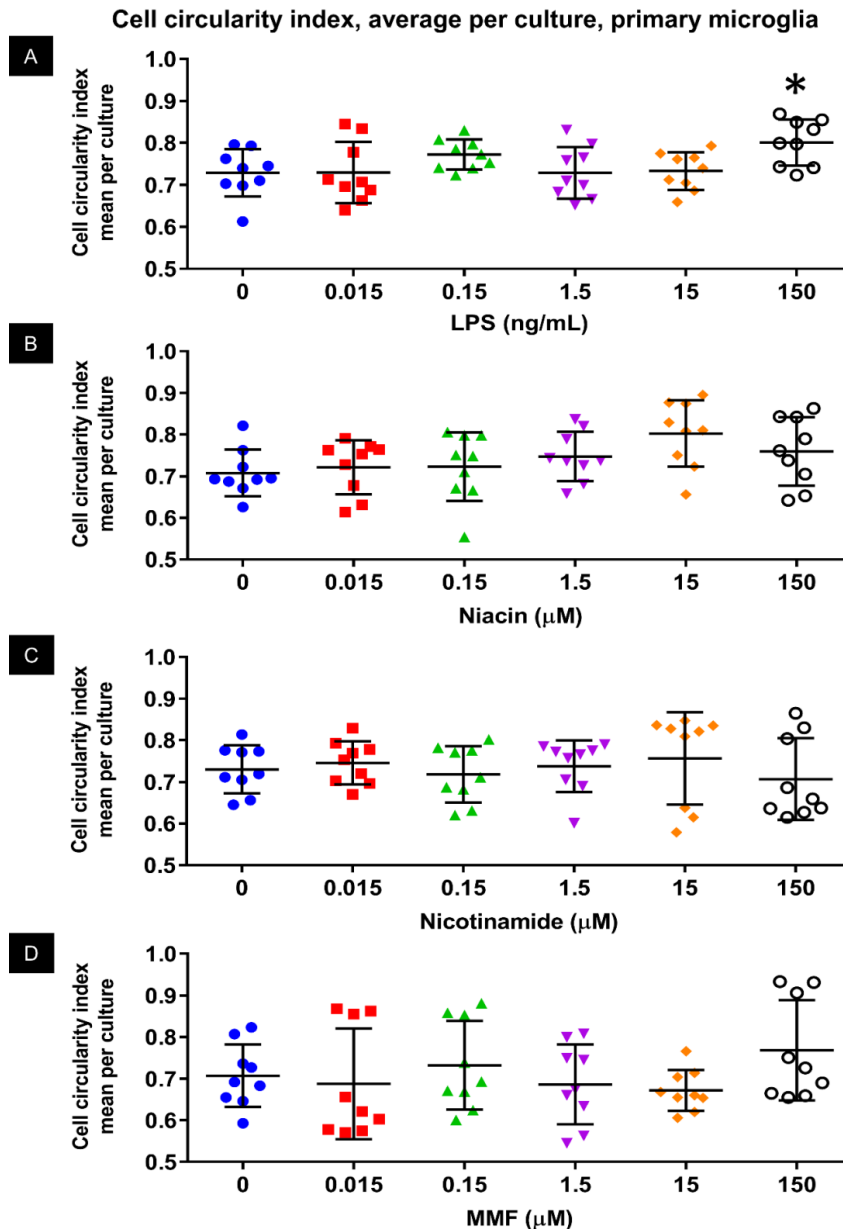


**Figure 3.19. Microglial cell circularity index was unaffected by Gpr109a ligands, or Nm, but increased at high LPS concentration.** Mean cell circularity index within each culture was increased by the greatest dose of LPS (A;  $F_{(5, 48)} = 2.720$ ,  $p = 0.030$ ; 150 ng/ml vs control:  $p < 0.05$ ), but unaltered by other treatments: NA (B;  $F_{(5, 48)} = 2.103$ ,  $p = 0.081$ ), Nm (C;  $F_{(5, 48)} = 0.4946$ ,  $p = 0.779$ ) or MMF (D;  $F_{(5, 48)} = 1.139$ ,  $p = 0.353$ ). One-way ANOVA with Dunnett's post-test; \* $p < 0.01$  versus control;  $n = 9$ .



### 3.3.13. Primary rat astrocytes expressed Gpr109a

In astrocyte cultures, >99% of GFAP<sup>+</sup> cells were immunopositive for Gpr109a with clear nuclear-localised immunostaining (Fig 3.20).

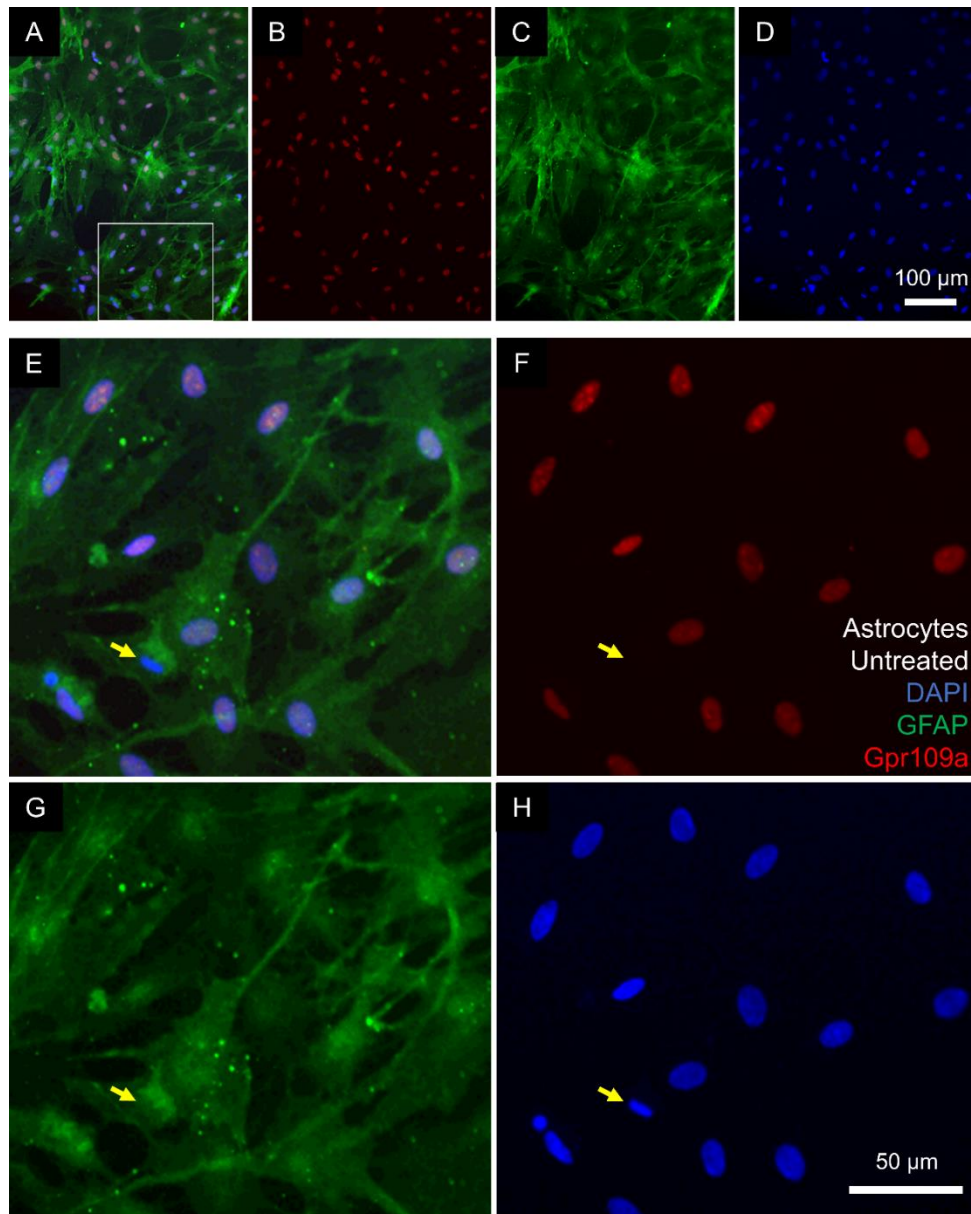


**Figure 3.20. Primary rat astrocytes expressed Gpr109a with nuclear localisation.** Fluorescence micrographs of astrocyte cultures, immunostained for GFAP and Gpr109a, with and without DAPI-merges. (A) Merged micrograph showing GFAP<sup>+</sup>/Gpr109a<sup>+</sup> cells. White rectangle is magnified below. (B-D) Single-colour micrographs, counterparts to (A). (E-H) Magnified region from (A), merged and single-colour micrographs. Gpr109a staining was obvious and nuclear-localised. There were very few cells (<1%) which were GFAP<sup>+</sup>/Gpr109a<sup>-</sup> (yellow arrows show an example).

### **3.4. Discussion**

The objectives of this study were to determine whether neural immune cells express Gpr109a, and whether these cells may respond to clinically-relevant Gpr109a ligands: NA and MMF. LPS was included as a positive inflammatory control. Nm was included as a control for non-Gpr109a-mediated effects. Gpr109a was shown to be expressed in CNS glia, although there was very little evidence that these cells responded to the Gpr109a ligands tested. Responses to LPS were shown. Marker expression was altered in several conditions, as determined by changes in immunostaining intensity. There was limited evidence of morphological changes due to treatment conditions.

#### **3.4.1. Efficacy of the anti-GPR109a antibody was confirmed**

At the highest concentration of anti-Gpr109a antibody tested, immunostaining was evident in individual cells in microglial and astrocyte cultures (**Fig 3.2, Fig 3.20**). Serial dilution of anti-Gpr109a antibody produced diminishing intensity of immunostaining in microglial cultures, with the lowest concentration tested being indistinguishable from the null primary control (absence of anti-Gpr109a antibody, but presence of secondary antibody) (**Fig 3.1**). The null primary control also showed no indication of non-specific binding of secondary antibody.

#### **3.4.2. Microglia express Gpr109a**

Microglia have previously been reported to express Gpr109a *in vivo*, in human, mouse, and rat tissue <sup>87,91,88</sup>. Expression levels are reportedly increased in some pathological conditions, with human PD tissue expressing higher levels of GPR109a compared with healthy (non-PD) controls <sup>87</sup>. However, microglial expression of Gpr109a has not been

closely studied at the level of individual cells, with data often being derived from whole tissue (e.g. PCR, Western blots), or being mentioned as visual observations, without quantification (e.g. percentage of positive cells).

**Fig 3.7** shows nuclear Gpr109a expression in control conditions and potential decreasing intensity with increasing concentrations of LPS treatment. This contradicts findings by Feingold *et al.* 2015<sup>170</sup> who explored the impact of LPS on Gpr109a in a RAW264.7 murine macrophage cell line. Feingold *et al.* showed using qPCR that Grp109a expression increases with increasing LPS concentration. This contradiction might be explained by cell type as Feingold *et al.* used the RAW 264.7 murine macrophage cell line contrasting to primary rat microglia. The lack of coherence between the data warrants the need for further investigation.

### **3.4.3. Astrocytes express Gpr109a**

Rezq *et al.*<sup>91</sup> reported that Gpr109a was expressed in only 7.5% of rat astrocytes *in vivo*. In contrast to Rezq *et al.*, we determined that the percentage of GFAP<sup>+</sup> cells expressing Gpr109a is >99% in untreated *in vitro* cultures (**Fig 3.20**). This was a pilot experiment only, and more detailed investigations are required to validate these observations of Grp109a expression by astrocytes.

The disparity between our data and Rezq *et al.* could be due to the CNS region from which the astrocytes were sourced, and/or differences in processing and analysis. Rezq *et al.* 2016<sup>91</sup> explored astrocyte expression using confocal microscopy of post-mortem RVLM tissue, whereas observations reported here were from *in vitro* primary glial cultures obtained from cerebral cortices. There is reason to believe that tissue source may affect expression, as studies have shown differences in transcriptomic profiles amongst astrocytes sourced from

different locations. Batiuk *et al.* 2020<sup>171</sup>, in an *in vitro* mouse model, used single cell RNA sequencing to identify five transcriptomically-distinct astrocyte subtypes (AST1, AST2, AST3, AST4 and AST5) defined by morphological and physiological differences, with differing expression across forebrain regions<sup>171</sup>. AST1 showed expression of genes related to synaptogenesis (*Nrxn1*), synaptic plasticity (*Agt*), and glutamatergic neurotransmission. AST2: glutamatergic transmission and synaptogenesis. AST3: GABAergic neurotransmission and different synaptogenesis-related genes. AST4 is thought to be a unique subtype linked to neurogenesis due to unique expression of genes for mitosis and cell cycle control (*Cdk4/Sirt2*) and neurogenesis and neuronal differentiation (*Dab1*). AST5 is thought to be an intermediate state between astrocyte precursors and mature astrocytes. AST1 and AST4 were predominant in the hippocampus whilst AST2 are found mainly in the cortical regions. AST3 and AST5 showed uniform presence across brain regions<sup>171</sup>.

However, no reports have specifically addressed Gpr109a transcriptomics. Pan *et al.* 2020<sup>172</sup> and Todd *et al.* 2021<sup>173</sup> show that disease models have varying transcriptomic profiles. Todd *et al.* 2021 showed that trauma induced via fluid percussion injury to mimic traumatic brain injury leads to a distinct astrocyte response and transcriptomic changes compared with models of neuroinflammatory disease and ischemia. In a mouse model of aging Pan *et al.* 2020 show that microglia and astrocytes of wild type mice at 4 months experience a consistent upregulation and downregulation of age related genes relative to their 2 months old control. When wild type were compared to age matched APP-PS1 (AD mouse model), APP-PS1 microglia and astrocytes experienced a greater upregulation of age related genes. In both wild-type and APP-PS1 aging resulted microglia upregulating inflammatory genes; whilst astrocytes upregulated AD risk genes and those associated with synaptic transmission and elimination.

Following from previous research identifying transcriptomic difference between astrocytes it could be possible that Gpr109a expression is lower in the RVLM than in cerebral cortices. Further still the model chosen has a proven impact on transcriptomic profile. Organotypic brain slices are a more accurate representation of living brain tissue whereas primary astrocytes cultures are not. It could follow that astrocytes are activated by the methods of extraction during *in vitro* culturing causing hyperactivation of Grp109a. Astrocytes express Gpr109a but it is still unknown to what extent it is expressed. Further investigations are required to address these questions.

#### **3.4.4. Gpr109a expression was nuclear localised in both microglia and astrocytes**

**Fig 3.7** shows nuclear expression in primary microglia; additionally, there appears to be no translocation of the Gpr109a receptor, with the Gpr109a receptor located at the nucleus regardless of increasing LPS concentration. This contradicts findings by Feingold *et al.* 2015<sup>170</sup> who using fluorescence microscopy demonstrated that Gpr109a expression is located throughout the cell membrane/cytoplasm in a mouse peripheral macrophage cell line, regardless of treatment condition. Whilst no Gpr109a translocation was noted upon treatment with Gpr109a ligands, it has been reported in other cell types that, upon treatment with niacin, Gpr109a co-localises with endosomes allowing it to be internalised and translocated to the nucleus: increasing concentration and longer incubation periods correlated with increased nuclear-associated Gpr109a staining intensity<sup>174,175</sup>.

Rezq *et al.*<sup>91</sup> do not comment on astrocytic intracellular localisation of Gpr109a expression, but published micrographs suggest it to be present in the cytoplasm and membrane. Thesis micrograph images suggest Gpr109a is nuclear localised (**fig 3.20**). The contrasting data between our findings and that of Rezq *et al.* have been discussed in **3.4.3**.

### 3.4.5. Primary rat microglia response to LPS, nicotinamide, and Gpr109a ligands

Microglial cell counts were reduced at the highest LPS concentration tested (150 ng/ml), suggesting toxicity (**Fig 3.3**). Statistical analysis indicated that cell counts were not reduced for any NA, Nm, or MMF concentration, although the greatest concentration for each treatment generated the lowest cell counts (**Fig 3.3**). Microglial morphologies at LPS concentration of 150 ng/ mL often appeared smaller and more rounded than controls, although morphological analyses only indicated a significant difference for the circularity index, which was increased (i.e. cells were more circular) at 150 ng/mL (**Fig 3.19**). Some cultures showed more evident microglial atrophy/rounding and reduced staining intensity than others, and perhaps this variation in extent of toxicity between cultures limited the ability to determine significant changes statistically. An evident dose-response was expected. The effects of LPS on marker intensity were expected to be large and statistically significant as LPS is expected to upregulate the M1 phenotype and reduce the M2 phenotype. Due to the expectation that culture-level effects would be evident averages were generated; however, the statistics generated did not indicate clear changes so additional analysis was performed pooling all individual cell values.

#### **LPS, nicotinamide and Gpr109a ligands: impact on M1 markers Iba1, Nox2**

Iba1 and Nox2 response to LPS concentration suggest dose-response, especially between the dose range of 0.15 - 15 ng/mL. However, statistical analyses only indicated elevated expression at 1.5 ng/mL for Iba1, and at 1.5 and 15 ng/mL for Nox2 (**Fig 3.4**). If these increases are genuine responses to LPS, they may indicate M1 activation of microglia, as Iba1 participates in membrane ruffling and phagocytosis and Nox2 is a superoxide-generating enzyme that produces ROS. ROS can have beneficial actions such as protecting

the CNS<sup>165</sup> from exogenous pathogens. However, when chronically produced at high levels ROS can damage cell membranes, proteins, and DNA causing cellular death. Further still excessive production can stimulate further production of pro-inflammatory molecules by microglia reinforcing the inflammatory response further. However, the small size of the increases, and the lack of a consistent dose-response make this an unreliable conclusion. The highest concentration of LPS (150 ng/mL) significantly reduced fluorescence for Iba1 and Nox2 (**Fig 3.4**). Paired with the reduced cell counts (Fig 3.3) this would be consistent with the other observations suggesting that 150 ng/mL LPS was toxic to these microglial cultures.

There were no consistent changes in Iba1 or Nox2 expression when microglial cultures were treated with NA, Nm, or MMF. There was only noted a very small increase at 1.5  $\mu$ M NA (Iba1) and 0.015  $\mu$ M NA (Nox2) alongside an inconsistent dose-response effect, therefore this is not considered to represent a genuine response (**Fig 3.8**). When treated with Nm the only significant alterations were at 1.5  $\mu$ M Nm leading to very small increases in expression of Iba1 and Nox2 and a decrease in Nox2 at 150  $\mu$ M Nm (**Fig 3.10**), this decreased expression might indicate a genuine effect or potential toxicity. MMF only produced a statistically significant alteration to Iba1 and Nox2 expression at the highest concentration (150  $\mu$ M), where there was a drastic reduction in fluorescence intensity for both markers (**Fig 3.12**).

Whilst treatment with MMF generated averages were consistently below controls; statistical testing only indicated a significant decrease at 150  $\mu$ M MMF (for Iba1 and Nox2). The decline in expression was so marked it could indicate genuine effects; however, these effects could be due to toxicity rather than desired alterations in microglial phenotype. Even if these changes were indicative of a genuine promotion of a therapeutically desired

microglial phenotype, 150  $\mu\text{M}$  might not be a realistic concentration to replicate in a patient without risk of undesirable side effects. Peng *et al.* 2016,<sup>100</sup> using a Sprague-Dawley rat model, monitored DMF/MMF kinetics when orally dosed with 100 mg/kg DMF. They noted the highest concentration to be 1,000 ng/mL in blood plasma (8.13  $\mu\text{M}$ ), and 500 ng/g in brain tissue (treating 1 g as equivalent to 1 mL, 4.1  $\mu\text{M}$ ), both concentrations being far lower than 150  $\mu\text{M}$ . This is however in a rat model and may not be indicative of concentrations found in humans.

### **LPS, nicotinamide and Gpr109a ligands: impact on Arg1 expression**

It could be predicted that Arg1 expression would decrease with increasing LPS concentration. However, LPS was only associated with a decrease in expression at the highest concentration (150 ng/mL) but this decrease was small in magnitude (**Fig 3.6**). Combined with results demonstrating a concentration of 150 ng/mL LPS decreased Nox2 and Iba1 staining intensity and decreased cell counts (**Fig 3.4**), this reduction in Arg1 expression may indicate a toxic level of LPS. It is not possible from the data available to determine whether Arg1 activity may have been affected by LPS treatment, even if quantity of protein was unaltered.

Niacin increased Arg1 expression at concentrations 0.015 and 0.15  $\mu\text{M}$  (**Fig 3.9**). MMF increased Arg1 expression at 0.015, 0.15, 1.5, 15  $\mu\text{M}$  (**Fig 3.12**). Nm did not elicit any changes to Arg1 expression (**Fig 3.11**). This was unexpected as Nm is thought to upregulate anti-inflammatory effect via Nrf2.

### **LPS, nicotinamide and Gpr109a ligands: impact on Gpr109a expression**

Increasing LPS concentration from 0.15-150  $\mu\text{M}$  led to decreased staining intensity for Gpr109a (Fig 3.6). This contradicts reports by Fu *et al.* 2015<sup>89</sup> and Feingold *et al.* 2015<sup>170</sup> where increasing LPS concentrations and incubation periods led to increases in Grp109a



expression in microglia, although this was measured as mRNA, not protein <sup>89</sup>. In a RAW264.7 mouse peripheral macrophage cell line, increasing concentrations induced increasing Gpr109a mRNA expression, with maximal response at 100 ng/ml (1,000 did not increase response). Time-dependent increased expression was seen peaking at 16 h (100 ng/ml), with a decline at 24 h <sup>170</sup>. Gpr109a was located within the cell membrane/cytoplasm in both control and treated cultures. As mentioned previously this data may not translate directly to a primary microglial cell culture as it originated from a macrophage cell line. During our experiments we used a 24 h incubation period which may be beyond peak Gpr109a expression. Future investigations should consider varying LPS incubation periods, as well as LPS concentration. Gpr109a expression for NA concentrations of 0.015  $\mu$ M, 0.15  $\mu$ M, 1.5  $\mu$ M, and 15  $\mu$ M were indicated to be statistically significantly increased, but these increases were very small (**Fig 3.9**). Arg1 expression for niacin concentrations of 0.015  $\mu$ M and 0.15  $\mu$ M were also very slightly greater than control. The small magnitude and lack of consistent dose-response effects suggest that these should not be considered as genuine cellular responses to NA.

Nm treatment resulted in no alteration in Arg1 expression (**Fig 3.11**). Statistical analysis indicated very slightly reduced expression for Gpr109a at 0.015  $\mu$ M, and very slightly elevated expression at 15 and 150  $\mu$ M (**Fig 3.11**). Nm is thought to act independently of the Gpr109a receptor. The small magnitude and lack of consistent dose-response effects suggest that these should not be considered as genuine cellular responses to Nm. MMF had a marked impact on Arg1 expression with MMF (0.015-15  $\mu$ M) resulting in statistically significant increases in Arg1 expression. Similarly MMF treatment increased Gpr109a expression significantly at 0.015  $\mu$ M, 1.5  $\mu$ M, and 15  $\mu$ M (**Fig 13**). The variations in response of Gpr109a expression to Gpr109a ligand concentration may reflect each individual ligand's

affinity for the Gpr109a receptor (explored in **table 2.1**). The tentative correlation between increased Arg1 and Gpr109a expression might indicate a morphological change from M1/M0 to M2. Further experimentation would be required to validate this.

#### **3.4.6. Morphometry**

Once data were pooled for morphological analysis, there were sufficient experimental repeats (n = 9) to reliably test for normality of the data. As the data passed normality testing, one-way ANOVA was used for statistical testing.

Of all six morphological features that were measured, only a single change was indicated by statistical testing: circularity index value greater at 150 ng/mL LPS. This is likely a genuine change, as cells did show signs of toxicity at this concentration of LPS, which would be consistent with a loss of processes/ramifications. However, it would be expected that features such as area would also be markedly reduced in response to obvious toxicity, and data analysis did not indicate this.

It could be predicted that a change from largely ramified morphologies to more amoeboid morphologies would occur with LPS treatment, consistent with M0 to M1 phenotypic changes. Further, these changes might be expected to be detected by morphometric analyses. However, no such changes were evident in the data produced here. The following text discusses comparisons between thesis data and that of the literature, and includes comparisons presented in Tables.

### **LPS and treatment impact on microglial morphology: analysis of morphologies**

Untreated microglia yielded an average area of 1,123  $\mu\text{m}^2$  which is higher than *in vitro* untreated N9 microglia<sup>68</sup> and naïve mouse microglia taken from a coronal section<sup>57</sup>(**Table 3.1**). Thesis results far area better align with those seen in an *in vitro* mouse primary microglial study by Caldeira *et al.* 2017<sup>66</sup> (**Table 3.1**) where untreated microglial cultures yielded 600  $\mu\text{m}^2$  at 2 DIV and 1,297  $\mu\text{m}^2$  at 16 DIV. This result might be explained by the culture methods and cell types used. Caldeira *et al.* used primary microglial culture similar to our experimental design; whereas Cunha *et al.* 2016<sup>68</sup> use a microglial cell line and Zanier *et al.* 2015<sup>57</sup> used coronal sections of mouse brain cortex. This highlights the importance considering microglial source and culture methods when analysing morphometry. *In vivo* and *ex vivo* studies allow for microglia to grow in 3D space whereas *in vitro* studies on glass coverslips restrict growth to a 2D plane. As the microglia continue to grow flat they may be the same size in terms of volume however they will have a greater surface area and perimeter. This implies that the physical environment in which microglia grow can directly impact morphology.

**Table 3.1 comparing thesis data vs literature for inflammatory stimuli impact on area and volume morphometric for microglia.**

Experiment and treatment conditions		Area ( $\mu\text{m}^2$ )	Perimeter ( $\mu\text{m}$ )	
Thesis data LPS	Concentration ng/mL, 24hr			
	0	1123	126.4	
	0.015	1288	148.8	
	0.15	1208	138.8	
	1.5	1361	153.2	
	15	1467	153.3	
	150	1085	126.2	
Mouse coronal brain slice <sup>57</sup>	Naïve (control)	54.57	61.46	
	tMCAO	85.78	75.27	
	pMCAO	57.13	47.69	
	TBI	71.90	58.26	
Mice, postnatal 1-2 days. <i>In vitro</i> primary microglia <sup>66</sup>	2 DIV	C	600	140
	2 DIV	A $\beta$ , 1 $\mu\text{M}$ 24hr	1231	148
	16 DIV	C	1297	216
	16 DIV	A $\beta$ 1 $\mu\text{M}$ 24 h	1467	160*
N9 microglia cell line <sup>68</sup>	Control	230	80	
	LPS 300 ng/mL 24 h	466	34.4	
Primary human, resected tissue (intractable epilepsy) <sup>65</sup>	<i>E. coli</i> bio-particle exposure, 1 h	Pseudopodic $\sim 90 \pm 10$ Amoeboid $\sim 190 \pm 10$ Ramified $\sim 305 \pm 30$		
~ indicates approximate value, estimated from graphs for example;				

LPS treatment at 300 ng/mL for 24 h increased microglial cell area <sup>68</sup>(Table 3.1). Thesis data indicated that increasing LPS concentrations had no significant impact on microglial area. Untreated microglia had an average perimeter of 126.4  $\mu\text{m}$ , similar to values noted by Caldeira *et al.* 2017 <sup>66</sup> (**Table 3.1**). Thesis average microglial perimeter values were, however, greater than those reported by Zanier *et al.* 2015 <sup>57</sup> and Cunha *et al.* 2016 <sup>68</sup> (**Table 3.1**). This might also be explained by differing culturing methods, as microglia grow flat when cultured in 2D planes therefore displaying larger perimeters.

When treated with LPS there was no significant change to microglial perimeter, whereas Cunha *et al.* 2016 <sup>68</sup> reported a significant reduction in cell perimeter. Cunha *et al.* used a LPS concentration of 300 ng/mL whereas our largest LPS concentration was 150ng/mL, at which toxicity was suspected, as indicated by a dramatic reduction in microglial cell number (**Fig 3.3**). Cunha *et al.* did not report toxicity at this concentration, however they used the N9 immortalised cell line which might account for variation in response to toxic stimulus. Considering methods of extraction when preparing primary microglial cultures, the cultures studied in this thesis may already be exhibiting an inflammatory response, due to exposure to inflammatory stimuli (e.g. cellular debris, DAMPs) during processing. This is predicted to cause microglia to adopt an amoeboid morphology, which we expected to be reflected in a decreased cell perimeter; however, this was not seen.

There was no statistically significant impact of LPS on Feret's maximum (**Table 3.6**). Untreated microglia gave a Feret's value of 54.0 most similar to Caldeira *et al.* 2017 <sup>66</sup> who in a 2DIV culture derived an average Feret's maximum value of 46.4 (**Table 3.2**). Similarly to cell area and perimeter, thesis values appear higher when compared to different culture conditions Cunha *et al.* 2016 <sup>68</sup> and Zanier *et al.* 2015 <sup>57</sup> (**Table 3.1**). When treated with LPS there was no significant trends noted.

<b>Table 3.2 comparing thesis data vs literature for inflammatory stimuli impact on Feret's Max and Circularity.</b>					
			Feret's Max	Aspect ratio (average, all cell values)	Circularity
Thesis data LPS	Concentration ng/mL				
	0		54.0	1.70	0.73
	0.015		55.9	1.77	0.73
	0.15		52.5	1.65	0.77
	1.5		59.1	1.74	0.73
	15		57.9	1.73	0.73
Mouse coronal brain slice <sup>57</sup>	Naïve (control)		17.10		0.26
	tMCAO		20.10		0.25
	pMCAO		14.92		0.38**
	TBI		17.73		0.37**
Mice, postnatal 1-2 days. In vitro primary microglia <sup>66</sup>	2 DIV	C	46.4		0.448
	2 DIV	A $\beta$ , 1 $\mu$ M 24 h	45.6		0.416
	16 DIV	C	74.4		0.380+
	16 DIV	A $\beta$ , 1 $\mu$ M 24 h	52.8		0.456*
N9 microglia cell line <sup>68</sup>	Control		26.4		
	LPS, 300ng/mL 24h		34.4		
Primary rat post-mortem fixed slice culture <sup>72</sup>	Cluster 1				0.011
	Cluster 2				0.007
	Cluster 3				0.016
	Cluster 4				0.031
Rat post-mortem fixed slice culture, hippocampus, hypothalamus, septofimbrial nucleus <sup>30</sup> .	Cluster 1.1	Saline, hypo, surveillant			>0.0145
	Cluster 1.2	Saline, Sept, surveillant			>0.0145
	Cluster 2.1	Saline, Sept, surveillant			0.0035-0.0145
	Cluster 2.2	Saline, hpc, surveillant			0.0035-0.0145

Aspect ratio is expressed as Feret's maximum divided by Feret's minimum. Values greater than 1 indicate elongation, and a circle has an aspect ratio of exactly 1. Regardless of treatment conditions aspect ratio values are consistently greater than 1 suggesting microglia are elongated (**Table 3.2**). At the smallest values for AR (1.65; least elongated), circularity was the greatest (0.77 and 0.80). At four different AR values (1.70, 1.73, 1.74 and

1.77), counterpart circularity was 0.73 in every case. So, AR and circularity were broadly in agreement, but did not completely predict each other.

This data on circularity gave higher values than previous reports by Caldeira *et al.* 2017<sup>66</sup>, Zanier *et al.* 2015<sup>57</sup>, and Fernández-Arjona 2019<sup>72</sup> (**Table 3.2**). A value of 1 indicates a perfectly circular object. This potentially indicates that microglia in our studies displayed an amoeboid morphology, even in control samples. This may be a result of pro-inflammatory microglial activation from being cultured on a 2D hard glass surface. LPS treatment had no statistically significant impact on circularity values.

### **Nicotinamide and Gpr109a ligand impact on microglial morphology: analysis of morphometrics**

Gpr109a ligand treatment has no impact on morphological measurement cell area, cell perimeter, Feret's diameter, Feret's minimum, aspect ratio, or circularity index. The lack on impact of Gpr109a ligands and LPS treatment on morphometric measurements may indicate their unreliability as indicators of microglial activation status (**Table 3.3**).

Table 3.3 comparing thesis data vs literature for Gpr109a ligand treatment of primary microglia				
		Area	Perimeter	Circularity (or Sphericity if stated)
	Concentration $\mu$ M			
Thesis data, Nm as control	0	1373.7	156.7	0.71
	0.015	1290.7	149.7	0.72
	0.15	1556.4	166.8	0.72
	1.5	1462.1	157.7	0.75
	15	1565.5	163.4	0.80
	150	1646.6	178.4	0.76
Thesis data, NA	0	1597.6	171.8	0.73
	0.015	1361.6	160.5	0.75
	0.15	1486.0	170.3	0.72
	1.5	1492.5	159.8	0.74
	15	1649.2	162.8	0.76
	150	1898.8	178.5	0.71
Thesis data, MMF	0	1391.1	158.8	0.71
	0.015	1780.4	183.7	0.69
	0.15	1641.4	169.5	0.73
	1.5	1458.3	165.5	0.69
	15	1488.0	165.6	0.67
	150	1355.2	147.5	0.77
C57BL/6J mice, brain cerebral cortices, microglial single cell culture <sup>71</sup>	Control			~0.48
	BHB 1mM			~0.40
	BHB 3mM			~0.33**
	BHB 5mM			~0.28**
	BHB 5mM 0 h			~0.42
	BHB 5mM 1 h			~0.36
	BHB 5mM 4 h			~0.28**
	BHB 5mM 8 h			~0.21**
	Niacin 0h, 1mM			~0.41
	Niacin 6h, 1mM			~0.38
	Niacin 12h, 1mM			~0.37
	Niacin 24h, 1mM			~0.35
C57BL/6J, ex vivo multiphoton live imaging, spinal cord injury model <sup>70</sup>	Control	850		~0.66 (Sphericity)
	Niacin 100 mg/kg for 7 days	~1350***		~0.62* (Sphericity)

There was no significant trend between cell area and increasing concentrations of Gpr109a ligands. The cell areas noted for both control and Gpr109a ligand are similar to those recorded for niacin treatment conditions by Rawji *et al.* 2020 <sup>70</sup> (Table 3.3). Since there was no significant difference between control and treatment conditions the increased cell area is likely due to culturing conditions. When *in vitro* conditions are compared to ex vivo and



*in vivo* tissue those cells cultured on a 2D plane have greater cell area and perimeter values (Table 3.1).

There was no significant trend between circularity and increasing concentrations of Gpr109a ligands. This is unlike the results obtained by Huang *et al.* 2018<sup>71</sup> which show a decreasing circularity with increasing BHB concentration. This may indicate that BHB promotes ramification. They however state whilst BHB is a Gpr109a ligand and that these effects are independent of Gpr109a instead acting through the Akt-RhoGTPase pathway. Sphericity is the 3D counterpart to circularity, with a value of 1 being perfectly spherical. Rawji *et al.* 2020<sup>70</sup> notes that there is a small but significant decrease in sphericity of microglia when mice receive niacin treatment. The sphericity values are similar to those we obtained for circularity, although it is not clear whether, for example, 0.7 circularity is readily comparable to 0.7 sphericity in terms of extent of cell deformation. Compared to the literature, cultures analysed here appeared more amoeboid in both control and treatment groups.

### 3.5. Summary / conclusions

Both microglia and astrocytes express Gpr109a, which is nuclear-localised. Although some statistical analyses suggested changes in marker expression, these were typically of very small magnitude, and did not show consistent dose-response effects, and so cannot be reliably described as genuine cell responses. For example, niacin treatment lacked a dose response only inducing a statistically significant increase in Nox2 expression 0.015  $\mu$ M concentration and in Iba1 expression at 1.5  $\mu$ M. Niacin at concentrations 0.015  $\mu$ M – 15  $\mu$ M did significantly increase Gpr109a expression compared to control; however, only the doses 0.015  $\mu$ M and 0.15  $\mu$ M caused a significant upregulation of Arg1. Additionally, niacin

still lacked a dose response for Arg1 and Gpr109 as whilst doses increased expression there was no evidence of a dose-response. LPS at 150 ng/mL seemed to induce toxicity, indicated by visual observations and reduced cell counts. Neither of the Gpr109a ligands tested (NA and MMF) were associated with consistent changes in marker expression. None of the treatments induced detectable and reliable changes in morphology. Further testing will be required to assess whether the chosen markers and morphological assessments are suitable for the intended investigations, but it seems likely that a different experimental setup will be required e.g. based on a different culture system, elaborated upon further in section 4.2.5.

# Chapter 4: General Discussion and Conclusions

## 4.1. Neural immune cells express Gpr109a, but did not show detectable responses to Gpr109a ligands

This project attempted to prove whether the immune competent neuroglial cell types express Gpr109a, and whether they respond to Gpr109a ligands. Gpr109a expression was identified in both neural cell types investigated: microglia and astrocytes. This finding is important, as previous reports on microglia and astrocyte expression of Gpr109a are ambiguous. However, despite confirmation of Gpr109a expression suggesting that both microglia and astrocytes have the potential to be modulated by Gpr109a ligands, neither of the two Gpr109a ligands tested here (niacin and MMF) demonstrated clear effects on marker expression (Arg1, Iba1, and Nox2) or cell morphology, each of which might be indicative of changes in activation status.

Thesis data provide evidence for widespread Gpr109a expression by almost all cells in culture, whereas other studies have presented qPCR and Western blot data, showing the presence of Gpr109a mRNA and protein within a culture, but leaving doubt as to whether these are generated by a subset of cells, rather than most/all cells, or whether expression levels vary across individual cells.

Cell responses to LPS were not as obvious as might have been predicted, and so this aspect of the experimental design should also be considered for planning future experimentation.

To accommodate for lack of obvious responses of markers to LPS more sensitive techniques

which may detect smaller changes could be used; e.g. qPCR, western blot analysis, or Fluorescence-Activated Cell Sorting (FACS). Chosen pro-inflammatory stimulus should be considered, along with validation of the untreated control culture condition; is the baseline representative of the largely M0 population expected in healthy CNS tissue?

#### **4.2. Limitations of experimental design used here and ideas for future experimental work**

It is possible that microglia and/or astrocytes do respond to Gpr109a ligands, but that the experimental design used here was inappropriate for detecting these responses, or inappropriate for eliciting any such responses. Various elements of the chosen culture system could possibly confound investigations into inflammatory behaviours, and/or morphological measurements. These include the process of dissecting and processing tissue, the presence of serum in the culture medium, features of the culture substrate, and/or the absence of other neural cell types, to be discussed in sections 4.2.5 and 4.2.4 respectively.

##### **4.2.1. Microglial responses to Gpr109a ligands were only assessed in the absence of pro-inflammatory stimuli**

Before studying whether Gpr109a ligands might reduce inflammation, it was decided to study Gpr109a ligand impact on untreated (non-inflammatory) microglia. There was a lack of clear evidence that microglia did respond to the two ligands: MMF and niacin. However, this experimental setup may be too simplistic, and not relevant to clinical usage: e.g. the treatment of disease/injury. Gpr109a ligands may only cause notable changes to microglial

phenotype if microglia are already in an inflamed state. Further experiments should be performed, in which inflammatory phenotypes are induced in microglia and astrocytes, for example by LPS treatment, or ideally a more accurate simulation of neural injury/disease, relevant to the intended application of the Gpr109a ligand therapy (e.g. stroke or MS). Such an experimental setup may more reliably indicate whether Gpr109a ligands do generate therapeutically beneficial changes in neural immune cells.

#### **4.2.2. 3D cultures may better replicate *in vivo* cellular functions**

It is increasingly recognised that 2D monocultures fail to accurately mimic various features of the *in vivo* CNS environment, and depending on the research question being investigated, these differences can be critical to accurately modelling cell behaviours. Examples relevant to microglia culture include the fact that 2D cell cultures restrict microglial motility and shape, as primary branches are restricted to movement along one plane. Also, the majority of cell contact is with plastic/glass, rather than with ECM or other cells, which also limits cell-cell interactions. 2D cultures may induce low-level inflammatory responses, as glass/plastic presents an unnaturally stiff surface to the cells, and mechanical cues are increasingly recognised to influence cell behaviours. A consequence of the 2D plane is that cells grow flattened, and medium/gas perfusion will only occur on the non-adhered side of the cell <sup>108</sup>. These conditions could alter microglial behaviour, with microglia cultured in 2D typically showing amoeboid morphologies, associated with “classical activation” or the M1 phenotype, even in supposedly inactivated control conditions, where M0 should predominate <sup>176</sup>. To test whether 3D culture methods better replicate *in vivo* cellular functions compared to 2D an experiment assessing microglial

activation states could be ran in parallel. Possible 3D culture methods e.g. hydrogels and organotypic slice cultures are discussed in section 4.2.5.

#### **4.2.3. The process of establishing cultures may alter inflammatory profiles, at least initially**

Caldeira *et al.* demonstrated microglia isolated and maintained for 2 days *in vitro* (DIV) show an inflammatory microglial response, induced by the process of isolation (dissection and tissue processing) <sup>177</sup>. Microglia isolated and maintained for 16 DIV were described as unresponsive/dormant.

Processing of the tissue may cause an inflammatory response. To obtain a pure microglia we shook mixed glial cultures on a rotary shaker. The use of a rotary shaker has been suggested to inflame microglia shown by a more heterogeneous microglial population with a higher proportion of “M1” amoeboid microglia. These microglia also showed higher baseline of activation markers Arg1(M2), iNOS (M1), CD86 (M1/M2b), CD206 (M2) higher levels of cytokines TNF $\alpha$  (M1), IL-1 $\beta$  (M1), IL-10 (M2), and IGF-1 (M2) as well as increased phagocytic capability <sup>178</sup>. A suitable replacement may be mild trypsinisation with researchers showing microglia isolated by trypsinisation demonstrating a lower baseline for inflammatory markers (iNOS, CD86, CD206, and Arg1) and cytokines (TNF $\alpha$ , IL-1 $\beta$ , IL-10, and IGF-1). In addition, they also demonstrate that trypsinisation gives a higher yield and purer cultures with a microglial purity of >98% compared to shaking <sup>178</sup>.

#### **4.2.4. Do other cell types need to be included during testing?**

Microglia and astrocytes were identified as the principle immune cells of the CNS, but peripheral immune cells can enter the CNS, especially in some pathological states, and

other neural cell types have been shown to express Gpr109a. These cell types should be considered, both individually, and in the contexts of multicellular tissue and disease states. A major area of contention is whether disease-specific neurotoxic effects are mediated by invading peripheral macrophages, resident microglia, or both. Macrophages do not typically occupy the parenchyma, however when the BBB is disrupted they may infiltrate. For neurological diseases demonstrating moderate to high levels of macrophage infiltration, studies concentrating solely upon microglia may be failing to model crucial aspects of the disease, and vice versa.

For example, Rahman *et al.*<sup>88</sup> demonstrated in a MCAO mouse model that Gpr109a was expressed by 87.5% of CD11b<sup>+</sup> cells and 98.7% of Iba1<sup>+</sup> cells; however, these markers do not distinguish between microglia and peripherally-derived macrophages. By generating chimeric mice through bone marrow transplantation, Rahman *et al.* concluded that the neuroprotective effect post-MCAO was mediated by invading macrophages not microglia. Confirmation that microglia and astrocytes express Gpr109a supports the idea that Gpr109a ligands may induce immunomodulatory effects. However, targeting remains an issue. Oral delivery of ligands would be expected to affect peripheral immune cells, and perhaps other peripheral tissues, in addition to reaching the CNS. Although treatments such as niacin appear to be well-tolerated, if greater-than-usual doses are required to achieve therapeutic concentrations in the CNS, then peripheral (side-)effects must be assessed more closely. Side effects including flushing and nausea occur at doses as low as 30mg per day which may reduce patient medication adherence. Care is also needed to avoid niacin toxicity which may be induced at 3g per day, this can cause adverse effects e.g. hepatotoxicity<sup>179</sup>. It may also produce unexpected anti-inflammatory effects for autoimmune diseases outside of the CNS, e.g. Type 1 diabetes, colitis, Crohn's, arthritis<sup>138</sup>.

Human peripheral macrophages express Gpr109a<sup>125</sup>, and there is debate over whether any beneficial effects of Gpr109a ligands within the CNS may be due to activation of invading macrophages, or activation of microglia, or both. Clinical evidence from ischemic stroke and MS, diseases where peripheral immune cells infiltrate the immune system, cannot easily indicate whether either cell type is critical. In diseases, such as Parkinson's, Alzheimer's, and depressive disorders there is less dramatic infiltration of peripheral macrophages. Therefore, microglia would comprise a greater percentage of the immune cells present, and would make better targets. To address this question future experimental work may involve carrying the out the experiments with macrophages and microglia in parallel, to determine if infiltrating macrophages and microglia react to Gpr109a ligands in a similar way.

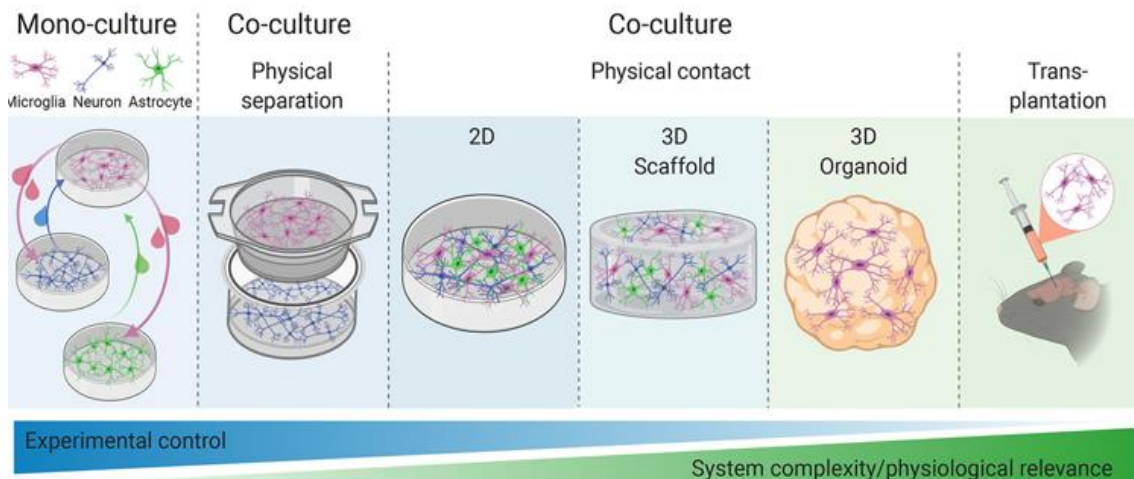
Beyond this, if Gpr109a ligands pass into the brain they are likely to activate other Gpr109a expressing neural cell types, which reportedly includes neurons<sup>91</sup>, and it is not clear whether this may be beneficial or detrimental, and would presumably lessen the signalling to target cells such as microglia or astrocytes. Further research should assess the effects of Gpr109a ligands on neural cells other than microglia and astrocytes, including to what extent they respond to these ligands in multi-cellular neural tissue. Research would also be warranted into whether delivery could be achieved directly into the CNS, for example nasally, to limit/avoid effects on peripheral immune cells and other peripheral tissues.

#### **4.2.5. More complex models: 3D co-cultures, organotypic slice cultures, *in vivo***

Models with greater complexity, incorporating both 3D environment and multiple cell types include co-cultures within hydrogels, organotypic brain slice cultures, and *in vivo* experiments (**Fig 4.1**). Hydrogels allow for researchers to study effects on cell types in



isolation or in conjunction with other cell types in mixed cultures in a 3D environment, where behaviours and especially morphologies may more closely resemble those *in vivo*. When compared to 2D culture, the immortalised microglial (BV2) cell line cultured in a 3D collagen construct demonstrated greater levels of cell viability with low levels of lactate dehydrogenase activity 48 h post-culture establishment. Untreated 3D cultures show lower levels of the inflammatory cytokines IL-6, TNF $\alpha$ , and MCP-1 when compared to untreated 2D coated and uncoated monolayers<sup>180</sup>. 3D models demonstrate different activation responses to LPS, compared to 2D monolayers<sup>180</sup>. LPS-treated 3D cultures also show a more noticeable increase in inflammatory cytokine expression (IL-6, TNF $\alpha$ , and MCP-1) relative to control, when compared to LPS-induced responses in 2D. However, untreated/treated 3D cultures still show lower expression of IL-6, TNF $\alpha$ , and MCP-1 compared to 2D. The inflammatory effect was seen more homogenously throughout the culture in 3D compared to 2D monolayers seen as a uniform upregulation of CD40. Authors did not speculate the reason for this but it could have been because of an inflammatory response induced by the unnatural environment of 2D cell culture, resulting in an already elevated inflammatory state within the 'control' condition.



**EXAMPLES OF WHAT EACH CULTURE FORMAT IS USEFUL FOR**

<p>Verification of cell-type identity</p> <p>Assessing basic cell-functions, but is affected by the lack of other cell types</p> <p>Elucidating how secretions from one cell type affects another</p> <p>Analysing secretome</p>	<p>Assessing maturational effects of cell types upon each other, but limited to secreted signals</p> <p>Analysing more complex bi-directional signalling</p>	<p>Most common, simple and reproducible co-culture format</p> <p>Studying secreted + contact mediated interactions, but limited cell-cell contact due to 2D</p> <p>Separate generation of cells prior to co-culture enables mix-and-match of cell-type proportions, genetic background and delivery of cell-type specific labels, tools, indicators etc.</p>	<p>Physiologically relevant cell-cell contact, retention of secreted molecules and proteins</p> <p>Scaffolds enable easy and reproducible imaging assays</p>	<p>Organoids mimic <i>in vivo</i> development of neuro- and gliogenesis but reproducibility is challenging</p>	<p>Examining microglia in an intact brain environment, allowing for investigation of microglial responses to brain injury/disease pathologies</p> <p>Possibility to study regional differences by varying the injection site</p> <p>Assessing the impact of peripheral factors</p>
--	--	--	--	--	--

**Figure 4.1: Experimental conditions typically involve a trade-off, with increasing complexity being associated with a loss of experimental control.** Schematic illustrating how increasing complexity of experimental conditions is inversely associated with extent of experimental control/monitoring <sup>144</sup>.

Differential microglial responses in 3D vs 2D culture were also seen in a study comparing the drug response of monocyte-derived microglia-like cells (MDMi) from AD patients in a thick matrigel layer (3D) compared to a matrigel coated surface (2D). These MDMi cells are described as behaving similarly to microglia, and in 3D models were reported to show a ‘more mature’ phenotype more closely resembling M0 microglia, with greater ramification and differing response to drug treatment <sup>181</sup>. MDMi cultured in 3D hydrogels were also reported to have greater cell viability, and lower levels of inflammation compared to 2D monolayers. The potential for priming during culture establishment has not been

completely bypassed by this method as cells still require extraction from tissue. Also, it is not clear whether there are any as-yet-undetected differences between *in vivo* microglia and these monocyte-derived cells, which seems possible as monocyte-derived macrophages are known to exhibit differences compared to microglia. Future experiments may seek to investigate a direct comparison studying differential responses between 2D microglial cultures and 3D microglial cultures, similar to this MDMi study <sup>181</sup>

In cultured brain slices, Stence *et al.* showed microglia becoming activated as early as 12 h post-dissection, suggesting that slices should perhaps be fixed at an earlier stage (<12 h), to limit the chances of this activation confounding the experiment <sup>176</sup>. Both organotypic cultures and hydrogels lack natural perfusion of tissue, due to loss of circulatory system, which can only be partly compensated for through regular/constant media changes.

*In vitro* organotypic slices cultures and *in vivo* models would allow for microglia and astrocytes to retain their physiologically relevant cell-cell and cell-ECM contact. Microglia and astrocytes are ubiquitous in the CNS, and so are always able to exchange signals. Culturing these cells in isolation has the potential to cause an inflammatory response, as microglia and astrocytes lose their natural interactions with other microglia, astrocytes, oligodendroglia, and neuronal cells <sup>5,182</sup>. For example, neuronal expression of fractalkine is detected by microglial receptors (CX3CR1), and has an anti-inflammatory effect on microglia. Microglia have been shown to induce a pro-inflammatory astrocyte state (A1), and an anti-inflammatory state (A2), under different conditions. Astrocytes have also been shown to influence microglial activation in a similar fashion <sup>182</sup>. *In vivo* studies are the most appropriate for studying microglia/astrocyte interaction in their natural microenvironment, as physiological perfusion of tissues is maintained. *In vivo* studies are, however, difficult to conduct and monitor due to technical, time and cost considerations,

and are correctly subject to greater ethical scrutiny. *In vivo* neurological injury models are usually particularly distressing to animal subjects. It would be beneficial for researchers to have simple, easily controlled, high throughput *in vitro* culture systems, to perform initial studies before a smaller, targeted set of *in vivo* experiments.

#### **4.2.6. Disease modelling**

LPS was used here as a pro-inflammatory control, and a basic simulation of an inflammatory disease state. However, the presence of LPS is representative of a bacterial infection, and immune responses may be subtly different, compared to responses to trauma or neurodegenerative conditions. There are also considerations around modelling injury or disease in tissue from animals during early development, in contrast to adult, aged or diseased individuals.

Aging is an important factor in microglial activation status, with advanced age being considered a priming stimulus<sup>183,184</sup>. Both Microglia and Astrocytes are susceptible to priming<sup>185</sup> and are potentially being primed or inflamed before LPS stimulation therefore not truly M0 or A0. Priming describes an exaggerated microglial response to sub-threshold inflammatory stimulus, usually the result of a 'priming' inflammatory stimulus. This priming effect may be present in many culture conditions, induced by the dissection process during culture establishment.

Advanced age is difficult to simulate *in vitro*, but may be highly relevant to neuroimmune responses. Rodents are the most common experimental animals, and although adult tissue could be used instead of neonatal, even adult rodents are not truly representative of aged humans, and rodents do not naturally develop degeneration resembling AD, PD, MS etc. In future investigations the use of an 'aged' culture could better mimic neurodegenerative

diseases associated with age such as AD or PD, and this may be best facilitated by using human-derived cells, possibly induced pluripotent stem cell cultures, and possibly derived from PD or AD patients.

LPS is the standard experimental pro-inflammatory stimulus. However, neurodegenerative diseases are not widely believed to be caused by elevated LPS levels in the brain. To address this issue future experiments might look to investigate the impact of inflammatory stimuli classically associated with neurodegeneration, for example, amyloid  $\beta$ ,  $\alpha$ -synuclein, or tau protein. It will be important to understand whether any of these pathology-related molecules alter Gpr109a expression levels in the CNS, and whether Gpr109a activation affects cell responses to these molecules, especially in terms of immune responses and/or degradation pathways.

#### **4.2.7. Assays and analyses**

Microglial activation status was assessed by marker expression and morphology, both via fluorescence microscopy. Fluorescence microscopy indicates relative levels of protein expression, and was expected to reveal substantial changes. However, it is not as precise a measurement as seen in qPCR and Western blot analysis. Fluorescent microscopy for morphology also introduces the potential for human error/bias. Microglia were delineated using the ImageJ hand drawn tool, which has an element of imprecision, especially around fine processes, although the use of this technique for all conditions should reduce the significance of this compromise.

Fluorescent microscopy offers the benefit of allowing for the observation of intracellular localisation and translocation. Fluorescent microscopy also allows for morphological analysis in particular measurements assessing the complexity of processes protruding from

microglia and astrocytes. Considering the limitations of only using fluorescent microscopy, a combination of fluorescent microscopy and qPCR/Western blot may be recommended for future experiments.

### 4.3. Phenotypic markers and terminology

There is emerging evidence, discussed in Chapter 1, suggesting that microglia activation states may not be as discrete as the terms M1 and M2 might imply. If genuine, reproducible/identifiable subtypes exist, they might be defined by morphological, gene expression, protein expression, and/or behavioural characteristics. To accurately define microglia it may be necessary to study all of these levels. However, the majority of microglial research still refers to these activation states (M1/M2, and to a lesser extent M0) when discussing microglial phenotypes.

There is not a completely predictable correlation between marker expression and outcome, so presence/increase of a single M1 marker should not be interpreted as detrimental. For example, M1 microglia typically release cytokines and ROS/RNS. iNOS is a metabolic enzyme catalysing the production of NO oxide, expressed by microglia, astrocytes, and neurons in the CNS. M1 microglia express high levels of iNOS but due to its potential to be expressed in other cell types, identification would require co-staining with a microglial marker. High/prolonged upregulation of iNOS in microglia is associated with bystander tissue damage, consistent with the proposal that M1 microglial activation may be detrimental. However, iNOS could have regulatory functions in CNS inflammation: iNOS<sup>-/-</sup> (knockout) mice are hyper-susceptible to Experimental Autoimmune Encephalomyelitis (EAE), suggesting that iNOS could have beneficial regulatory functions in CNS inflammation

115.

For future investigations it may be more accurate to consider monitoring their activity in terms of function as well as morphology and marker expression. The following behaviours

could be considered: phagocytosis, secretion of cytokines/ROS/RNS, and potential neurotoxic/neuroprotective effects on other cell types.

Microglial phagocytosis is an important physiological process allowing for microglia engulfment and clearance of pathogens, dead or degenerating cells, and cellular debris.

Phagocytosis also has roles in development of mature neuronal circuits and neural plasticity where they prune redundant and excessive synapses. Malfunction of this process can lead to ineffective pruning. Excessive pruning has been implicated in both autism spectrum disorders (ASD) and AD. Phagocytosis may be responsible for disrupting the balance between excitatory and inhibitory synapses in cases of ASD<sup>186</sup>.

Meanwhile, it may be responsible for excessive elimination of synapses in AD. CD47 protects synapses from excessive pruning during development by binding to SIRP $\alpha$  a CD47 receptor. Knockdown of SIRP $\alpha$  resulted in increased synaptic loss and enhanced cognitive impairment. Phagocytosis was assayed by measuring engulfment of synaptosome. This was analysed by calculating the fraction of Iba1 (microglial) area that overlapped pHrodo red conjugated synaptosome area <sup>187</sup>. In models of AD the A $\beta$  molecule has been shown to induce microglial phagocytosis of neurons <sup>188</sup>. Therefore, phagocytosis of A $\beta$  may be protective.

Further phagocytic assay methods include measuring the amount of internalised A $\beta$ <sub>1-42</sub> using enzyme-linked immunosorbent assay <sup>189</sup> or by measuring the uptake of fluorescently labelled carboxylate-modified microspheres <sup>188</sup>.

Phagocytosis is demonstrated by both M1 and M2 thus is unable to identify microglial activation. Therefore, it is desirable to use in conjunction with other functional assays, such as measuring the secretion of pro-inflammatory and anti-inflammatory molecules, and neuronal survival.



Ultimately, assessments are most concerned with whether microglial responses lead to improved functional outcomes, e.g. reduced pathology or improved neurological performance, rather than being strictly tied to a specific marker or morphological feature, and testing in disease models. Examples of functional assays to be used in rodent models is the Basso, Beattie, and Bresnahan locomotor score method. This measures functional recovery by rating recovery stages by monitoring rat locomotor activity, e.g. assessing trunk position and stability, paw placement, and tail position <sup>54</sup>. When studied in clinical trials functional studies include UPDRS and MMSE, as explained previously in sections 1.9 and 1.6 respectively.

The need to monitor the effects of microglia on nearby cells, i.e. destruction of tissues, neurotoxic effect, astrogliosis, highlights the advantage of studying overall outcomes in simulated tissues/disease states, rather than simply studying microglia alone, or expression of a single marker alone.

#### **4.4. Prophylaxis as a clinical consideration**

A potential therapeutic avenue could be prophylactic treatment. To use Gpr109a ligands as a way of priming the anti-inflammatory activity of the immune system against inflammatory stimulus. Fu *et al.* <sup>89,90</sup> pre-treated microglia with 1.5 mM BHBA (Gpr109a ligand) before treatment with 10 ng/ml LPS. BHBA pre-treatment attenuated the LPS induced increase in iNOS, COX-2, TNF- $\alpha$ , IL-1 $\beta$ , and NF- $\kappa$  $\beta$ . Additionally Fu *et al.* saw an inversely proportional time-dependent response of NF- $\kappa$  $\beta$  levels with LPS and LPS+BHBA. This also indicates that incubation times also an important factor to consider.

If pre-treatment was reliably shown to be immunomodulatory in ways that may have therapeutic utility, then prophylactic drug treatment may be trialled for people at risk of developing neurological diseases; e.g., stroke, or MS patients, ahead of disease episodes.

#### **4.5. Conclusion**

Gpr109a expression has been demonstrated in the two major immune-competent cells of the CNS. Although no obvious responses to Gpr109a ligands were observed, it remains possible that the test conditions used here were unsuitable for detecting cellular responses. For example, a 3D culture, better reproducing *in vivo* cell morphologies, coupled with simulated disease/injury (an inflammatory state before ligand treatment), may be more likely to generate identifiable phenotypic and morphological responses. Given that (i) neural cells express Gpr109a, (ii) Gpr109a ligands cross the BBB, and (iii) the clinical use of such ligands, it is important to understand the effects of these ligands on all neural cells. This is increasingly important, as such ligands are being employed in clinical trials for MS, stroke and possibly other neurological conditions. Understanding these responses, and perhaps exploiting any therapeutically beneficial responses, could provide novel treatments for poorly-served patient populations.

# Appendix

Table 1.2 Studies reporting objective morphometric values for microglia

Table 1.8 Evidence for microglial involvement in neurological conditions, from human patients

Table 1.9: Microglial involvement in neuroinflammation in animal models

For space reasons, and to keep a simple flow in the introduction, several Tables are placed in this Appendix

<b>Table 1.2: Studies reporting objective morphometric values for microglia</b>			
<b>Source/ culture details</b>	<b>Treatment</b>	<b>Phenotypes (morphology, protein expression) present, assays</b>	<b>Morphometric measurements</b>
Adult male rats, coronal sections, layers I-VI <sup>190</sup>	No treatment; examined healthy cells within layers of prefrontal cortex	Microglial morphology is consistent across cortical layers of the prefrontal cortex.	Convex hull area, and cell body perimeter ( $\mu\text{m}$ ), branch points, total process length ( $\mu\text{m}$ ), total process volume ( $\mu\text{m}^3$ ), number of processes.  'Microglia size affects the extent of ramification, convex hull vs soma perimeter, branch point, primary processes, total process length, total number of processes, radius vs nodes, intersections, process length, process volume, process diameter, surface area'
Mouse coronal slice sections (fixed) <sup>57</sup>	tMCAO, pMCAO or TBI of mice	<p>CX3CR1 and CD11b are microglia markers.</p> <p>CX3CR1<sup>+</sup> cells Post-tMCAO: hypertrophic all over lesion Co-localised staining with <b>CD11b<sup>+</sup> ramified</b> microglia but <b>not CD11b<sup>+</sup> amoeboid</b>. Post-pMCAO and TBI: hypertrophic CX3CR1<sup>+</sup> cells seen in the lesion core.</p> <p>CD11B<sup>+</sup> cells Post-tMCAO: Mostly round, not co-localised with CX3CR1. Post-pMCAO and TBI: round and CX3CR1.</p>	<p><b>Higher percentage of ramified CD11b<sup>+</sup> cells after tMCAO than after either pMCAO or TBI.</b></p> <p><u>tMCAO</u> Area: increased between naïve (54.57) and tMCAO (85.78*). Suggested as indicative of hypertrophic cells. Perimeter: increase between naïve (61.46) and tMCAO (75.27*) Circularity: no difference between naïve (0.26) and tMCAO (0.25) Feret's diameter (calliper): increase between naïve (17.10) and tMCAO (20.10*) Aspect ratio: no significant differences Solidity: no significant changes between naïve cortex (0.55) and tMCAO (0.55) Grid crossings: increase between naïve (3.8) and tMCAO (4.39*)</p> <p><u>pMCAO</u> Area: no difference between naïve (54.57) and pMCAO (57.13) Perimeter: reduction between naïve (61.46) and pMCAO (47.69*) Circularity: increase between naïve (0.26) and pMCAO (0.38*) Feret's diameter (calliper): decrease between naïve (17.10) and pMCAO (14.92*) Aspect ratio: no significant differences Solidity: increase between naïve (0.55) and pMCAO (0.68*) Grid crossings: decrease between naïve cortex (3.8) and pMCAO (2.66*)</p> <p><u>TBI</u> Area: no difference between naïve (54.57) and TBI (71.90) Perimeter: decreased, naïve (61.46) and TBI (58.26*) Circularity: increase between naïve (0.26) and TBI (0.37*) Feret's diameter (calliper): increase from naïve (17.10) to TBI (17.73*) Aspect ratio: no significant differences Solidity: increase between naïve (0.55) and TBI (0.65*) Grid crossings: decrease between naïve (3.8) and TBI (3.22*)</p>

N9 microglia cell line <sup>68</sup>	300 ng/ml LPS, 24 h	<u>qRT-PCR.</u> M1 markers: NOS2, MHC-II M2 markers: Arg1, Fizz1 <u>Morphological characterization</u> Using Iba1 marker to delineate Area Perimeter Feret's diameter <u>Inflammation</u> NF- $\kappa$ B activation	Increased expression of NOS2 and MHC-II Decreased expression of Arg1 and Fizz1 Induced microgliosis (change from oval or ramified shape to amoeboid and increased cell density) Amoeboid microglia lacked ramifications or had shorter and thicker branches (hypertrophied?) These branched amoeboid microglia account for 75% of the cells incubated with LPS.  <u>Area</u> Control ~230 $\mu$ m <sup>2</sup> LPS ~466 $\mu$ m <sup>2</sup>  <u>Perimeter</u> Control ~ 80 $\mu$ m    LPS ~ 97.6 $\mu$ m  <u>Feret's diameter</u> Control ~26.4 $\mu$ m    LPS ~ 34.4 $\mu$ m
Primary microglia, 1-2 day old mice. Pure microglia cultures <sup>66</sup>	Amyloid beta (1-42) oligomers and fibrils (2 or 16 days)	<u>Morphological analysis</u> Using Iba1 marker to delineate Area Perimeter Circularity Feret's diameter  <u>miRNA expression</u> miR-155, miR-124, TNF $\alpha$ , IL-1 $\beta$ , IL-6, HMGB1, IL-18, NLRP3 <u>Protein expression</u> CD11b and CD86	<u>Area</u> 2 DIV    Control ~600    Amyloid Beta ~ 1231 16 DIV    Control ~1297    Amyloid Beta ~ 1467  <u>Perimeter</u> 2 DIV    Control ~140    Amyloid Beta ~ 148 16 DIV    Control ~216    Amyloid Beta ~ 160  <u>Feret's Max (diameter)</u> 2 DIV    Control ~46.4    Amyloid Beta ~45.6 16 DIV    Control ~74.4    Amyloid Beta ~52.8  <u>Circularity</u> 2 DIV    Control ~0.448    Amyloid Beta ~0.416 16 DIV    Control ~0.38    Amyloid Beta ~0.456
Primary human resected tissue (intractable epilepsy) <sup>65</sup>	<i>In vitro</i> cell culture. <i>E.coli</i> bio-particle exposure	Amoeboid, ramified, pseudopodic Subjective labelling, rather than measurements	<u>Area</u> ('cell body size, excluding membrane sheets'; methods do not make clear whether processes are included with soma; membrane overlapping with other cells seems to be excluded) Pseudopodic    ~90 $\pm$ 10 $\mu$ m <sup>2</sup> Amoeboid    ~190 $\pm$ 10 $\mu$ m <sup>2</sup> Ramified    ~305 $\pm$ 30 $\mu$ m <sup>2</sup> .

2-3 month old male mice, coronal slice culture <sup>191</sup>	Unilateral deafferentation of trigeminal nuclear complex	Software reconstructed 3D microglia.	Cell numbers: microglia density Length of processes: [see <b>Table 1.4</b> ] 'Cell body size': frequency graph of cell sizes Number of primary processes: [no numerical data given]
Rat post-mortem fixed sections, hippocampus, hypothalamus, septofimbrial nucleus <sup>30</sup>	Intra-cerebro-ventricular injection: neuraminidase (500 mU).	<p>'Clusters' of similar profiles were identified, and described based on appearance and location:</p> <p>Cluster1 (<b>largest</b>): large soma, ramified with thick primary processes and short secondary processes 1.1 activated, septofimbrial nucleus and surveillant hypothalamic 1.2 surveillant hippocampal</p> <p>Cluster2: Small soma, highly ramified, thin primary and secondary processes 2.1 surveillant, septofimbrial nucleus 2.2 surveillant, hippocampal</p> <p>Cluster3: highly ramified, thick processes 3.1 activated, hippocampal 3.2 surveillant hypothalamic</p> <p>Cluster4 (<b>smallest</b>): Short poorly ramified processes of varying thickness around swollen cell bodies, termed either activated, "unramified", "bushy" "type IV" or "R3". 4.1 activated, septofimbrial nucleus, hypothalamic 4.2 activated, septofimbrial nucleus, hypothalamic</p>	<p>Neuraminidase induced morphological changes and increased IL-1<math>\beta</math> expression (indicating acute inflammatory response). Area, Perimeter, Circularity Index, Mean radius, Convex hull perimeter, Bounding circle diameter, Max span convex hull, Roughness, Convex hull area, Density, Lacunarity, The ratio convex hull radii, Convex hull circularity, Convex hull span ratio</p> <p>'Only <b>cell circularity (index; CI)</b>, <b>convex hull area (CHA)</b>, <b>perimeter</b>, and <b>convex hull span ratio (CHSR)</b> were suitable for hierarchical cluster analysis (MMI&gt;0.55)' Hierarchical cluster analysis identifies four microglia clusters, numbered <b>largest to smallest</b>, 1-4. Linear discriminant analysis predicts allocation of microglia to one of the four clusters, based on CHSR, CC, and CHA, in this order.</p> <p>Principle component analysis suggests <b>maximum span across the convex hull (MSACH)</b> and <b>convex hull circularity (CHC)</b> may be useful in further classifying microglia.</p> <p>Cluster 1, CHSR &lt;1.35 with CI &gt;0.0145 or CHSR between 1.35-1.93 with CHA&lt;1915. 1.1: MSACH: 52 <math>\mu</math>m                      1.2: MSACH: 63 <math>\mu</math>m</p> <p>Cluster 2, CHSR&lt;1.35 with CI between 0.0035-0.0145 2.1: CHC: 0.80                              2.2: CHC: 0.88</p> <p>Cluster 3, CHSR&lt;1.35 with CI &lt;0.0035 or CHSR between 1.35-1.93 with CHA&gt;1915 3.1: MSACH: 60 <math>\mu</math>m                      3.2: MSACH: 82 <math>\mu</math>m</p> <p>Cluster 4 CHSR &gt; 1.93 4.1: CHC: 0.73                              4.2: CHC: 0.85</p>
Rat post-mortem fixed slice culture, hypothalamus, coronal brain <sup>72</sup>	Intra-cerebro-ventricular injection:	Identified 4 clusters each defined by their inflammatory status and specific morphological parameters.	<p><b><u>Assessed relationship between parameter and IL-1<math>\beta</math> expression</u></b> Cell perimeter, Circularity index, Mean radius, Convex hull perimeter, Bounding circle diameter, Max span convex hull, Roughness, Convex hull area, Density, Cell area, Lacunarity, The ratio convex hull radii, Convex hull circularity, Convex hull span ratio.</p>

	neuraminidase (500 mU).	<p>Cluster1: intermediate activation, "less elongated"</p> <p>Cluster2: slightly activated, highly ramified.</p> <p>Cluster3: intermediate activation, rod shaped</p> <p>Cluster4: highly activated, highly circular</p>	<p>Significant relationship seen between parameter and IL-1<math>\beta</math> in all but The ratio convex hull radii, Convex hull circularity, Convex hull span ratio.</p> <p>MMI &gt; 0.55 are multimodal and therefore suitable to perform cluster analysis.</p> <p>Based on MMIs, only <b>lacunarity, circularity index (CI), and convex hull span ratio (CHSR)</b> were suitable for hierarchical cluster analysis.</p> <p>Cluster1: intermediate activation, lacunarity (0.4), CI (0.011), CHSR (1.52).</p> <p>Cluster2: slightly activated, lacunarity (0.6, highest), CI (0.007), CHSR (1.43)</p> <p>Cluster3: intermediate activation, lacunarity (0.38), CI (0.016), CHSR (2.55)</p> <p>Cluster4: highly activated, lacunarity (0.37), CI (0.031, highest), CHSR (1.57)</p>
Mice. Sagittal section at 30 $\mu$ m or 50 $\mu$ m thickness <sup>67</sup>	Npc1nmf <sup>164</sup> mutant mouse model of Niemann-Pick Type-C1 disease (NPC1). Western diet.	<p>Morphological changes occur early in cerebellar layer of Npc1nmf<sup>164</sup> mice: increased soma size thicker and retracted processes</p> <p>Becoming more amoeboid with age.</p>	<p><b>Cell volume <math>\mu</math>m<sup>3</sup></b></p> <p>WT WK4 ~700 (** vs NPC1 WK4)</p> <p>NPC1 WK4 ~1500</p> <p>NPC1 WK12 ~1000</p> <p><b>Process length <math>\mu</math>m</b></p> <p>WT WK4 ~300 (***) vs NPC1WK12)</p> <p>NPC1 WK4 ~280 (***) vs NPC1WK12)</p> <p>NPC1 WK12 ~160</p> <p><b>Process mean volume <math>\mu</math>m<sup>3</sup></b></p> <p>WT WK4 ~6 (** vs NPC1 WK4), (***) vs NPC1 WK12)</p> <p>NPC1 WK4 ~9</p> <p>NPC1 WK12 ~14</p> <p><b>Number of intersections</b></p> <p>WT WK4 ~190 (****vs NPC1 WK4)</p> <p>NPC1 WK4 ~190 (****vs NPC1 WK12)</p> <p>NPC1 WK12 ~80</p> <p><b>Total volume of phagosomes <math>\mu</math>m<sup>3</sup></b></p> <p>WT WK4 - ~280 (**** vs NPC1 WK4), (***)vs NPC1 WK12)</p> <p>NPC1 WK4 ~950</p> <p>NPC1 WK12 ~750</p>
Male Long-Evans rats. 100 $\mu$ m coronal sections of prelimbic cortex (PL) and nucleus accumbens (NAc) <sup>69</sup>	Chronic ethanol exposure via vapour inhalation from postnatal day 5.	<p>Used 3D reconstruction (Imaris software)</p> <p><b>Prelimbic cortex (PL)</b></p> <p><b>CIE compared to control</b></p> <p>Lower cell density, cell volume, and number of branch points.</p>	<p>Microglia density, soma volume, cell volume, branch points, Sholl intersections.</p> <p>Authors suggest may be indicative of amoeboid or hypertrophic morphology.</p> <p>Significant difference: *(versus LPS),</p>

	Iba1 staining	<p>Larger in soma intensity.</p> <p><b><u>LPS compared to control</u></b> Larger soma volume, cell volume, soma intensity, number of branch points.</p> <p><b><u>LPS compared to CIE</u></b> Larger soma volume, cell volume, soma intensity, number of branch point, Sholl intersections.</p> <p><b><u>Nucleus accumbens (NAc)</u></b> <b><u>LPS compared to control</u></b> Larger soma volume, soma intensity. Lower cell density.</p> <p><b><u>LPS compared to CIE</u></b> Larger in soma volume, cell volume.</p>	<p>*(versus CIE)</p> <p><b><u>Soma volume (<math>\mu\text{m}^3</math>)</u></b> PL control ~400    LPS ~700****+    CIE ~480 NA Control ~350    LPS ~390    CIE ~600****+</p> <p><b><u>Cell volume(<math>\mu\text{m}^3</math>)</u></b> PL Control ~1700    LPS ~2100****+    CIE ~1000* NA Control ~1510    LPS ~1570    CIE ~1480</p> <p><b><u>Branch points</u></b> PL Control ~0.0018    LPS ~0.0012    CIE ~0.0024 NA Control ~0.021    LPS ~0.17    CIE ~0.19</p> <p><b><u>Sholl intersections</u></b> PL Control ~0.011    LPS ~0.014    CIE ~0.009 NA Control ~0.015    LPS ~0.013    CIE ~0.014</p> <p><b><u>Territory (<math>\mu\text{m}^3</math>)</u></b> PL Control ~60,000    LPS ~58,000    CIE ~64,000 NA Control ~44,000    LPS ~58,000    CIE ~50,000</p>
C57BL/6J mice cerebral cortical microglial monoculture <sup>71</sup>	<p><i>In vivo</i> studies- Mice BHB (6 days) Then either saline or LPS challenge</p> <p><i>In vitro</i> studies –</p>	<ul style="list-style-type: none"> <li>• BHB prevented microglial process retraction when exposed to LPS.</li> <li>• However this was mediated by the Akt-small RhoGTPase axis</li> <li>• Inhibition of the Akt-small RhoGTPase axis and BHB treatment lead to microglial process retraction in the presence of LPS.</li> </ul>	<p>Only measurement taken was circularity index. Measure of ramification. 1 perfectly circular and 0 highly ramified.</p> <p><b><u>Concentration</u></b> Control ~0.48    BHB 1 mM ~0.40    BHB 3 mM ~0.33**    BHB 5 mM ~0.23**</p> <p><b><u>Incubation period, BHB at 5 mM</u></b> Control 0 h ~0.42    BHB 1 h ~0.364    BHB 4 h ~0.28**    BHB 8 h ~0.21** <i>In vivo</i>: BHB and LPS BHB- LPS- ~0.44</p>



	Primary microglial cultures LPS priming Then BHB	BHB was ruled not to act through Gpr109a as Gpr109a agonist's niacin and MK-6892 failed to elicit the same response.	BHB+ LPS- ~0.21** BHB- LPS+ ~0.41 BHB+ LPS+ ~0.23**(compared to BHB-LPS+)  <i>In vitro</i> : LPS treatment (1 µg/mL, 24 h; priming), then BHB (5 mM, 8 h) LPS- BHB- ~0.41 LPS- BHB+ ~0.19** LPS+ BHB- ~0.43 LPS+ BHB+ ~0.21** (compared to BHB-LPS+)												
C57BL/6J, ex vivo multiphoton live imaging, spinal cord injury model <sup>70</sup>	Intraperitoneal niacin treatment  100 mg/kg daily for 7 days.	<ul style="list-style-type: none"> <li>Niacin upregulates CD36 and enhances myelin debris phagocytosis by microglia in culture.</li> <li>Niacin promotes clearance of myelin debris in lesions by phagocytosis, enhances oligodendrocyte progenitor cell number, and improves remyelination.</li> </ul> <p>Treatment with Niacin also increases Gpr109a expression in both young and middle-aged mice.</p>	<p>Cell area (µm<sup>2</sup>)</p> <table> <tr> <td>Control</td> <td>~ 850***</td> <td>Niacin</td> <td>~1350***</td> </tr> </table> <p>Volume (µm<sup>3</sup>)</p> <table> <tr> <td>Control</td> <td>~1300***</td> <td>Niacin</td> <td>~2200***</td> </tr> </table> <p>Sphericity</p> <table> <tr> <td>Control</td> <td>~0.66*</td> <td>Niacin</td> <td>~0.62*</td> </tr> </table>	Control	~ 850***	Niacin	~1350***	Control	~1300***	Niacin	~2200***	Control	~0.66*	Niacin	~0.62*
Control	~ 850***	Niacin	~1350***												
Control	~1300***	Niacin	~2200***												
Control	~0.66*	Niacin	~0.62*												
<p>BHB: Beta Hydroxybutyric acid; CIE: chronic intermittent ethanol; Cluster: microglial categorisation based on morphology; DIV: days <i>in vitro</i>; LPS: lipopolysaccharide; MCAO: middle cerebral artery occlusion ; NF-κβ: Nuclear Factor Kappa Beta; NPC1: Niemann-Pick disease; pMCAO: permanent medial cerebral artery occlusion; qRT-PCR: Real-Time Quantitative Reverse Transcription PCR; TBI: traumatic brain injury; tMCAO: transient middle cerebral artery occlusion; type C1; WK: week; WT: wild type</p>															

**Table 1.8: Evidence for microglial involvement in neurological conditions, from human patients**

Model	Review	Cohort	Methods	Results
Alzheimer's disease:  Mild cognitive impairment (MCI) with cortical amyloid deposition <sup>86</sup>	Phase1 longitudinal study  Microglia mediated inflammation accompanied amyloid in cases of MCI due to AD.	42 MCI cases  12 age-matched healthy controls	<ul style="list-style-type: none"> <li>• Inclusion criteria: declining memory function over 6 months, age 50-85, good employment history, amnesic MCI.</li> <li>• Exclusion criteria: recreational drug use, sedative medications, significant neurologic or psychiatric disease.</li> <li>• Participants with amyloid deposition: PET scan (markers for beta amyloid and microglia activation [TSPO]).</li> <li>• Participants with MCI: neuropsychological assessment</li> </ul>	<p>MCI: 26 of 42 cases showed raised cortical amyloid load.</p> <p>Amyloid+ MCI: 22 of 26 cases showed clusters of increased cortical microglial activation accompanying amyloid deposition.</p> <p>This positive correlation was seen in frontal, parietal, and temporal lobes.</p>
Prodromal Alzheimer's disease:  MCI with cortical amyloid and Tau deposition <sup>192</sup>	<p>Results support the theory of a biphasic trajectory of inflammation in AD.</p> <p>First stage rising A<math>\beta</math> load correlates with increasing levels of inflammation, this resolves.</p> <p>As Tau tangles form in prodromal AD cases the rising Tau load is associated correlates with increasing levels of inflammation.</p>	<p>Longitudinal cross-sectional study following MCI cases <sup>86</sup></p> <p>Comparison of MCI cohort to measurements taken 2 years earlier as published in 2017 paper <sup>86</sup>.</p>	<ul style="list-style-type: none"> <li>• Cohort from 2017 paper<sup>86</sup></li> <li>• Same inclusion/exclusion criteria.</li> <li>• Within 10 weeks after PiB and PK PET scans <sup>18</sup>FF-PET became available of which 25 participants with MCI consented.</li> <li>• 38 MCI patients returned for the follow up appointment 2 years later.</li> <li>• Of the 38 MCI subjects</li> <li>• with baseline high PiB (prodromal; n=23) had 23 PiB+PK scans, 13 FTP scans</li> <li>• with baseline low PiB (n=15) had 15 PiB+PK cans, 9 FTP scans</li> <li>• Returning participant repeated cognitive tests</li> </ul>	<p>In early prodromal AD cases participants show increased amyloid dep over 2 years which correlates with increasing levels of inflammation.</p> <p>Levels of inflammation decline in prodromal AD cases with high A<math>\beta</math> but not Tau.</p> <p>Prodromal AD cases showing both high AB and Tau at baseline show further increase in Tau tangle load over 2 years that correlated with a rise in inflammation.</p>
MCI with cortical amyloid deposition, or early AD <sup>77</sup>	Microglia may be protective to axons in the early stages of AD	27 MCI or early AD cases	MCI and AD cases showing raised cortical beta amyloid had 11C-PK11195 PET, structural and diffusion magnetic resonance imaging.	<p>In MCI cases brain inflammation correlated inversely with plasma NfL levels, in the frontal, parietal, precuneus, occipital, and sensorimotor cortices.</p> <p>Potential use of NfL to measure protective efficacy of immune stimulation and monitoring efficacy of putative neuroprotective agents.</p>

<p>Alzheimer's disease <sup>193</sup></p>	<p>The protein module most strongly associated with AD is enriched in astrocyte and microglia proteins.</p> <p>The M4 astro/microglia module correlates most strongly with cognitive impairment.</p>	<p>Dorsolateral prefrontal cortex (DLPFC)</p> <p>Control = 94</p> <p>asymAD =102</p> <p>AD=305</p>	<p><u>Measuring protein levels with label-free MS and WGCNA</u></p> <p>CERAD amyloid plaque score</p> <p>Braak Tau neurofibrillary tangle score</p> <p>CDR – overall function status</p>	<p>The protein module M4 (sugar metabolism) correlates most closely with CERAD, Braak, and CDR.</p> <p>Its expression correlates most strongly with astrocytes and microglia.</p>
<p>Neuroinflammation and protein aggregation co-localize across the frontotemporal dementia (FTD) spectrum <sup>194</sup></p>	<p>Close association between inflammation and protein aggregation in FTD</p> <p>Activated amoeboid microglia closely associated with protein aggregates.</p> <p>Relationship between density of aggregates and density of microglia</p>	<p>Cross-sectional study</p> <p>FTD patients: 31</p> <ul style="list-style-type: none"> <li>• bvFTD: 10</li> <li>• svPPA: 11</li> <li>• nfvPPA: 10</li> </ul> <p>Age matched controls: 14</p> <p>Cambridge Brain Bank samples: FTLT-Picks' (Tauopathy) (n=3) FTLD-TDP Type C (n=3) FTLP-TDP Type A (n=3) Braak stage V AD (n=3)</p>	<ul style="list-style-type: none"> <li>• PET imaging, marker for microglial activation (proxy for neuroinflammation)</li> <li>• PET imaging markers for Tau, including aggregates (TDP-43)</li> <li>• No published information on inclusion and exclusion criteria.</li> <li>• Immunohistochemical analysis using CD68 to mark for active microglia.</li> </ul>	<ul style="list-style-type: none"> <li>• Neuroinflammation and protein aggregation elevated and co-localized</li> <li>• Most strongly in svPPA, where predominant aggregates are TDP-43</li> <li>• This relationship seen throughout disease course (<i>in vivo</i> PET imaging and post-mortem immunohistochemical analysis)</li> <li>• Post-mortem: colocalisation of CD68+ amoeboid microglia and protein aggregates</li> <li>• Positive proportional relationship with disease severity</li> </ul>
<p>Multiple sclerosis <sup>81</sup></p>	<p>TSPO expression: increased in active and chronic active lesions.</p> <p>Marks astrocytes and microglia. TSPO indicates cell density, not activation/polarisation</p> <p>TSPO PET: indirect marker of "glial" activation</p> <p>Successful therapeutic interventions that modulate microglia from pro- to anti-inflammatory may not affect the TSPO signal</p>	<p>42 patients with MS and 12 aged matched controls, 4 biopsy of suspected MS tumour-like lesions.</p>	<p>Immunohistochemistry for TSPO using antibodies on brain and spinal cord samples</p>	<ul style="list-style-type: none"> <li>• TSPO expression not associated exclusively with pro or anti-inflammatory microglia/macrophage based markers</li> <li>• TSPO expression not restricted to microglia, with GFAP+ astrocytes being TSPO+ <ul style="list-style-type: none"> <li>○ Seen in spinal cord as well as brain</li> </ul> </li> <li>• Of TSPO+ cells, &lt;1% were lymphocytes <ul style="list-style-type: none"> <li>○ Not considered significant proportion</li> </ul> </li> <li>• TSPO expression seen in lesions and spinal cords <ul style="list-style-type: none"> <li>○ This is increased in active lesions</li> </ul> </li> </ul>

	May show if treatments reduce "activated" microglia numbers			
Alzheimer's disease and Parkinson's Disease Dementia <sup>73</sup>	In AD and PD increased microglia activation correlation with decrease in mini mental state examination (MMSE; cognitive) performance.	10 AD 10 MCI 11 PD dementia (PDD) 16 controls	Magnetic resonance imaging. PET imaging for cerebral glucose metabolic rate: proxy for neuronal synaptic function	AD, MCI, and PD: correlation between increased microglia activation and reduced glucose metabolism. AD and MCI: negative correlation between increased microglia activation and MMSE. In AD and MCI: positive correlation between amyloid beta deposition and microglial activation
Human post-mortem brain samples (PD patients) <sup>82</sup>	Increased number of CD68+ amoeboid microglia in HC of incidental lewy body disease cases and PD patients	Tissue from clinically diagnosed PD patients (Braak stage 4-6) and incidental Lewy body disease (Braak stage 1-3),  with no symptoms, but showing a-synuclein deposition, [therefore can be considered prodromal PD]  All clinical patients have age and gender matched healthy controls	Immunofluorescence and immunohistochemistry of post-mortem tissue	Significantly more amoeboid microglia in PD patients compared to the age and gender matched controls. Extensive loss of dopaminergic neurons in the substantia nigra of PD patients. Positive correlation between a-synuclein pathology and an increase in amoeboid microglia in both the HC and SN in PD patients.
Abbreviations; Aβ: Amyloid Beta ; AD:Alzheimer's Disease ; bvFTD: behavioural variant FTD; CDR: clinical dementia rating; CERAD: Consortium to Establish a Registry for Alzheimer's disease; DLPFC:Dorsolateral prefrontal cortex; FTD: frontotemporal dementia; FTLD-TDP: frontotemporal lobar degeneration-TAR DNA-binding protein; <sup>18</sup> FF-PET: <sup>18</sup> F-flortaucipir-PET; Hpc: hippocampus; MCI: mild cognitive impairment ; MMSE: mini mental state examination; NfL: neurofilament light; nfvPPA: non-fluent variant primary progressive aphasia; PD: Parkinson's Disease; PET: Positron emission tomography ; PiB: Pittsburg compound B; svPPA: semantic variant primary progressive aphasia; TPSO: Translocator protein (18kDa) ; WGCNA: weight correlation network analysis.				

**Table 1.9: Microglial involvement in neuroinflammation in animal models**

Model	Outcome	Culture conditions	Methods	Results
<b>Parkinson's disease MPP<sup>+</sup> treated rat cell culture</b> <sup>84</sup>	Astrocyte signalling to microglia within the midbrain is a key factor "underlying the selective vulnerability of SN DA neurons seen in PD pathogenesis."	Homo and heterotypic co-cultures of neurons and astrocytes were established. Microglia transcriptomic analysis of cells derived from CTX, SN, and VTA.  <u>Neuron-astrocyte-microglia culture permutations:</u>  <b>SN neurons: SN astrocytes: microglia</b> <b>SN neurons: VTA astrocytes: microglia</b> <b>VTA neurons: SN astrocytes: microglia</b> <b>VTA neurons: VTA astrocytes: microglia</b> At the following N:A:M ratios 1:2:1, 1:4:1, 1:2:2, 1:4:2  Microglia were obtained from the cortex due to experimental limitations.	50 μM MPP <sup>+</sup> 24-48 h	<ul style="list-style-type: none"> <li>Microglia exhibit regional differences in their cytokine profiles in both MPP<sup>+</sup> treated and untreated control.</li> <li>MPP<sup>+</sup> induced ~50% loss of SN DA neurons in neurone-astrocyte culture</li> <li>Microglia from either CTX, SN, or VTA did not induce neuronal cell death in untreated cultures. <ul style="list-style-type: none"> <li>Instead microglia exacerbated neural cell loss in MPP<sup>+</sup> cultures, with ~75% neuron loss. This was reversed by TLR4 antagonist reverting cell loss back to ~50%.</li> </ul> </li> <li>SN astrocytes at either 2x or 4x were unable to protect SN and VTA neurons, with MPP<sup>+</sup> cultures experiencing ~60% neuron loss.</li> <li>VTA astrocytes at proportions 2 fold and 4 fold with respect to both SN and VTA neurons saw partial reversal of neurotoxic effect in N:A:M cultures (1:2:1, 1:4:1). <ul style="list-style-type: none"> <li>VTA astrocyte treated cultures experiencing ~20% neuron cells.</li> </ul> </li> <li>VTA astrocyte protection could be abolished by doubling the number of microglia, SN and VTA neurons ~40% and 50% neuron loss respectively.</li> </ul>
<b>Macaques with MPTP induced Parkinsonism</b> <sup>83</sup>	Microglia interact directly with SNpc neurons.  Microglia presence is correlated with DA neurons.	Brain bank tissue samples from chronic Parkinsonian Monkeys.	MPTP weekly 0.3 mg/kg IV  Analysis of primates was completed years after MPTP treatment	<ul style="list-style-type: none"> <li>Parkinsonian macaques shows loss of dopaminergic neurons in the SNpc alongside persistent microglial activation</li> <li>Whilst overall number of microglia did not change, number of activated microglia and microglia phagocytic activation increased.</li> <li>Seen by morphological changes: increased body size and number of terminal tips</li> <li>Even years after induction of Parkinsonian symptoms there is a prominent increase of interactions between microglia filopodia and DA neurons, compared to control.</li> </ul>

<b>Mouse model obesity-associated cerebro-vascular dysfunction</b> <sup>195</sup>	7-OZ treatment reduced cerebrovascular dysfunction (BA) in DIO mice  via blockade of microglia expressed Tak1.	Mouse model of DIO and control group.  MCAO, DIO groups and control groups. Immunohistochemistry. Brains sectioned into 30 µm.	Diet induced obesity.  MCAO.  Immuno-histochemistry. Brain sections, 30 µm  Western blot ELISA RT-qPCR	<ul style="list-style-type: none"> <li>• Microglia in brainstem after prolonged-DIO show overactivation of Tak1. This impaired BA function.</li> <li>• Deletion of microglial Tak1 reduced cerebrovascular dysfunction in DIO mice</li> <li>• In models of ischemic stroke microglia-selective deletion of Tak1 improved cerebrovascular outcome.</li> <li>• Blockade of Tak1 with 7-OZ reduced BA dysfunction in DIO mice.</li> <li>• Prolonged DIO: overproduction of IL-18 in brainstem microglia.</li> <li>• Blockade of IL-18Ra reduces dysfunction of BA in prolonged DIO mice.</li> </ul>
<b>Persistent toxoplasma infection associated with neurodegeneration</b> <sup>196</sup>	Degenerating CX3CL1+ neurons were surrounded by activated microglia and complement proteins, providing evidence that neurons were interacting with microglia	Mouse model  Half of the brain was processed for immunofluorescence staining and the other used for dissection of the prefrontal cortex for mRNA and protein analysis	Markers: Toxoplasma – toxoplasma IgG Cysts-MAG1 Neurons.  GABAergic neurons – GAD67  Glutamatergic neurons – NMDA1  Degenerating neurons – FJB  Microglia – IBA1	<ul style="list-style-type: none"> <li>• Cyst-associated neurodegeneration presents in the SC and ACC of mouse brain.</li> <li>• Both glutamatergic and GABAergic neurons display degeneration.</li> <li>• Cyst-associated elevation of cerebral complement components.</li> <li>• Complement C1q and C3 deposited on the surfaces of FJB-positive cells (neurons)</li> <li>• <u>Degenerating neurons surrounded/infiltrated by activated microglia.</u></li> <li>• Determined microglia activation by morphology.</li> <li>• Description of activated cell morphology: “enlarged perikarya and thicker processes”</li> <li>• <u>Fractalkine (CX3CL1) increased significantly in degenerating neurons</u></li> <li>• CX3CL1 is produced by neurons and its sole receptor is on microglia</li> </ul>
Abbreviations; ACC: anterior cingulate cortex; BA: basilar artery; CTX: cortex; DIO: diet induced obesity ; DA: dopamine; MCAO: Middle cerebral artery occlusion ;MPP+: 1-methyl-4-phenylpyridinium ; SC: somatomotor cortex; SN: Substantia Nigra ; SNpc: Substantia nigra pars compacta ;Tak1: Transforming growth factor β-activated kinase ; VTA: Ventral tegmental area ; 7-OZ: 5Z-7-oxozeanol a potent Tak-1 inhibitor.				

# References

1. World Health Organization. Neurological disorders: a public health approach. *Neurological disorders: public health challenges*. 41–176 (2006) doi:10.1001/archneurol.2007.19.
2. Who & Alzheimer's. WHO | Dementia: a public health priority. *who* (2012).
3. Graeber, M. B., Li, W. & Rodriguez, M. L. Role of microglia in CNS inflammation. *FEBS Lett* **585**, 3798–3805 (2011).
4. Notter, T., Coughlin, J. M., Sawa, A. & Meyer, U. Reconceptualization of translocator protein as a biomarker of neuroinflammation in psychiatry. *Nature Publishing Group* 1–12 (2017) doi:10.1038/mp.2017.232.
5. Jha, M. K., Jo, M., Kim, J. H. & Suk, K. Microglia-Astrocyte Crosstalk: An Intimate Molecular Conversation. *Neuroscientist* (2018) doi:10.1177/1073858418783959.
6. Joers, V., Tansey, M. G., Mulas, G. & Carta, A. R. Progress in Neurobiology Microglial phenotypes in Parkinson's disease and animal models of the disease. *Prog Neurobiol* **155**, 57–75 (2017).
7. Joers, V., Tansey, M. G., Mulas, G. & Carta, A. R. Progress in Neurobiology Microglial phenotypes in Parkinson's disease and animal models of the disease. *Prog Neurobiol* **155**, 57–75 (2017).
8. Satoh, J. I. Gene expression profiles of M1 and M2 microglia characterized by comparative analysis of public datasets. *Clin Exp Neuroimmunol* **9**, 124–138 (2018).

9. Kim, C. C., Nakamura, M. C. & Hsieh, C. L. Brain trauma elicits non-canonical macrophage activation states. *J Neuroinflammation* **13**, 117 (2016).
10. Ransohoff, R. M. perspective A polarizing question : do M1 and M2 microglia exist ? **19**, 987–991 (2016).
11. Moehle, M. S. & West, A. B. M1 and M2 immune activation in Parkinson’s Disease: Foe and ally? *Neuroscience* **302**, 59–73 (2015).
12. Bell-Temin, H. *et al.* Novel molecular insights into classical and alternative activation states of microglia as revealed by SILAC-based proteomics. *Mol Cell Proteomics* **14**, 1–36 (2015).
13. Lam, D., Lively, S. & Schlichter, L. C. Responses of rat and mouse primary microglia to pro- and anti-inflammatory stimuli: molecular profiles, K<sup>+</sup> channels and migration. *J Neuroinflammation* **14**, 166 (2017).
14. Stratoulis, V., Venero, J. L., Tremblay, M. & Joseph, B. Microglial subtypes: diversity within the microglial community. *EMBO J* **38**, 1–18 (2019).
15. Tan, Y. L., Yuan, Y. & Tian, L. Microglial regional heterogeneity and its role in the brain. *Mol Psychiatry* **25**, 351–367 (2020).
16. wang, J. *et al.* Treatment targets for M2 microglia polarization in ischemic stroke. *Biomedicine and Pharmacotherapy* **105**, 518–525 (2018).
17. Franco, R. & Fernández-Suárez, D. Alternatively activated microglia and macrophages in the central nervous system. *Prog Neurobiol* **131**, 65–86 (2015).
18. Jurga, A. M., Paleczna, M. & Kuter, K. Z. Overview of General and Discriminating Markers of Differential Microglia Phenotypes. *Front Cell Neurosci* **14**, 1–18 (2020).



19. Freilich, R. W., Woodbury, M. E. & Ikezu, T. Integrated expression profiles of mRNA and miRNA in polarized primary murine microglia. *PLoS One* **8**, e79416 (2013).
20. Al-Shaheeb, S. Characterising microglial activation: refinement and validation of primary in vitro models (PhD Thesis). (Keele University, 2019).
21. Lee, C. G. *et al.* Role of Chitin and Chitinase/Chitinase-Like Proteins in Inflammation, Tissue Remodeling, and Injury. *Annu Rev Physiol* **73**, 479–501 (2011).
22. Vinet, J. *et al.* Neuroprotective function for ramified microglia in hippocampal excitotoxicity. *J Neuroinflammation* **9**, 27 (2012).
23. Qiao, O. *et al.* New insights in drug development for Alzheimer’s disease based on microglia function. *Biomedicine and Pharmacotherapy* vol. 140 Preprint at <https://doi.org/10.1016/j.biopha.2021.111703> (2021).
24. Saijo, K. & Glass, C. K. Microglial cell origin and phenotypes in health and disease. *Nat Rev Immunol* **11**, 775–787 (2011).
25. Amadio, S. *et al.* Plasticity of primary microglia on micropatterned geometries and spontaneous long-distance migration in microfluidic channels. *BMC Neurosci* **14**, 121 (2013).
26. Torres-Platas, S. G. *et al.* Morphometric characterization of microglial phenotypes in human cerebral cortex. *J Neuroinflammation* **11**, 1–13 (2014).
27. Okajima, T. & Tsuruta, F. Microglial dynamics during brain development. *Neural Regen Res* **13**, 222–223 (2018).
28. Kalla, R. *et al.* Loss of microglial ramification in microglia-astrocyte cocultures: involvement of adenylate cyclase, calcium, phosphatase, and Gi-protein systems. *Glia* **41**, 50–63 (2003).

29. Taylor, S. E., Morganti-Kossmann, C., Lifshitz, J. & Ziebell, J. M. Rod microglia: A morphological definition. *PLoS One* **9**, (2014).
30. Fernández-Arjona, M. del M., Grondona, J. M., Granados-Durán, P., Fernández-Llebrez, P. & López-Ávalos, M. D. Microglia Morphological Categorization in a Rat Model of Neuroinflammation by Hierarchical Cluster and Principal Components Analysis. *Front Cell Neurosci* **11**, 1–22 (2017).
31. Zhang, S. *et al.* CD200-CD200R dysfunction exacerbates microglial activation and dopaminergic neurodegeneration in a rat model of Parkinson's disease. *J Neuroinflammation* **8**, 154 (2011).
32. Oria, M. *et al.* CD200-CD200R imbalance correlates with microglia and pro-inflammatory activation in rat spinal cords exposed to amniotic fluid in retinoic acid-induced spina bifida. *Sci Rep* 1–12 (2018) doi:10.1038/s41598-018-28829-5.
33. Zhao, X., Li, J. & Sun, H. CD200-CD200R interaction: An important regulator after stroke. *Front Neurosci* **13**, (2019).
34. Ridolfi, E., Barone, C., Scarpini, E. & Galimberti, D. The Role of the Innate Immune System in Alzheimer ' s Disease and Frontotemporal Lobar Degeneration : An Eye on Microglia. **2013**, (2013).
35. Gaikwad, S., Naveen, C. & Agrawal-Rajput, R. Toll-like receptor-4 antagonism mediates benefits during neuroinflammation. *Neural Regeneration Research* vol. 11 552–553 Preprint at <https://doi.org/10.4103/1673-5374.180732> (2016).
36. Tang, Y. & Le, W. Differential Roles of M1 and M2 Microglia in Neurodegenerative Diseases. *Mol Neurobiol* **53**, 1181–1194 (2016).

37. Kauppinen, T. M. *et al.* Poly(ADP-ribose)polymerase-1 modulates microglial responses to amyloid  $\beta$ . *J Neuroinflammation* **8**, 1–17 (2011).
38. Weightman, A. P., Jenkins, S. I. & Chari, D. M. Using a 3-D multicellular simulation of spinal cord injury with live cell imaging to study the neural immune barrier to nanoparticle uptake. *Nano Res* **9**, 2384–2397 (2016).
39. Chhor, V. *et al.* Characterization of phenotype markers and neuronotoxic potential of polarised primary microglia In vitro. *Brain Behav Immun* **32**, 70–85 (2013).
40. Lisi, L., Stigliano, E., Lauriola, L., Navarra, P. & dello Russo, C. Proinflammatory-activated glioma cells induce a switch in microglial polarization and activation status, from a predominant M2b phenotype to a mixture of M1 and M2a/B polarized cells. *ASN Neuro* **6**, 171–83 (2014).
41. Cherry, J. D. J. J. D. *et al.* Neuroinflammation and M2 microglia: the good, the bad, and the inflamed. *J Neuroinflammation* **11**, 98 (2014).
42. Walker, D. G. & Lue, L. F. Immune phenotypes of microglia in human neurodegenerative disease: Challenges to detecting microglial polarization in human brains. *Alzheimer's Research and Therapy* vol. 7 Preprint at <https://doi.org/10.1186/s13195-015-0139-9> (2015).
43. Durante, W., Johnson, F. K. & Johnson, R. A. *ARGINASE: A CRITICAL REGULATOR OF NITRIC OXIDE SYNTHESIS AND VASCULAR FUNCTION.*
44. Kang, Q., Li, L., Pang, Y., Zhu, W. & Meng, L. An update on Ym1 and its immunoregulatory role in diseases. *Frontiers in Immunology* vol. 13 Preprint at <https://doi.org/10.3389/fimmu.2022.891220> (2022).

45. He, Y. *et al.* IL-4 Switches Microglia/macrophage M1/M2 Polarization and Alleviates Neurological Damage by Modulating the JAK1/STAT6 Pathway Following ICH. *Neuroscience* **437**, 161–171 (2020).
46. Yu, T. *et al.* Promising Neuroprotective Function for M2 Microglia in Kainic Acid-Induced Neurotoxicity Via the Down-Regulation of NF- $\kappa$ B and Caspase 3 Signaling Pathways. *Neuroscience* **406**, 86–96 (2019).
47. Gensel, J. C. & Zhang, B. Macrophage activation and its role in repair and pathology after spinal cord injury. *Brain Res* **1619**, 1–11 (2015).
48. Mosser, D. M. The many faces of macrophage activation. *J Leukoc Biol* **73**, 209–212 (2003).
49. Norden, D. M., Fenn, A. M., Dugan, A. & Godbout, J. P. TGF $\beta$  produced by IL-10 redirected astrocytes attenuates microglial activation. *Glia* **62**, 881–895 (2014).
50. Novak, M. L. & Koh, T. J. Phenotypic transitions of macrophages orchestrate tissue repair. *Am J Pathol* **183**, 1352–63 (2013).
51. Bell-Temin, H. *et al.* Novel molecular insights into classical and alternative activation states of microglia as revealed by SILAC-based proteomics. *Mol Cell Proteomics* **14**, 1–36 (2015).
52. Mandrekar-Colucci, S. & Landreth, G. E. Microglia and inflammation in Alzheimer's disease. *CNS Neurol Disord Drug Targets* **9**, 156–67 (2010).
53. Varnum, M. M. & Ikezu, T. The classification of microglial activation phenotypes on neurodegeneration and regeneration in Alzheimer's disease brain. *Arch Immunol Ther Exp (Warsz)* **60**, 251–66 (2012).

54. Kisuck, A. & Bař, M. Activation of Neuroprotective Microglia and Astrocytes at the Lesion Site and in the Adjacent Segments Is Crucial for Spontaneous Locomotor Recovery after Spinal Cord Injury. (2021).
55. Zhang, L., Zhang, J. & You, Z. Switching of the microglial activation phenotype is a possible treatment for depression disorder. *Frontiers in Cellular Neuroscience* vol. 12 Preprint at <https://doi.org/10.3389/fncel.2018.00306> (2018).
56. Shahidehpour, R. K. *et al.* Dystrophic microglia are a disease associated microglia morphology in the human brain. *bioRxiv* 1–17 (2020).
57. Zanier, E. R., Fumagalli, S., Perego, C., Pischiutta, F. & de Simoni, M.-G. Shape descriptors of the “never resting” microglia in three different acute brain injury models in mice. *Intensive Care Med Exp* **3**, 1–18 (2015).
58. Wyatt-Johnson, S. K., Herr, S. A. & Brewster, A. L. Status epilepticus triggers time-dependent alterations in microglia abundance and morphological phenotypes in the hippocampus. *Front Neurol* **8**, 1–10 (2017).
59. Bisht, K. *et al.* Dark microglia: A new phenotype predominantly associated with pathological states. *Glia* **64**, 826–839 (2016).
60. Kavetsky, L. *et al.* Increased interactions and engulfment of dendrites by microglia precede Purkinje cell degeneration in a mouse model of Niemann Pick Type-C. *Sci Rep* **9**, 1–15 (2019).
61. Roth, T. L. *et al.* Transcranial amelioration of inflammation and cell death after brain injury. *Nature* **505**, 223–228 (2014).

62. Levtova, N. *et al.* Comparative morphology and phagocytic capacity of primary human adult microglia with time-lapse imaging. *J Neuroimmunol* **310**, 143–149 (2017).
63. Holloway, O. G., Canty, A. J., King, A. E. & Ziebell, J. M. Rod microglia and their role in neurological diseases. *Semin Cell Dev Biol* **94**, 96–103 (2019).
64. Holloway, O. G., Canty, A. J., King, A. E. & Ziebell, J. M. Rod microglia and their role in neurological diseases. *Semin Cell Dev Biol* **94**, 96–103 (2019).
65. Levtova, N. *et al.* Comparative morphology and phagocytic capacity of primary human adult microglia with time-lapse imaging. *J Neuroimmunol* **310**, 143–149 (2017).
66. Caldeira, C. *et al.* Key Aging-Associated Alterations in Primary Microglia Response to Beta-Amyloid Stimulation . *Frontiers in Aging Neuroscience* **9**, 277 (2017).
67. Kavetsky, L. *et al.* Increased interactions and engulfment of dendrites by microglia precede Purkinje cell degeneration in a mouse model of Niemann Pick Type-C. *Sci Rep* **9**, 1–15 (2019).
68. Cunha, C., Gomes, C., Vaz, A. R. & Brites, D. Exploring New Inflammatory Biomarkers and Pathways during LPS-Induced M1 Polarization. *Mediators Inflamm* **2016**, (2016).
69. Siemsen, B. M. *et al.* Chronic intermittent ethanol and lipopolysaccharide exposure differentially alter Iba1-derived microglia morphology in the prelimbic cortex and nucleus accumbens core of male Long-Evans rats. *J Neurosci Res* **1**, 1–18 (2020).
70. Rawji, K. S. *et al.* Niacin-mediated rejuvenation of macrophage/microglia enhances remyelination of the aging central nervous system. *Acta Neuropathol* **139**, 893–909 (2020).

71. Huang, C. *et al.* The ketone body metabolite  $\beta$ -hydroxybutyrate induces an antidepressant-associated ramification of microglia via HDACs inhibition-triggered Akt-small RhoGTPase activation. *Glia* **66**, 256–278 (2018).
72. Fernández-Arjona, M. del M., Grondona, J. M., Fernández-Llebrez, P. & López-Ávalos, M. D. Microglial Morphometric Parameters Correlate With the Expression Level of IL-1 $\beta$ , and Allow Identifying Different Activated Morphotypes. *Front Cell Neurosci* **13**, 1–15 (2019).
73. Fan, Z. *et al.* Influence of microglial activation on neuronal function in Alzheimer’s and Parkinson’s disease dementia. *Alzheimer’s and Dementia* **11**, 608-621.e7 (2015).
74. Arevalo-Rodriguez, I. *et al.* Mini-Mental State Examination (MMSE) for the detection of Alzheimer’s disease and other dementias in people with mild cognitive impairment (MCI). *Cochrane Database of Systematic Reviews* vol. 2015 Preprint at <https://doi.org/10.1002/14651858.CD010783.pub2> (2015).
75. Parbo, P. *et al.* Brain inflammation accompanies amyloid in the majority of mild cognitive impairment cases due to Alzheimer’s disease. *Brain* 2002–2011 (2017) doi:10.1093/awx151.
76. Parbo, P. *et al.* Low plasma neurofilament light levels associated with raised cortical microglial activation suggest inflammation acts to protect prodromal Alzheimer’s disease. *Alzheimers Res Ther* **12**, 1–7 (2020).
77. Parbo, P. *et al.* Low plasma neurofilament light levels associated with raised cortical microglial activation suggest inflammation acts to protect prodromal Alzheimer’s disease. *Alzheimers Res Ther* **12**, 1–7 (2020).

78. Nutma, E. *et al.* A quantitative neuropathological assessment of translocator protein expression in multiple sclerosis. *Brain* **142**, 3440–3455 (2019).
79. Wang, M. *et al.* Macroglia-microglia interactions via TSPO signaling regulates microglial activation in the mouse retina. *Journal of Neuroscience* **34**, 3793–3806 (2014).
80. Leyns, C. E. G. & Holtzman, D. M. Glial contributions to neurodegeneration in tauopathies. *Mol Neurodegener* **12**, 1–16 (2017).
81. Nutma, E. *et al.* A quantitative neuropathological assessment of translocator protein expression in multiple sclerosis. *Brain* **142**, 3440–3455 (2019).
82. Doorn, K. J. *et al.* Microglial phenotypes and toll-like receptor 2 in the substantia nigra and hippocampus of incidental Lewy body disease cases and Parkinson’s disease patients. *Acta Neuropathol Commun* **2**, 1–17 (2014).
83. Barcia, C. *et al.* Persistent phagocytic characteristics of microglia in the substantia nigra of long-term Parkinsonian macaques. *J Neuroimmunol* **261**, 60–66 (2013).
84. Kostuk, E. W., Cai, J. & Iacovitti, L. Regional microglia are transcriptionally distinct but similarly exacerbate neurodegeneration in a culture model of Parkinson’s disease. *J Neuroinflammation* **15**, 1–11 (2018).
85. Block, M. L., Zecca, L. & Hong, J. S. Microglia-mediated neurotoxicity: Uncovering the molecular mechanisms. *Nat Rev Neurosci* **8**, 57–69 (2007).
86. Parbo, P. *et al.* Brain inflammation accompanies amyloid in the majority of mild cognitive impairment cases due to Alzheimer’s disease. *Brain* 2002–2011 (2017) doi:10.1093/awx151.



87. Wakade, C., Chong, R., Bradley, E., Thomas, B. & Morgan, J. Upregulation of GPR109A in Parkinson's disease. *PLoS One* **9**, 1–10 (2014).
88. Rahman, M. *et al.* The  $\beta$ -hydroxybutyrate receptor HCA2 activates a neuroprotective subset of macrophages. *Nat Commun* **5**, 3944 (2014).
89. Fu, S. *et al.* Anti-inflammatory effects of BHBA in both in vivo and in vitro Parkinson's disease models are mediated by GPR109A-dependent mechanisms. 1–14 (2015) doi:10.1186/s12974-014-0230-3.
90. Fu, S. P. *et al.* BHBA suppresses LPS-induced inflammation in BV-2 cells by inhibiting NF- $\kappa$ B activation. *Mediators Inflamm* **2014**, (2014).
91. Rezaq, S. & Abdel-Rahman, A. A. Central GPR109A Activation Mediates Glutamate-Dependent Pressor Response in Conscious Rats. *Journal of Pharmacology and Experimental Therapeutics* **356**, 457–466 (2016).
92. Wakade, C., Chong, R., Bradley, E. & Morgan, J. C. Low-dose niacin supplementation modulates GPR109A, niacin index and ameliorates Parkinson's disease symptoms without side effects. *Clin Case Rep* **3**, 635–637 (2015).
93. Fish, J. Unified Parkinson's Disease Rating Scale. in *Encyclopedia of Clinical Neuropsychology* 2576–2577 (Springer New York, 2011). doi:10.1007/978-0-387-79948-3\_1836.
94. Getts, D. R. *et al.* Ly6c+ “inflammatory monocytes” are microglial precursors recruited in a pathogenic manner in West Nile virus encephalitis. *J Exp Med* **205**, 2319–2337 (2008).
95. Lund, H. *et al.* Competitive repopulation of an empty microglial niche yields functionally distinct subsets of microglia-like cells. *Nat Commun* **9**, (2018).

96. Yamasaki, R. *et al.* Differential roles of microglia and monocytes in the inflamed central nervous system. *Journal of Experimental Medicine* **211**, 1533–1549 (2014).
97. Al-Jaderi, Z. & Maghazachi, A. A. Utilization of dimethyl fumarate and related molecules for treatment of multiple sclerosis, cancer, and other diseases. *Front Immunol* **7**, 1–8 (2016).
98. Mills, E. A., Ogrodnik, M. A., Plave, A. & Mao-Draayer, Y. Emerging understanding of the mechanism of action for dimethyl fumarate in the treatment of multiple sclerosis. *Front Neurol* **9**, 1–8 (2018).
99. Schulze-Topphoff, U. *et al.* Dimethyl fumarate treatment induces adaptive and innate immune modulation independent of Nrf2. *Proceedings of the National Academy of Sciences* **113**, 4777–4782 (2016).
100. Peng, H. *et al.* Dimethyl fumarate alters microglia phenotype and protects neurons against proinflammatory toxic microenvironments. *J Neuroimmunol* **299**, 35–44 (2016).
101. Ambrosius, B. *et al.* Teriflunomide and monomethylfumarate target HIV-induced neuroinflammation and neurotoxicity. *J Neuroinflammation* **14**, 1–10 (2017).
102. Jiang, D. *et al.* Monomethyl fumarate protects the retina from light- induced retinopathy. *Invest Ophthalmol Vis Sci* **60**, 1275–1285 (2019).
103. Jiang, D. *et al.* Monomethyl fumarate protects the retina from light- induced retinopathy. *Invest Ophthalmol Vis Sci* **60**, 1275–1285 (2019).
104. Kronenberg, J. *et al.* Fumaric acids directly influence gene expression of neuroprotective factors in rodent microglia. *Int J Mol Sci* **20**, (2019).

105. Zhou, X. D. *et al.* Neuroprotective effect of targeted regulatory Nrf2 gene on rats with acute brain injury induced by carbon monoxide poisoning. *Environ Toxicol* **36**, 1742–1757 (2021).
106. Zhu, F., Shao, J., Tian, Y. & Xu, Z. Sulfiredoxin-1 protects retinal ganglion cells from high glucose-induced oxidative stress and inflammatory injury by potentiating Nrf2 signaling via the Akt/GSK-3 $\beta$  pathway. *Int Immunopharmacol* **101**, (2021).
107. Tang, H., Lu, J. Y. L., Zheng, X., Yang, Y. & Reagan, J. D. The psoriasis drug monomethylfumarate is a potent nicotinic acid receptor agonist. *Biochem Biophys Res Commun* **375**, 562–565 (2008).
108. Brennan, M. S. *et al.* Dimethyl fumarate and monoethyl fumarate exhibit differential effects on KEAP1, NRF2 activation, and glutathione depletion in vitro. *PLoS One* **10**, (2015).
109. Brennan, M. S., Matos, M. F., Richter, K. E., Li, B. & Scannevin, R. H. The NRF2 transcriptional target , OSGIN1 , contributes to monomethyl fumarate-mediated cytoprotection in human astrocytes. *Nature Publishing Group* 1–15 (2017) doi:10.1038/srep42054.
110. Biber, K. *et al.* Microglial drug targets in AD: Opportunities and challenges in drug discovery and development. *Front Pharmacol* **10**, 1–19 (2019).
111. Yang, S. *et al.* Baicalein administered in the subacute phase ameliorates ischemia-reperfusion-induced brain injury by reducing neuroinflammation and neuronal damage. *Biomedicine and Pharmacotherapy* **117**, 109102 (2019).
112. Nakano-Kobayashi, A. *et al.* Therapeutics potentiating microglial p21-Nrf2 axis can rescue neurodegeneration caused by neuroinflammation. *Sci Adv* **6**, 1–13 (2020).

113. Ding, Y. *et al.* Effects of SC99 on cerebral ischemia-perfusion injury in rats: Selective modulation of microglia polarization to M2 phenotype via inhibiting JAK2-STAT3 pathway. *Neurosci Res* **142**, 58–68 (2019).
114. Yang, S. *et al.* Baicalein administered in the subacute phase ameliorates ischemia-reperfusion-induced brain injury by reducing neuroinflammation and neuronal damage. *Biomedicine and Pharmacotherapy* **117**, 109102 (2019).
115. Xiang, B., Xiao, C., Shen, T. & Li, X. Anti-inflammatory effects of anisalcohol on lipopolysaccharide-stimulated BV2 microglia via selective modulation of microglia polarization and down-regulation of NF- $\kappa$ B p65 and JNK activation. *Mol Immunol* **95**, 39–46 (2018).
116. Ding, Y. *et al.* Effects of SC99 on cerebral ischemia-perfusion injury in rats: Selective modulation of microglia polarization to M2 phenotype via inhibiting JAK2-STAT3 pathway. *Neurosci Res* **142**, 58–68 (2019).
117. Sigfridsson, E., Marangoni, M., Hardingham, G. E., Horsburgh, K. & Fowler, J. H. Deficiency of Nrf2 exacerbates white matter damage and microglia/macrophage levels in a mouse model of vascular cognitive impairment. *J Neuroinflammation* **17**, 1–15 (2020).
118. Nakano-Kobayashi, A. *et al.* Therapeutics potentiating microglial p21-Nrf2 axis can rescue neurodegeneration caused by neuroinflammation. *Sci Adv* **6**, 1–13 (2020).
119. Ahmed, S. M. U., Luo, L., Namani, A., Wang, X. J. & Tang, X. Nrf2 signaling pathway: Pivotal roles in inflammation. *Biochim Biophys Acta Mol Basis Dis* **1863**, 585–597 (2017).

120. Cummings, J., Lee, G., Ritter, A., Sabbagh, M. & Zhong, K. Alzheimer's disease drug development pipeline: 2020. *Alzheimer's and Dementia: Translational Research and Clinical Interventions* **6**, 1–29 (2020).
121. Zhang, C. *et al.* Cromolyn Reduces Levels of the Alzheimer's Disease-Associated Amyloid  $\beta$ -Protein by Promoting Microglial Phagocytosis. *Sci Rep* **8**, 1–9 (2018).
122. Brazier, D., Perry, R., Keane, J., Barrett, K. & Elmaleh, D. R. Pharmacokinetics of Cromolyn and Ibuprofen in Healthy Elderly Volunteers. *Clin Drug Investig* **37**, 1025–1034 (2017).
123. Burstein, A. H. *et al.* Development of Azeliragon, an Oral Small Molecule Antagonist of the Receptor for Advanced Glycation Endproducts, for the Potential Slowing of Loss of Cognition in Mild Alzheimer's Disease. *J Prev Alzheimers Dis* **5**, 149–154 (2018).
124. Giri, B. *et al.* Niacin Ameliorates Neuro-Inflammation in Parkinson's Disease via GPR109A. 1–14 (2019).
125. Wakade, C. *et al.* Niacin modulates macrophage polarization in Parkinson's disease. *J Neuroimmunol* **320**, 76–79 (2018).
126. Williams, A. C. & Ramsden, D. B. Nicotinamide: A double edged sword. *Parkinsonism Relat Disord* **11**, 413–420 (2005).
127. Li, R. *et al.* Pellagra Secondary to Medication and Alcoholism: A Case Report and Review of the Literature. *Nutrition in Clinical Practice* **31**, 785–789 (2016).
128. Williams & Dunbar, R. Big Brains, Meat, Tuberculosis, and the Nicotinamide Switches: Co-Evolutionary Relationships with Modern Repercussions? *International Journal of Tryptophan Research* **6**, 73–88 (2013).

129. Singh, L. K. *et al.* Rapid resolution of delusional parasitosis in pellagra with niacin augmentation therapy. *Gen Hosp Psychiatry* **30**, 581–584 (2008).
130. Sakai K, Nakajima T, F. N. A suspected case of alcoholic pellagra encephalopathy with marked response to niacin showing myoclonus and ataxia as chief complaints. *Brain and Nerve*. **Feb;58**, 141–144 (2006).
131. Singh, L. K. *et al.* Rapid resolution of delusional parasitosis in pellagra with niacin augmentation therapy. *Gen Hosp Psychiatry* **30**, 581–584 (2008).
132. Wang, W. & Liang, B. Case report of mental disorder induced by niacin deficiency. *Shanghai Arch Psychiatry* **24**, 352–354 (2012).
133. Sharma, B., Sannegowda, R. B., Jain, R., Dubey, P. & Prakash, S. A rare case of alcoholic pellagra encephalopathy with startle myoclonus and marked response to niacin therapy: time for a new dictum? *BMJ Case Rep* 1–3 (2013) doi:10.1136/bcr-2013-008906.
134. Gopal, S. *et al.* Evidence of activation of the Nrf2 pathway in multiple sclerosis patients treated with delayed-release dimethyl fumarate in the Phase 3 DEFINE and CONFIRM studies. *Multiple Sclerosis* **23**, 1875–1883 (2017).
135. di Nuzzo, L., Orlando, R., Nasca, C. & Nicoletti, F. Molecular pharmacodynamics of new oral drugs used in the treatment of multiple sclerosis. *Drug Des Devel Ther* **8**, 555–567 (2014).
136. Parodi, B. *et al.* Fumarates modulate microglia activation through a novel HCAR2 signaling pathway and rescue synaptic dysregulation in inflamed CNS. *Acta Neuropathol* 279–295 (2015) doi:10.1007/s00401-015-1422-3.

137. Mills, E. A., Ogrodnik, M. A., Plave, A. & Mao-Draayer, Y. Emerging understanding of the mechanism of action for dimethyl fumarate in the treatment of multiple sclerosis. *Front Neurol* **9**, 1–8 (2018).
138. Glehn, F. von *et al.* Dimethyl fumarate downregulates the immune response through the HCA 2 / GPR109A pathway : Implications for the treatment of multiple sclerosis. *Mult Scler Relat Disord* **23**, 46–50 (2018).
139. Wang, W. & Liang, B. Case report of mental disorder induced by niacin deficiency. *Shanghai Arch Psychiatry* **24**, 352–354 (2012).
140. Sharma, B., Sannegowda, R. B., Jain, R., Dubey, P. & Prakash, S. A rare case of alcoholic pellagra encephalopathy with startle myoclonus and marked response to niacin therapy: time for a new dictum? *BMJ Case Rep* 1–3 (2013) doi:10.1136/bcr-2013-008906.
141. Kronenberg, J. *et al.* Fumaric acids directly influence gene expression of neuroprotective factors in rodent microglia. *Int J Mol Sci* **20**, (2019).
142. Garrido-gil, P., Joglar, B., Rodriguez-perez, A. I., Guerra, M. J. & Labandeira-garcia, J. L. Involvement of PPAR-  $\gamma$  in the neuroprotective and anti-inflammatory effects of angiotensin type 1 receptor inhibition : effects of the receptor antagonist telmisartan and receptor deletion in a mouse MPTP model of Parkinson ' s disease. *J Neuroinflammation* **9**, 38 (2012).
143. Sigfridsson, E., Marangoni, M., Hardingham, G. E., Horsburgh, K. & Fowler, J. H. Deficiency of Nrf2 exacerbates white matter damage and microglia/macrophage levels in a mouse model of vascular cognitive impairment. *J Neuroinflammation* **17**, 1–15 (2020).

144. Hedegaard, A., Stodolak, S., James, W. S. & Cowley, S. A. Honing the Double-Edged Sword: Improving Human iPSC-Microglia Models. *Front Immunol* **11**, 1–9 (2020).
145. Schmid, C. D. *et al.* Differential gene expression in LPS/IFN $\gamma$  activated microglia and macrophages: in vitro versus in vivo. *J Neurochem* **109 Suppl**, 117–25 (2009).
146. Galatro, T. F. *et al.* Transcriptomic analysis of purified human cortical microglia reveals age-associated changes. *Nat Neurosci* **20**, 1162–1171 (2017).
147. Guerrero, J. & Reiter, R. Melatonin-Immune System Relationships. *Curr Top Med Chem* **2**, 167–179 (2002).
148. Satoh, T. & Lipton, S. Recent advances in understanding NRF2 as a druggable target: development of pro-electrophilic and non-covalent NRF2 activators to overcome systemic side effects of electrophilic drugs like dimethyl fumarate. *F1000Res* **6**, 2138 (2017).
149. Xie, X. *et al.* Dimethyl fumarate induces necroptosis in colon cancer cells through GSH depletion/ROS increase/MAPKs activation pathway. *Br J Pharmacol* **172**, 3929–3943 (2015).
150. Satoh, T. & Lipton, S. Recent advances in understanding NRF2 as a druggable target: development of pro-electrophilic and non-covalent NRF2 activators to overcome systemic side effects of electrophilic drugs like dimethyl fumarate. *F1000Res* **6**, 2138 (2017).
151. Wilms, H. *et al.* Dimethylfumarate inhibits microglial and astrocytic inflammation by suppressing the synthesis of nitric oxide, IL-1 $\beta$ , TNF- $\alpha$  and IL-6 in an in-vitro model of brain inflammation. *J Neuroinflammation* **7**, 1–8 (2010).



152. Offermanns, S. Hydroxy-Carboxylic Acid Receptor Actions in Metabolism. *Trends in Endocrinology and Metabolism* **28**, 227–236 (2017).
153. Wise, A. *et al.* Molecular identification of high and low affinity receptors for nicotinic acid. *Journal of Biological Chemistry* **278**, 9869–9874 (2003).
154. Garrido-gil, P., Joglar, B., Rodriguez-perez, A. I., Guerra, M. J. & Labandeira-garcia, J. L. Involvement of PPAR-  $\gamma$  in the neuroprotective and anti-inflammatory effects of angiotensin type 1 receptor inhibition: effects of the receptor antagonist telmisartan and receptor deletion in a mouse MPTP model of Parkinson ' s disease. *J Neuroinflammation* **9**, 38 (2012).
155. Izuta, Y. *et al.* Ketone body 3-hydroxybutyrate mimics calorie restriction via the Nrf2 activator, fumarate, in the retina. *Aging Cell* **17**, (2018).
156. Wise, A. *et al.* Molecular identification of high and low affinity receptors for nicotinic acid. *Journal of Biological Chemistry* **278**, 9869–9874 (2003).
157. Tang, H., Lu, J. Y. L., Zheng, X., Yang, Y. & Reagan, J. D. The psoriasis drug monomethylfumarate is a potent nicotinic acid receptor agonist. *Biochem Biophys Res Commun* **375**, 562–565 (2008).
158. Offermanns, S. Hydroxy-Carboxylic Acid Receptor Actions in Metabolism. *Trends in Endocrinology and Metabolism* **28**, 227–236 (2017).
159. Shen, H. C. *et al.* Discovery of a biaryl cyclohexene carboxylic acid (MK-6892): A potent and selective high affinity niacin receptor full agonist with reduced flushing profiles in animals as a preclinical candidate. *J Med Chem* **53**, 2666–2670 (2010).
160. McCarthy, K. D. & de Vellis, J. Preparation of separate astroglial and oligodendroglial cell cultures from rat cerebral tissue. *J. Cell Biol.* **85**, 890–902 (1980).

161. Cătălin, B., Stopper, L., Bălșeanu, T. A. & Scheller, A. The in situ morphology of microglia is highly sensitive to the mode of tissue fixation. *J Chem Neuroanat* **86**, 59–66 (2017).
162. Kenkhuis, B. *et al.* Co-expression patterns of microglia markers Iba1, TMEM119 and P2RY12 in Alzheimer's disease. *Neurobiol Dis* **167**, (2022).
163. Waller, R. *et al.* Iba-1-/CD68+ microglia are a prominent feature of age-associated deep subcortical white matter lesions. *PLoS One* **14**, (2019).
164. Koyama, R. & Ikegaya, Y. Microglia in the pathogenesis of autism spectrum disorders. *Neuroscience Research* vol. 100 1–5 Preprint at <https://doi.org/10.1016/j.neures.2015.06.005> (2015).
165. Simpson, D. S. A. & Oliver, P. L. Ros generation in microglia: Understanding oxidative stress and inflammation in neurodegenerative disease. *Antioxidants* vol. 9 1–27 Preprint at <https://doi.org/10.3390/antiox9080743> (2020).
166. Kumar, A. *et al.* NOX2 drives M1-like microglial/macrophage activation and neurodegeneration following experimental traumatic brain injury. *Brain Behav Immun* **58**, 291–309 (2016).
167. Liao, S. *et al.*  $\beta$ -Hydroxybutyrate Mitigated Heart Failure with Preserved Ejection Fraction by Increasing Treg Cells via Nox2/GSK-3 $\beta$ . *J Inflamm Res* **14**, 4697–4706 (2021).
168. Gautam, J. *et al.* 4-Hydroxynonenal-induced GPR109A (HCA 2 receptor) activation elicits bipolar responses, G  $\alpha$ i -mediated anti-inflammatory effects and G  $\beta$  $\gamma$  -mediated cell death. *Br J Pharmacol* **175**, 2581–2598 (2018).

169. Cherry, J. D., Olschowka, J. A. & O'Banion, M. K. Arginase 1+ microglia reduce A $\beta$  plaque deposition during IL-1 $\beta$ -dependent neuroinflammation. *J Neuroinflammation* **12**, (2015).
170. Feingold, K. R., Moser, A., Shigenaga, J. K. & Grunfeld, C. Inflammation stimulates niacin receptor (GPR109A/HCA2) expression in adipose tissue and macrophages. *J Lipid Res* **55**, 2501–2508 (2015).
171. Batiuk, M. Y. *et al.* Identification of region-specific astrocyte subtypes at single cell resolution. *Nat Commun* **11**, 1–15 (2020).
172. Pan, J., Ma, N., Yu, B., Zhang, W. & Wan, J. Transcriptomic profiling of microglia and astrocytes throughout aging. *J Neuroinflammation* **17**, 1–19 (2020).
173. Todd, B. P. *et al.* Traumatic brain injury results in unique microglial and astrocyte transcriptomes enriched for type I interferon response. 1–15 (2021).
174. Li, G. *et al.* Internalization of the Human Nicotinic Acid Receptor GPR109A Is Regulated by G $\beta$ 1, GRK2, and Arrestin3. **285**, 22605–22618 (2010).
175. Richman, J. G. *et al.* Nicotinic Acid Receptor Agonists Differentially Activate Downstream Effectors. **282**, 18028–18036 (2007).
176. Stence, N., Waite, M. & Dailey, M. E. Dynamics of microglial activation: a confocal time-lapse analysis in hippocampal slices. *Glia* **33**, 256–66 (2001).
177. Caldeira, C. *et al.* Microglia change from a reactive to an age-like phenotype with the time in culture. *Front Cell Neurosci* **8**, (2014).
178. Lin, L., Desai, R., Wang, X., Lo, E. H. & Xing, C. Characteristics of primary rat microglia isolated from mixed cultures using two different methods. *J Neuroinflammation* **14**, 1–10 (2017).

179. Habibe MN, K. JZ. Niacin Toxicity. *In: StatPearls [Internet]. Treasure Island (FL): StatPearls Publishing (2022).*
180. Haw, R. T. Y. *et al.* A three-dimensional collagen construct to model lipopolysaccharide-induced activation of BV2 microglia. *J Neuroinflammation* **11**, 1–10 (2014).
181. Cuní-lópez, C. *et al.* 3D models of Alzheimer’s disease patient microglia recapitulate disease phenotype and show differential drug responses compared to 2D. (2021).
182. Yun, S. P. *et al.* Block of A1 astrocyte conversion by microglia is neuroprotective in models of Parkinson’s disease. *Nat Med* **24**, 931–938 (2018).
183. Bussian, T. J. *et al.* Clearance of senescent glial cells prevents tau-dependent pathology and cognitive decline. *Nature* **562**, 578–582 (2018).
184. Norden, D. M. & Godbout, J. P. Review: Microglia of the aged brain: Primed to be activated and resistant to regulation. *Neuropathol Appl Neurobiol* **39**, 19–34 (2013).
185. Lopez-Rodriguez, A. B. *et al.* Microglial and Astrocyte priming in the APP/PS1 model of Alzheimer’s Disease: increased vulnerability to acute inflammation and cognitive deficits. 344218 (2018) doi:10.1101/344218.
186. Koyama, R. & Ikegaya, Y. Microglia in the pathogenesis of autism spectrum disorders. *Neuroscience Research* vol. 100 1–5 Preprint at <https://doi.org/10.1016/j.neures.2015.06.005> (2015).
187. Ding, X. *et al.* Loss of microglial SIRP $\alpha$  promotes synaptic pruning in preclinical models of neurodegeneration. *Nat Commun* **12**, (2021).

188. Neniskyte, U., Fricker, M. & Brown, G. C. Amyloid  $\beta$  induces microglia to phagocytose neurons via activation of protein kinase Cs and NADPH oxidase. *International Journal of Biochemistry and Cell Biology* **81**, 346–355 (2016).
189. Jiang, T. *et al.* TREM1 facilitates microglial phagocytosis of amyloid beta. *Acta Neuropathol* **132**, 667–683 (2016).
190. Kongsui, R., Beynon, S. B., Johnson, S. J. & Walker, F. Quantitative assessment of microglial morphology and density reveals remarkable consistency in the distribution and morphology of cells within the healthy prefrontal cortex of the rat. *J Neuroinflammation* **11**, 182 (2014).
191. García-Magro, N. *et al.* Multiple Morphometric Assessment of Microglial Cells in Deafferented Spinal Trigeminal Nucleus. *Front Neuroanat* **13**, 1–13 (2020).
192. Ismail, R. *et al.* The relationships between neuroinflammation, beta-amyloid and tau deposition in Alzheimer's disease: A longitudinal PET study. *J Neuroinflammation* **17**, 1–11 (2020).
193. Johnson, E. C. B. *et al.* Large-scale proteomic analysis of Alzheimer's disease brain and cerebrospinal fluid reveals early changes in energy metabolism associated with microglia and astrocyte activation. *Nat Med* **26**, 769–780 (2020).
194. Bevan-Jones, W. R. *et al.* Neuroinflammation and protein aggregation co-localize across the frontotemporal dementia spectrum. *Brain* **143**, 1010–1026 (2020).
195. Shen, Q. *et al.* Reversal of prolonged obesity-associated cerebrovascular dysfunction by inhibiting microglial Tak1. *Nat Neurosci* **23**, 832–841 (2020).

196. Li, Y., Severance, E. G., Viscidi, R. P., Yolken, R. H. & Xiao, J. Persistent toxoplasma infection of the brain induced neurodegeneration associated with activation of complement and microglia. *Infect Immun* **87**, 1–12 (2019).